SUPPORTED BY

GLOBAL CCS INSTITUTE

Evaluating technology options to mitigate greenhouse gas emissions

ieaghg

EFFECTS OF IMPURITIES ON GEOLOGICAL STORAGE OF CO_2

Report: 2011/04

June 2011

INTERNATIONAL ENERGY AGENCY

The International Energy Agency (IEA) was established in 1974 within the framework of the Organisation for Economic Co-operation and Development (OECD) to implement an international energy programme. The IEA fosters co-operation amongst its 28 member countries and the European Commission, and with the other countries, in order to increase energy security by improved efficiency of energy use, development of alternative energy sources and research, development and demonstration on matters of energy supply and use. This is achieved through a series of collaborative activities, organised under more than 40 Implementing Agreements. These agreements cover more than 200 individual items of research, development and demonstration. IEAGHG is one of these Implementing Agreements.

DISCLAIMER

COPYRIGHT

ACKNOWLEDGEMENTS AND CITATIONS

This report describes research sponsored by IEAGHG and wholly funded by the Global CCS Institute.
This report was prepared by:

- CanmetENERGY, Natural Resources Canada

The principal researchers were:

- Jinsheng Wang
- David Ryan
- Edward J. Anthony
- Andrew Wigston

To ensure the quality and technical integrity of the research undertaken by IEAGHG each study is managed by an appointed IEAGHG manager. The report is also reviewed by a panel of independent technical experts before its release.

The IEAGHG manager for this report was:

- Neil Wildgust

The expert reviewers for this report were:

- Dr Todd Schaef, PNNL
- Brian Moffatt, BG Group
- Marc Parmentier, BRGM
- Stanley Santos, IEAGHG
- Ziqiu Xue, RITE
- Yann Le Gallo, Geogreen
- Franz May, BGR
- Linda Stalker, CSIRO
- Lingli Wei, Shell
- Malcolm Wilson, PTRC

The report should be cited in literature as follows:

'IEAGHG, "Effects of Impurities on Geological Storage of CO_2", 2011/04, June, 2011.'

Further information or copies of the report can be obtained by contacting IEAGHG at:

IEAGHG, Orchard Business Centre,
Stoke Orchard, Cheltenham,
GLOS., GL52 7RZ, UK
Tel: +44 (0)1242 680753 Fax: +44 (0)1242 680758
E-mail: @ieaghg.org
Internet: .ieaghg.org

EFFECTS OF IMPURITIES ON GEOLOGICAL STORAGE OF CARBON DIOXIDE

Background to the Study

Geological storage of CO_2 as a means to mitigate global warming would entail capture of CO_2 from a range of point source industrial emissions. Capture technology represents the major cost element of the CCS chain and the required purity of CO_2 can have a major bearing on actual capture costs. Impurities in the CO_2 stream have the potential to affect the efficiency and safety of transport and storage systems, for example through increased risks associated with corrosion, or changes in the phase behaviour of the CO_2 stream.

The presence of impurities is likely to have a significant effect on the phase behaviour or CO_2 streams, with implications for the design and operation of pipelines and injection wells. The presence of impurities could also pose a significant threat of increased corrosion of pipeline and well materials.

The presence of impurities in the CO_2 stream may have an effect on all types of geological storage scenarios, especially in terms of changes in storage capacity and injectivity due to changes in phase behaviour with respect to pure CO_2. In addition, impurities could have a significant effect on injectivity through geochemical reactions in the vicinity of injection wells. Geochemical effects such as dissolution of CO_2 and reactions with minerals may determine the long term fate of injected CO_2, especially CO_2 injected into deep saline formations; and thus the effects of impurities on geochemistry may affect the risk profile of storage sites, as geochemical reactions are widely seen as a key mechanism for the stabilisation of pressure and brine displacement. Geochemical reactions also have the potential to affect the integrity of caprock sequences above storage complexes.

IEA GHG Report PH/4-32 (2004) looked at the maximum level of impurities which might be expected in captured CO_2 from a wide range of fuels and from a selection of the contending capture processes; there has been a considerable advance since in the understanding of purity in CO_2 captured using oxy-combustion processes. It is now unlikely that SO_2 and NO_x would be co-captured with CO_2 for transport and storage at the levels previously suggested of 0.5 – 3%.

Natural Resources Canada, were commissioned by IEAGHG and GCCSI in 2009 to undertake a study, aiming to provide an overview of the effects of impurities on storage, with key issues and limiting factors highlighted. The study will also aim to identify the current state of knowledge and/or gaps and recommend further research priorities on these topics.

Scope of Work

This study provides a review of existing information and published research on the potential impact of CO_2 waste stream purity on storage engineering and associated costs. A range of

storage scenarios are considered including deep saline formations (DSF), depleted gas fields and CO_2-EOR schemes, although the study focuses primarily on DSF since this scenario has the largest theoretical storage capacity and the most significant potential for complex geochemical reactions.

Other geological storage scenarios, such as coal beds and basalts are not considered by this study.

Particular aspects considered include:

- The potential effects of impurities on phase behaviour and storage capacity calculations,
- Effects on the rates of geochemical reactions with both formation and caprock and associated buoyant forces and trapping mechanisms,
- Potential effects on injectivity, reservoir permeability and caprock integrity both near well-bore and deeper in the formation,
- Potential for corrosion of well components and estimated impact on system reliability if not mitigated.

The findings of the literature and research review, combined with use of engineering judgement, are used to identify key issues, uncertainties and knowledge gaps. The results of the study may contribute to development of risk assessment methodologies for CO_2 storage and relevant sections of 'best practice' manuals.

NRCan was asked to refer to the following recent or ongoing IEAGHG reports/studies relevant to this study, to avoid obvious duplication of effort and to ensure that the reports issued by the programme provide a reasonably coherent output:

- Development Issues for Saline Aquifer Storage, CO2CRC, Report 2008/12.
- Storage Capacity Coefficients, EERC, 2009/13.
- Safety in CO_2 Capture Transport and Storage, UK HSL Laboratory, 2009/06
- Well Abandonment Practices, TNO, final report due July 2009/08
- Impact of impurities on CO2 capture, transport and storage Ph4-32 Aug 2004
- Injection Strategies for Storage Sites, CO2CRC, 2010/04.
- Pressurisation and Brine Displacement issues for Deep Saline Formation CO_2 Storage, Permedia, 2010/15
- Potential Impacts on Groundwater Resources, CO_2GeoNet, project commenced March 2010

Findings of the Study

Data from the COORETEC study (Kather et al, 2009) was used to define expected impurities from each combustion process (Table 1)

Impurities from an oxyfuel combustion power plant could be subdivided into three classes namely: bulk or major non-CO_2 components which consisting of (numbers are usually greater

than 0.5%):- N_2, Ar, O_2, H_2O, and may be further classified as condensable and non-condensable components; minor impurities consisting of (numbers are usually in ppm level but less than 0.5%): SO_2, SO_3, NO, NO_2, N_2O (usually from oxy-CFB boiler), CO, and particulate matters; and micro-impurities which consists of the HCl, HF, Hg and other heavy metals.

For any oxyfuel combustion power plant with CO_2 capture, there are three possible scenarios with regard to the level of CO_2 purity namely:

- Scenario 01 – low purity option (CO_2 purity between 85% - 90%)
- Scenario 02 – medium purity option (CO_2 purity between 95% - 97%)
- Scenario 03 – high purity option (CO_2 purity greater than 99%).

Table 1 Composition of CO_2 Streams

Component	Pre-combustion		Post-combustion			Oxyfuel		
	Selexol	Rectisol	Comp.1	Comp.2	Comp.3	Comp.1	Comp.2	Comp.3
CO_2 (vol %)	97.95	99.7	99.93	99.92	99.81	85.0	98.0	99.94
O_2 (vol %)	-	-	0.015	0.015	0.03	4.70	0.67	0.01
N_2 (vol %)	0.9	0.21	0.045*	0.045*	0.09*	5.80	0.71	0.01
Ar (vol %)	0.03	0.15				4.47	0.59	0.01
H_2O (ppm)	600	10	100	100	600	100	100	100
NO_x (ppm)	-	-	20	20	20	100	100	100
SO_2 (ppm)	-	-	10†	10†	20†	50	50	50
SO_3 (ppm)	-	-				20	20	20
CO (ppm)	400	400	10	10	20	50	50	50
H_2S+COS (ppm)	100	100	-	-	-	-	-	-
H_2	1 vol%	20 ppm	-	-	-	-	-	-
CH_4 (ppm)	100	100	-	-	-	-	-	-
NH_3 (ppm)	-	-	-	50	-	-	-	-
CH_3OH (ppm)	-	200	-	-	-	-	-	-

*Total concentration of N_2 + Ar

†Total concentration of SO_2 + SO_3

Potential effects of impurities on geological storage of CO_2 can be divided into chemical and physical processes.

Physical Effects

Physical effects are those caused by the changes in physical properties with respect to pure CO_2, such as changes in phase and density. Density changes, mostly due to the presence of non-condensable impurities which cannot be liquefied at ambient temperature such as N_2, O_2 and Ar, can affect storage capacity, injectivity and buoyancy.

Phase Behaviour

To determine the phase behaviour of various mixtures of impurities compared to pure CO_2, the Peng-Robinson equation of state was used. The non-condensable impurities have the effect of increasing the bubble-point pressure and decreasing the critical temperature, due to their low critical temperatures. The stream with the greatest effect compared to pure CO_2 is the high impurity oxyfuel stream, as can be seen in figure 1. The horizontal line at 10MPa shows the minimum pressure needed to avoid two phase flow at all temperatures.

Figure 1 Calculated Phase diagram comparing pure CO_2 and Oxyfuel composition 1

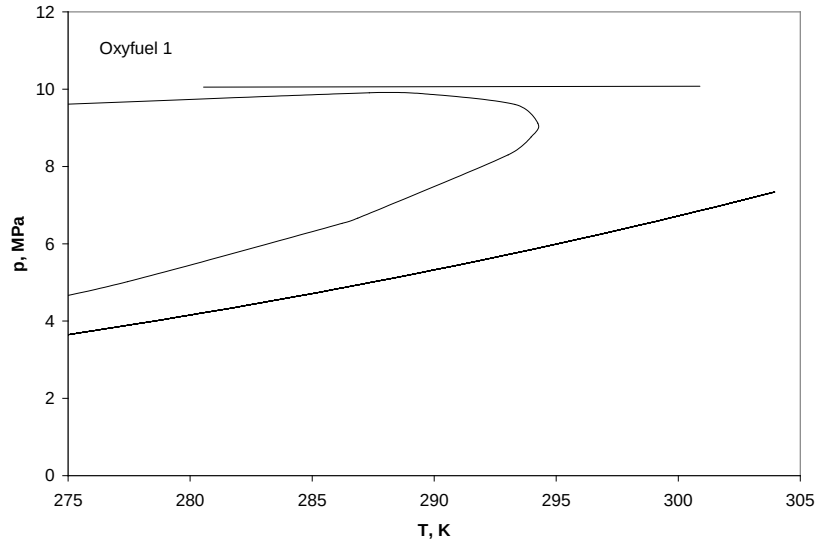

The impacts of changed phase behaviour on pipeline transport for transportation in the supercritical phase are that a higher pressure would be needed to avoid two phase flow. If transportation is in the liquid phase then the lower critical temperature would require a lower pipeline temperature, which could necessitate better insulation or cooling. Also note there are no experimental data using impure mixtures of CO_2 to calibrate parameter values for the equations of state.

Effects on Storage Capacity

Non-condensable impurities may potentially cause reduction of capacity firstly by replacement of CO_2, but also by reducing the density as they do not compress to as great a degree as CO_2. This study proposes that the storage capacity can be quantified by the following equation:

$$\frac{M}{M_0} = \frac{\bar{\rho}}{\rho_0 (1 + \sum_i m_i / m_{CO2})}$$

where M and M_0 denote the mass of CO_2 in the mixture and in the pure stream respectively, which occupy the same volume. $\bar{\rho}$ and ρ_0 are the density of the mixture and the pure stream, and m_i/m_{CO2} is the ratio of the mass of impurity i to the mass of CO_2 in the mixture. The ratio M/M_0 on the left hand side of this relation can also be viewed as the ratio of the mass of CO_2 per unit volume in the mixture to that in the pure state and represents a normalised storage capacity for CO_2 in its supercritical phase, *i.e.* the capacity for structural trapping of CO_2.

Therefore the high impurity streams can expect to reduce the storage capacity by a greater amount, though the degree to which the capacity differs compared to pure CO_2 is dependent on pressure and temperature. The effect of pressure at a constant temperature of 330K (58˚C) can be seen in Figure 2. The largest effect is when the high impurity oxyfuel stream is used. The results for this are similar to those of 15% Ar, i.e. when all light impurities are represented by Ar and calculations show that when assessing the physical effects Ar can be used to represent all light impurities.

Figure 2 Normalised capacity for various impurity streams

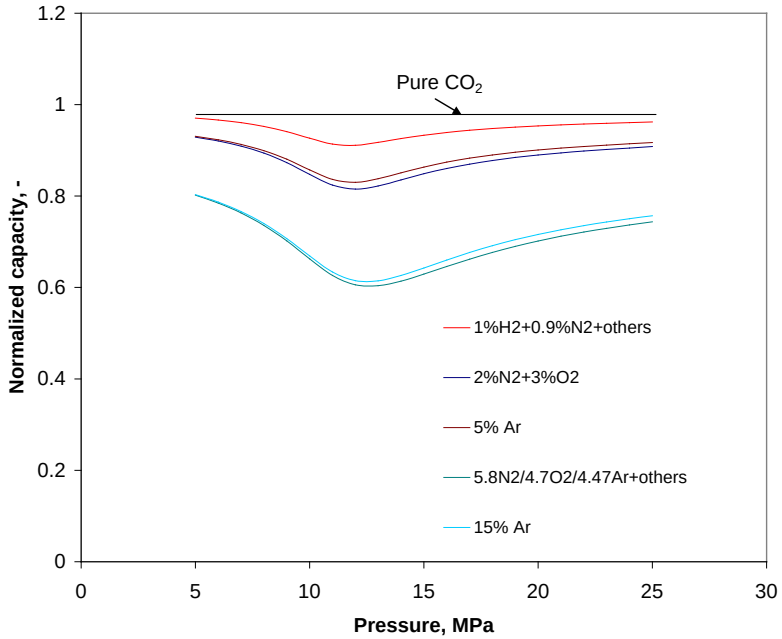

For all mixtures of supercritical CO_2 and non-condensable gases, there is a maximum decrease of the storage capacity at a certain pressure under a given temperature. An increasing temperature will shift this maximum decrease to a higher pressure and its magnitude decreases.

A range of storage conditions were considered to assess the potential impacts of a high impurity stream (15% non-condensables) on the storage capacity (Table 2). This range of

representative cases was taken from a previous IEAGHG study on establishing storage coefficients for DSF (2009/13).

The storage coefficient is defined as

$$E = \frac{G_{CO2}}{V_{CO2}\rho_{CO2}}$$

where G_{CO2} is the estimate of storage capacity in terms of CO_2 mass and V_{CO2} is the total pore space available for CO_2 storage. An impurity factor F is introduced for estimation of the storage capacity for impure CO_2:

$$G_{CO2} = V_{CO2}\rho_{CO2}EF$$

Numerically F is equal to the normalised storage capacity defined earlier.

Table 2 Effect of impurities on CO_2 storage capacity

Cases	Depth (m)	P (MPa)	T (°C)	T grad (°C/m)	Ea (-)	Storage Capacity		Fb (-)
						Pure	Impure	
Shallow-Low Temp	895	9.2	33	0.020	0.07	647.68	253.96	0.392
Shallow-Mid Temp	895	9.2	38	0.025	0.10	540.97	231.20	0.427
Shallow-High Temp	895	9.2	45	0.033	0.09	364.48	208.72	0.573
Median-Low Temp	2338	24	62	0.020	0.12	750.04	550.35	0.734
Median-Mid Temp	2338	24	75	0.025	0.13	675.00	493.67	0.731
Median-High Temp	2338	24	92	0.033	0.13	584.92	432.23	0.739
Deep-Low Temp	3802	38.8	92	0.020	0.15	777.66	611.13	0.786
Deep-Mid Temp	3802	38.8	113	0.025	0.16	700.29	551.25	0.787
Deep-High Temp	3802	38.8	141	0.033	0.17	611.35	485.19	0.794

[a] Storage coefficient.

[b] Capacity factor given as the ratio of the CO_2 storage capacity in the presence of impurities to that in the absence of impurities.

This shows the greatest effect from a high impurity stream of 15% non-condensables could potentially be a reduced capacity of around 40% at pressures and temperatures found in relatively shallow, low temperature CO_2 storage reservoirs. As the depth of the formations increase, the effect of impurities on CO_2 storage capacity decreases; at a depth of 3800 m, the capacity approaches 80% of that for pure CO_2.

Effects on Injectivity

The presence of these impurities have a potential effect on injectivity, as a decrease in density will decrease mass flux over the same pressure drop, however, the addition of impurities will also cause a decrease in viscosity, which would increase the mass flux. A normalised permeation flux can be demonstrated by the following equation:

$$\frac{\dot{M}_{CO2}}{\dot{M}_0} = \frac{\rho(\mu_0/\mu)}{\rho_0(1+\sum_i m_i/m_0)}$$

Where $\dot{M}_{CO2}$ and $\dot{M}$ are the mass flow per unit area for CO_2 in the mixture and in its pure state, ρ ρ_0 are the densities of the injected stream and that of pure CO_2 and μ and μ_0 are the viscosities of the injected fluid and that of pure CO_2.

Both viscosity and density will be determined by the temperature and pressure, though it should be noted that there is not experimental data to validate the viscosity calculations. With 15% impurities, the injectivity could be reduced by 15% at lower pressures (50-70 bar), but is likely to increase to the same as pure CO_2 as the pressure increases to around 20MPa. Table 3 shows, the effect of injectivity over the same range of scenarios used to examine storage capacity. It is clear the effect on injectivity is much less, though has the potential to be significant under certain circumstances

Table 3 Effect of impurities on CO_2 injectivity

Cases	Depth (m)	P (MPa)	T (°C)	T grad (°C/m)	Viscosity[a] (-)	Injectivity[b] (-)
Shallow-Low Temp	895	9.2	33	0.020	0.38	1.0
Shallow-Mid Temp	895	9.2	38	0.025	0.45	0.94
Shallow-High Temp	895	9.2	45	0.033	0.77	0.74
Median-Low Temp	2338	24	62	0.020	0.72	1.0
Median-Mid Temp	2338	24	75	0.025	0.75	0.98
Median-High Temp	2338	24	92	0.033	0.79	0.93
Deep-Low Temp	3802	38.8	92	0.020	0.81	0.97
Deep-Mid Temp	3802	38.8	113	0.025	0.83	0.95
Deep-High Temp	3802	38.8	141	0.033	0.87	0.91

[a] Relative viscosity given as the ratio of the viscosity in the presence of impurities to that in the absence of impurities.

[b] Relative injectivity given as the ratio of the injectivity in the presence of impurities to that in the absence of impurities.

Effects on Buoyancy

Decreased density is also likely to cause an increase in buoyancy of the plume. If changes in relative permeability and capillary pressure are neglected, normalised buoyancy can be given as:

$$\frac{F}{F_0} = \frac{\rho_{H2O} - \rho_m}{\rho_{H2O} - \rho_{CO2}}$$

where F and F_0 are buoyancy forces for the CO_2 mixture and pure CO_2 respectively, ρ_{H20}, ρ_m, *and* ρ_{CO2} are the densities of the formation water, plume and pure CO_2 respectively.

The greater density difference, the greater buoyancy and consequently rising velocity, which can be given as:

$$\frac{v}{v_0} = \frac{F/(\rho\mu)}{F_0/(\rho_0\mu_0)}$$

For the case of 15% light impurities, buoyancy can be increased by up to 50%, depending on the temperature and pressure, which could in turn increase the rising velocity of an injected CO_2 plume in the reservoir by up to three times. This would have the potential to reduce residual trapping and increase lateral spreading of the plume at the caprock, though this is subject to reservoir heterogeneity as this effect might be more pronounced in relatively uniform formations.

Chemical Effects

When looking at the chemical effects on rocks and wellbore cements, the most significant species are SO_x, NO_x and H_2S.

Effects on capacity and injectivity

NO_x catalyses the oxidation of SO_2 to form sulphuric acid, which lowers the pH and may then cause mineral dissolution and precipitation of sulphates. With fast dissolving and precipitating species, such as calcite and calcium sulphate, porosity can be affected and a decrease in porosity could potentially affect the capacity and injectivity. The rate of precipitation of $CaSO_4$ is quantified based on the concentration of calcium and sulphate ions, though also to be taken into account is the dry-out zone. Previous simulations have assumed that SO_2 is injected as an aqueous solution or that the injection zone is wet. When supercritical CO_2 is injected into the formation it displaces in-situ waters creating a dry-out zone and any dissolution and precipitation is assumed to take place at the front of the plume and a two phase flow region, but ceases once the dry-out front arrives. This decreases the impact on rock porosity and injectivity that could otherwise take place.

Simulations were carried out in the study for calcite dissolution and calcium sulphate precipitation and for an injection stream with 2.9% SO_2; the maximum porosity decrease would be 0.44%, which is much less significant then when compared to the wet case.

Simulations were carried out for other minerals all with porosity decreases much lower than the equivalent wet cases, however, for alunite, the associated volume changes is 5.6%, which could be considered significant.

Injection of H_2S has taken place during acid gas injection projects for many years with no serious effects, but there could be issues if it is injected in conjunction with SO_2, which could result in deposition of elemental sulphur causing severe pore blocking. This could be an issue if streams from pre-combustion and post-combustion sources were to be injected at the same storage site.

Effects on Caprocks

Potential chemical effects on caprock integrity over the long term are dissolution of both carbonate and aluminosilicate rocks, due to the presence of SO_x and NO_x which can form sulphuric and nitric acid. Thermochemical evaluations show that for 1.5% concentration of SO_x and NO_x, dissolution can increase by 50%, however, for CO_2 streams considered in this study SO_x and NO_x concentrations are within 200 ppm, for which the impact on the dissolution of the rocks is likely to be insignificant.

The effect of O_2 is mainly related to oxidation of SO_x and NO_x, but can react with certain minerals on its own, for example it can react with pyrite to form iron sulphate which is soluble, resulting in acidic pockets which can cause dissolution of the rock. To have a significant effect this would require a relatively large amount of O_2 which has not been consumed by oxidation of metallic minerals and/ or retained in the residual CO_2 phase, which is likely due to its low solubility.

Effect on Well Materials

Well materials may be affected after injection is terminated as there would be a return of water containing acidic impurities. Results of thermochemical calculations suggest that the effect of acid impurities on dissolution of cement constituents may be more significant than on dissolution of rocks. If protection from the cement sheaths is lost, the steel casings could also be attacked. Appropriate measures may be required for countering adverse effects, such as improving cement and casing quality prior to sealing wells.

Expert Review Comments

Expert comments were received from 10 reviewers, representing industry (corporate sponsors of IEAGHG) and academia. The feedback was constructive and supportive of the work that had been carried out. There was comment that the paper adds importantly to the literature in presenting the issue of physical impacts of impurities on capacity.

Key technical suggestions made by reviewers included reviewing the effects impurities on interfacial tension and capillary pressures and the potential impact on caprocks of the water dissolution in supercritical CO_2. These comments were addressed in the final report.

There were comments that current procedures for monitoring which include analyses of He, H and in others Ar is measured (e.g. Otway and Frio), were not referenced, but this topic will be covered fully in another IEAGHG Study – Feasibility of Monitoring techniques for substances mobilised by CO_2. There was also a comment that there could be further work carried out analysing reaction rates and kinetics.

Conclusions

In the studied scenarios of impure CO_2 streams where O_2, N_2 and Ar have the highest levels, the greatest impact of impurities is physical, i.e., reducing storage efficiency and injectivity.

The most significant effect is the reduction of storage capacity. It has been shown that the non-condensable impurities cause reduction of CO_2 capacity by a degree greater than their molar fractions when the temperature is not high above the critical temperature of CO_2. Particularly, there is a maximum reduction of the storage capacity in a certain pressure range, where the capacity can drop to below 40 % for the 15% light impurities case compared with that of pure CO_2. The injectivity of impure CO_2 streams reduces as a result of lower density. However, due to the compensation by increased viscosity the reduction of injectivity is smaller than that of storage capacity. In the studied scenarios using the 15% light impurities case, the average reduction of injectivity is 6%, with the largest reduction 26%. The higher buoyancy of impure CO_2 streams will reduce the efficiency of CO_2 dissolution in formation water and CO_2 trapping in rock pores, and thus has the potential reduce the security of CO_2 storage in the near to medium terms.

With regard to chemical effects on rocks, the most significant species are SO_x, NO_x and H_2S. NO_x can catalyze the oxidation of SO_2 to sulphuric acid. The impact of SO_2 on reduction of rock porosity and injectivity appears much smaller than previously thought, because its contact with water is limited with the development of the dry-out zone. NO_x will also promote dissolution of minerals, but will not cause precipitation and therefore reduction of rock porosity. H_2S on its own has not been found to reduce the injectivity in acid gas injection operations and computer simulations. However, if H_2S and SO_2 are co-injected, deposition of elemental sulphur, in the pores over the whole injection period can be a serious concern.

For evaluation of chemical effects on caprock integrity, thermochemical calculations show that SO_x and NO_x increase dissolution of carbonate rocks and aluminosilicate rocks. However, for CO_2 streams considered in this study where SO_x and NO_x concentrations are within 200 ppm, the impact on the dissolution of the rocks is insignificant.

Corrosion of injection well materials may not be serious when the CO_2 stream is dry, due to desiccation of the well zone in the injection period. However, after termination of injection and return of water, corrosion by the acidic impurities could be an issue of concern.

The results of the study have implications on site selection for different CO_2 streams, i.e. a relatively shallow storage site may be appropriate for a low impurity stream, whereas a high impurity stream may reduce the storage capacity by a significant amount. There are also

implications for designing pipeline systems, for multiple CO_2 streams and mixing of the streams.

Recommendations

The literature on the effects of impurities on the geological storage of CO_2 is currently limited and the some of the theoretical effects examined in the study cannot yet be verified by experimental data. It is important that IEAGHG keeps updated on further experimental work which would be able to verify the effects.

The outcome of this study may have implications on site selection for different impure streams of CO_2 and injection of different streams into the same storage site.

IEAGHG should ensure that adequate attention is paid to these topics through future storage network meetings and by the study programme.

SUPPORTED BY

GLOBAL CCS INSTITUTE

Effects of Impurities on Geological Storage of Carbon Dioxide

Jinsheng Wang, David Ryan, Edward J. Anthony, Andrew Wigston

Final version

April 2011

CanmetENERGY, Natural Resources Canada
1 Haanel Drive,
Ottawa, Ontario, Canada
K1A 1M1

Prepared for the IEA Greenhouse Gas R&D Programme
The Orchard Business Centre
Stoke Orchard, Cheltenham
Gloucestershire, United Kingdom

under Contract IEA/CON/09/172

Executive Summary

Carbon capture and storage (CCS) is one of the major transformative technologies identified worldwide for reducing atmospheric CO_2 emissions and this technology is particularly applicable where large CO_2 emitters are located and a large potential for CO_2 storage exists. Since CO_2 originates from a variety of sources, such as coal-fired power plants, refineries, bitumen upgraders, gas plants, steel and cement plants, the CO_2 stream contains various impurities, such as N_2, O_2, Ar, SO_x, NO_x, H_2S, H_2, *etc*., in various concentrations. A requirement on purity of the effluent CO_2 stream will greatly increase the cost of capture, and may eliminate from choice some of the more cost-effective capture processes that are not capable of achieving high purity. However, impurities in the injected CO_2 may affect the efficiency and safety of CO_2 storage in underground formations in various ways, such as decreasing storage capacity and CO_2 injectivity, and reducing storage integrity through chemical reactions.

Natural Resources Canada (NRCan) has been leading Canada's federal CCS programs. Along with a range of R&D projects for capturing CO_2 from coal-fired power plants and other sources, NRCan has also conducted studies on the injection of CO_2 in underground reservoirs, data and information acquisition, geological, geophysical and geochemical assessments, and reservoir model simulations. The effects of impurities on transport, injection and storage of captured CO_2 are of vital importance to successful implementation of Canada's CCS research strategies for now and in the future.

In this context we have undertaken a study on evaluation of the effects of impurities on CO_2 transport, injection and storage, sponsored by the International Energy Agency Greenhouse Gas R&D Programme (IEA GHG). The IEA GHG's objectives of this study are:

- To provide a review of existing information and published research on the potential impact of CO_2 stream purity on storage reservoir and caprock performance and associated engineering costs;

- To provide a high level overview of available knowledge. The focus is on storage of impure CO_2 in deep saline formations, since this scenario has the largest theoretical storage capacity and the most significant potential for complex geochemical reactions, although depleted gas fields and CO_2-EOR are also relevant.

Particular aspects to be considered include:

- The potential effects of impurities on phase behaviour and storage capacity calculations;
- Effects on the rates of geochemical reactions with both formation and caprocks, and the impacts on injectivity, reservoir permeability and caprock integrity.

- Effects on buoyancy forces and trapping mechanisms;
- Potential for corrosion of well components and estimated impact on system reliability if not mitigated.

The literature related to the effects of impurities is scarce, and mainly concerns transport of impure CO_2 by pipeline. The rest of the literature reports limited simulation work on co-injection of H_2S and SO_2 with CO_2, where the important desiccation effect near the injection zone is not taken into account, and the coexistence of NO_x, which could significantly affect the behaviour of SO_2, has not been considered. Accordingly, for the major part of the above issues there is little or no information available. Combined with NRCan's own research efforts on CO_2 capture and storage in Canada, we have carried out extensive investigations by ourselves. Through our work, all aspects specified by IEA GHG have been addressed. Significant achievements and findings are:

1. The measure of storage capacity for impure CO_2 and the impact of the impurities have been established. With a simple formula proposed in this work, normalized CO_2 storage capacity can be calculated for any CO_2 mixtures, and the impact of the impurities can be clearly seen.
2. Non-condensable impurities which cannot be liquefied at ambient temperature, such as N_2, O_2 and Ar, result in significant decrease in CO_2 storage capacity. The degree of decrease in the capacity is a function of pressure, temperature, and composition.
3. For all mixtures of supercritical CO_2 and non-condensable gases, there is a maximum decrease of the storage capacity at given temperature. This pressure corresponding to the maximum decrease changes with temperature.
4. In contrast to non-condensable gases, impurities which are more easily condensable than CO_2, such as SO_2, could increase the storage capacity, and there is a maximum increase at a certain pressure.
5. For a supercritical CO_2 stream with high levels of N_2, O_2 and Ar, which are common impurities from oxyfuel combustion, the volume and density may be determined by the use of Ar to represent all impurities, computationally and/or experimentally.
6. The change of density caused by non-condensable gas impurities results in lower injectivity of impure CO_2 into geological formations. Above a threshold pressure range the injectivity could reach the level of pure CO_2 due to lowered viscosity. However, more condensable impurities like SO_2 may have an effect of increasing the injectivity, through increasing density of the CO_2 stream.
7. Non-condensable gas impurities increase the buoyancy of the CO_2 plume. This would decrease the sweep efficiency of injected CO_2. As a result, the efficiency of solubility trapping and residual trapping of CO_2 would decrease.
8. A formula has been developed to enable quick determination of the effect of SO_x on CO_2 injectivity through precipitation of sulphates, which reduces rock porosity, an issue of substantial concern. With this formula, the degree of the porosity reduction could be directly predicted from the SO_x content of the injected CO_2.

9. Among reactive impurity species, SO_x, H_2S and NO_x would have the greatest chemical effects on the rocks. Based on our analysis, the effect of SO_x on reduction of rock porosity and injectivity would be much smaller than commonly thought. However, if H_2S and SO_x are co-injected, such as in the case where CO_2 streams from pre-combustion capture and oxyfuel combustion are merged, deposition of elemental sulphur in the pore space could be a concern for pore plugging and hence injectivity reduction.
10. The potential of corrosion of injection well materials has been assessed. The corrosion would be lower if the CO_2 stream is dry, due to desiccation of the well zone during the injection period. However, after termination of injection the acidic impurities would promote the corrosion of cements in the presence of water. CO_2 containing SO_x, NO_x and O_2 impurities would be more corrosive to cements and steels than pure CO_2 or CO_2/H_2S mixtures.

In addition to the above, phase envelopes for various impure CO_2 streams have been calculated, and issues related to calculations analyzed. The impacts of the impurities on pipelines and injection wells, due to changed critical temperature and liquefaction pressure, are discussed.

Moreover, the fate of hazardous impurities in the subsurface has been assessed. The impurities of major concern, including CO, SO_x, H_2S, NO_x and Hg, would eventually form dissolved and/or precipitated species. In the event of CO_2 leakage, these dissolved hazardous impurities may be released. The harmfulness of these impurities, however, will likely be overshadowed by that of the leaked CO_2, which is hazardous by itself at high concentrations, if breathed in for prolonged periods.

It should be emphasized that the existing literature does not currently provide solutions to the problems that will be inevitably encountered in CO_2 storage operations. None of the above issues have been addressed in the previous IEA GHG report (PH4/32) on impurity effects, and most of them have not been investigated elsewhere either. The results obtained from the present work are expected to have important applications or implications to all CO_2 storage operations, as illustrated in discussions for selected scenarios.

Contents

Figures

Tables

1. Background

Carbon capture and storage (CCS) has been identified as a key potential technology in reducing CO_2 emissions. The capture process represents the major cost component of CCS. CO_2 may be captured by different technologies from various sources, and various gaseous impurities exist in the CO_2 stream, such as N_2, O_2, SO_x and H_2S. Separation of these impurities would drastically increase the cost of capture and it would be more cost effective to co-inject these impurities with CO_2 for underground storage. Moreover, some technologies aim at co-capture and co-sequestration of multiple air pollutants together with CO_2. For such technologies the feasibility of co-sequestration is a prerequisite.

However, there are concerns over negative effects of impurities in CO_2 streams on the transport, injection and storage of CO_2. For instance, non-condensable impurities such as N_2 and O_2 would increase the saturation pressure of liquid CO_2 and decrease the critical temperature. As a result, lower temperature and additional overpressure is required to avoid two-phase flow in pipeline transport of CO_2. Non-condensable impurities would also increase the pressure for injection and reduce the capacity of the storage sites by decreasing not only volume fraction but also density of CO_2. Moreover, impurities like SO_x and NO_x will form acids in the presence of water, which may react with caprocks and well components and affect the storage integrity. The fate of hazardous impurities, in particular CO, H_2S, SO_x and Hg, in the subsurface is of special concern, as the impurities may escape the confinement in the event of CO_2 leakage.

Natural Resources Canada (NRCan) has been leading Canada's federal CCS programs. Along with a range of R&D projects for capturing CO_2 from coal-fired power plants and other sources, NRCan is also involved in and collaborating in research endeavours for CO_2 storage, including CO_2 injection, monitoring, measurement and verification, storage integrity assessment, and capacity estimation. The effects of impurities on transport, injection and storage of captured CO_2 are of vital importance to successful implementation of the CCS programs.

In this context NRCan has undertaken the study on evaluation of the effects of impurities on CO_2 storage, sponsored by the International Energy Agency Greenhouse Gas R&D Programme (IEA GHG).

1.1 Scope of the Current Study

IEA GHG has sponsored investigations of impurities in CO_2 streams. A previous report was issued in 2004 (PH/4-32), where the impacts on storage in saline aquifers were not a focus. The scope of the current study specified by IEA GHG is as follows:

"Review of existing information and published research on the potential impact of CO_2 waste stream purity on storage engineering and associated costs; aiming to provide a 'high level' overview of available knowledge. A range of storage scenarios may be considered including deep saline formations, depleted gas fields and CO_2-EOR schemes,

although the study should focus primarily on deep saline storage as this scenario has the largest theoretical storage capacity. Consideration of other geological storage scenarios, such as coal beds and basalts, is not required by this study.

Particular aspects that should be considered include:

- The potential effects of impurities on phase behaviour and storage capacity calculations
- Effects on the rates of geochemical reactions with both formation and caprock and associated buoyancy forces and trapping mechanisms
- Potential effects on injectivity, reservoir permeability and caprock integrity both near the well-bore and deeper in the formation
- Potential for corrosion of well components and estimated impact on system reliability if not mitigated

The findings of the literature and research review, combined with use of engineering judgment should identify key issues, uncertainties and knowledge gaps. The results of the study should be able to contribute to development of risk assessment methodologies for CO_2 storage and relevant sections of 'best practice' manuals."

In this study the data on impurity species and their concentration levels have been provided by IEA GHG, based on CO_2 quality recommended for evaluation under the COORETEC study for fossil-fueled power plants (Kather, 2009), as shown in Table 1.1. It should be noted that the effects of impurities studied in this work are also expected to be applicable to other CCS scenarios, such as those for oil refineries, iron and steel making, and cement production. Whereas the composition spectra may vary, the types of impurities in the other scenarios would be largely the same, as long as the CO_2 is from burning fossil fuels.

A number of relevant physical properties of the major impurities are given in Appendix A. From Table 1.1 it can be seen that the impurities vary with the sources of CO_2 streams. Reductive impurities H_2, H_2S and CH_4 are present in pre-combustion streams. Oxide impurities, including nitrogen oxides (NO_x) and sulphur oxides (SO_x), are present in oxyfuel and post-combustion streams. Hg is not shown in the table but is expected to be present in trace amounts in pre-combustion and post-combustion streams. Air-derived impurities N_2, O_2 and Ar exist in high levels in oxyfuel combustion streams, which have the highest total impurity levels among the three types of CO_2 streams. IEA GHG has considered three scenarios for CO_2 purity from oxyfuel combustion streams:

- Scenario 1 – low-purity (CO_2 purity between 85 - 90%)
- Scenario 2 – medium-purity (CO_2 purity between 95 - 97%)
- Scenario 3 – high-purity (CO_2 purity greater than 99%)

where N_2, O_2 and Ar comprise the major part of the impurities. Clearly, increasing impurity concentrations will have more significant effects on storage, thus the oxyfuel

streams are most important for the current study because of their high impurity concentrations.

Table 1.1 Compositions of CO_2 streams

Component	Pre-combustion		Post-combustion			Oxyfuel		
	Selexol	Rectisol	Comp.1	Comp.2	Comp.3	Comp.1	Comp.2	Comp.3
CO_2 (vol %)	97.95	99.7	99.93	99.92	99.81	85.0	98.0	99.94
O_2 (vol %)	-	-	0.015	0.015	0.03	4.70	0.67	0.01
N_2 (vol %)	0.9	0.21	0.045*	0.045*	0.09*	5.80	0.71	0.01
Ar (vol %)	0.03	0.15				4.47	0.59	0.01
H_2O (ppmv)	600	10	100	100	600	100	100	100
NO_x (ppmv)	-	-	20	20	20	100	100	100
SO_2 (ppmv)	-	-	10†	10†	20†	50	50	50
SO_3 (ppmv)	-	-				20	20	20
CO (ppmv)	400	400	10	10	20	50	50	50
H_2S+COS(ppmv)	100	100	-	-	-	-	-	-
H_2	1 vol%	20 ppm	-	-	-	-	-	-
CH_4 (ppmv)	100	100	-	-	-	-	-	-
NH_3 (ppmv)	-	-	-	50	-	-	-	-
CH_3OH (ppmv)	-	200	-	-	-	-	-	-

*Total concentration of N_2 + Ar
†Total concentration of SO_2 + SO_3

1.2 Previous and Ongoing Studies

Previous studies on the impurities are mostly related to pipeline transport. Seevam *et al.* (2007) discussed potential impacts of impurities on pipeline transport, focusing on recompression distance, flow assurance, and phase equilibrium. Oosterkamp and Ramsen (2008) gave an overview for offshore pipelines and summarized a number of uncertainties related to impurities, regarding corrosion, degrading of non-steel materials, lack of measurement data, water solubility, modeling, chemical reactions between impurities, and allowable impurity levels for pipeline transport. With respect to the allowable impurity levels, there have been recommendations by the European project DYNAMIS on CO_2 quality for transporting of CO_2 streams from pre-combustion and post-combustion processes (de Visser *et al.* 2008; 2009), as summarized in Table 1.2. In this table the considerations for setting the concentration limits are also given, which are based on both technical and safety perspectives from the transport point of view. By comparison with Table 1.1 it can be seen that the impurity levels considered by IEA GHG are within or lower than the limits recommended by DYNAMIS, except for the levels of O_2, N_2 and Ar from oxyfuel combustion. High levels of O_2, N_2 and Ar will result in higher energy consumption for compressing CO_2 for pipeline transport. However, in most cases the injection pressure will be higher than the liquefaction pressure of impure

CO_2, and thus the energy related to the additional compression work is not lost. This will be seen in the discussion of typical reservoir conditions.

Table 1.2. DYNAMIS recommendation for CO_2 quality (de Visser *et al.* 2009)

Component	Concentration	Limitation
H_2O	500 ppm	Technical: below solubility limit of H_2O in CO_2. No significant cross effect of H_2O and H_2S. Cross effect of H_2O and CH_4 is significant but within limits for water solubility.
H_2S	200 ppm	Health & safety considerations
CO	2000 ppm	Health & safety considerations
O_2*	Aquifer < 4 vol%, EOR 100 – 1000 ppm	Technical: range for EOR, because of lack of practical experiments on effects of O_2 underground.
CH_4*	Aquifer < 4 vol%, EOR < 2 vol %	Energy consumption for compression and miscibility pressure for EOR
N_2*	< 4 vol % (all non-condensable gases)	Energy consumption for compression
Ar*	< 4 vol % (all non-condensable gases)	Energy consumption for compression
H_2*	< 4 vol % (all non-condensable gases)	Further reduction of H_2 is recommended because of its energy content
SO_x	100 ppm	Health & safety considerations
NO_x	100 ppm	Health & safety considerations
CO_2	>95.5%	Balanced with other compounds in CO_2

* The concentration limit of all non-condensable gases taken together, including O_2, CH_4, N_2, Ar and H_2, should not exceed 4 vol %.

With regard to the subsurface side, acid gas injection, where H_2S is injected together with CO_2, has been successfully carried out for years (see, *e.g.*, Bachu and Gunter, 2004; Bachu, 2008), and substantial knowledge has been acquired. However, H_2S is less reactive than SO_x and NO_x under the considered conditions, because of its lower acidity

and low concentration level. Besides, H_2S is not present in CO_2 streams from oxyfuel combustion, which are most relevant to the present study. Brine acidification by SO_2 in injected CO_2 has been predicted based on model brine composition (Ellis *et al.*, 2010), where 1% SO_2 is predicted to decrease the pH of the brine from 4.6 in the case of CO_2 alone to 1 – 2.5, depending on reaction and rate-limiting mechanism. However, the effect of mineral buffering is not included for the prediction. Palandri and Kharaka (2005) presented simulation results for the effect of H_2S and SO_2 on CO_2 sequestration as siderite $FeCO_3$(siderite), through reducing ferric iron in sediments. The conclusion is that, with an excess of sulphur relative to CO_2, the iron can be transformed almost entirely into siderite thereby trapping CO_2 whereas the sulphur is converted predominantly into H_2SO_4. The applicability of this study, however, depends on the ferric iron content in the formations. Studies on the effect of H_2S and SO_2 on CO_2 injectivity have been performed by Knauss *et al.*(2005), Xu *et al.* (2007), and Bacon *et al.* (2009), which do not include the impact of desiccation due to injection of dry CO_2, and thus are not considered applicable to the scenarios of the present study, as will be discussed later.

Bachu and coworkers (2009 a, b) investigated chromatographic partitioning of impurities under CO_2 injection conditions. The results are interesting and have potential applications in monitoring of injected CO_2. This will also be discussed later.

de Visser *et al.* (2009) pointed out that the presence of impurities in the CO_2 lowers the density of the CO_2 stream, and thus decreases the amount of CO_2 stored per unit volume of storage space. As a consequence, the storage efficiency decreases. However, the effect of impurities on the reduction of storage space is not precisely known yet. Such comments arising from the large European program (DYNAMIS) provide evidence of the knowledge status in this field – no quantitative methods for the assessment have been developed yet.

Sass et al.(2009) discussed a number of issues concerning storage of flue gas from oxyfuel combustion, where CO_2 content is below 80%, including reduction of storage capacity and permeability by non-condensable gases, increase of injection pressure, reduction of injection lifetime due to precipitation of solids such as calcium sulphate, etc. However, no qualitative results are presented.

White and Johnson (2009) disclosed that, during the final phase (2007-2011) of the IEAGHG Weyburn-Midale CO_2 monitoring and storage project, the consequences of injecting impure CO_2 (with H_2S and SO_2 contaminants on reservoir and seal integrity at Weyburn (Saskatchewan, Canada) will be assessed experimentally using reservoir and caprock samples. Computer simulations will also be performed using lab-scale reactive transport modeling. It should be noted that in this project CO_2 is also used for enhanced oil recovery, and the composition is dictated by a Rectisol purification system. The concentration level of non-condensable gases and SO_x/NO_x in such a CO_2 stream is low and not comparable to that of oxyfuel CO_2 streams.

Overall the literature concerning the impurity effects is scarce. For the majority of the questions raised by IEA GHG, very limited data and information are available. The

knowledge gaps are substantial and comprehensive investigations are required to fill the gaps.

Combining with NRCan's own research programs on CCS, we have carried out extensive assessments for the effects of the impurities on CO_2 injection and storage. We will discuss the findings for each specified issue, respectively. For the discussions we divide the effects into two types: physical effects and chemical effects, *i.e.* those that do not involve chemical reactions and those that do. Evaluations of selected scenarios concerning both types of effects will also be presented.

2. Physical Effects of the Impurities

2.1. Phase Behaviour and the Impacts

Changes in phase behaviour of CO_2 due to the presence of impurities may be evaluated by equations of state. Cubic equations of state are often used to calculate phase diagrams of fluids owing to their relative simplicity. A very commonly used cubic equation of state is the Peng-Robinson equation (Peng and Robinson, 1976):

$$p = \frac{RT}{V_m - b} - \frac{a\alpha}{V_m^2 + 2bV_m - b^2} \qquad (2.1)$$

where p is pressure, T is temperature, V_m is the molar volume, and R is the universal gas constant. The parameters a, b and α are related to the critical temperature T_c, the critical pressure p_c, and the acentric factor ω in the following way:

$$a = \frac{0.45724 R^2 T_c^2}{p_c}$$

$$b = \frac{0.07780 R T_c}{p_c}$$

$$\alpha = (1 + (0.37464 + 1.54226\omega - 0.26992\omega^2)(1 - T_r^{0.5}))^2$$

$$T_r = \frac{T}{T_c}$$

This equation has also been used to calculate properties of supercritical CO_2 (see, *e.g.*, Clifford, 2007). Another commonly used equation of state is the Soave-Redlich-Kwong equation (Soave, 1972):

$$p = \frac{RT}{V_m - b} - \frac{a\alpha}{V_m(V_m + b)} \qquad (2.2)$$

where

$$a = \frac{0.42747 R^2 T_c^2}{p_c}$$

$$b = \frac{0.08664 R T_c}{p_c}$$

$$\alpha = (1 + (0.48508 + 1.55171\omega - 0.17613\omega^2)(1 - T_r^{0.5}))^2$$

$$T_r = \frac{T}{T_c}$$

In the present work the Peng-Robinson equation has been used for most calculations, because of its relatively simple form, whereas the Soave-Redlich-Kwong equation has been used redundantly in limited cases to verify calculated trends. For mixtures the following mixing rules are applied to the parameters:

$$a = \sum_i \sum_j x_i x_j (a_i \alpha_i)^{1/2} (a_j \alpha_j)^{1/2} (1 - k_{ij}) \qquad (2.3)$$

$$b = \sum_i x_i b_i \qquad (2.4)$$

where x_i and x_j denote mole fractions of mixture components; k_{ij} is the binary interaction constant for components *i* and *j*, whose values can be determined from fitting the equations to experimental pressure-volume-temperature (PVT) data. The k_{ij} values for CO_2 with each individual impurity component can be found in the literature. For instance, Li and Yan (2009 a, b) have reported k_{ij} values for cubic equations of state, including the Peng-Robinson and Soave-Redlich-Kwong equations, for mixtures of CO_2 with CH_4, H_2S, SO_2, Ar, N_2 and O_2, respectively. Not all k_{ij} values are available, especially k_{ij} values for impurity pairs. However, the contribution of k_{ij} is negligible to the calculated properties of CO_2 streams when the impurity fractions are low. This can be seen from the mixing rule (Equation 2.3): when the fraction x_i or x_j is small the resultant term will be small. Particularly, the product of x_i and x_j will be negligible for any impurity pair compared with the products for CO_2 and high-concentration impurities. The k_{ij} values used in our calculations are given in Appendix B. For component pairs where the k_{ij} values are not available, zero values (corresponding to ideal mixing) have been assumed.

Figure 2.1 shows representative phase diagrams calculated with the Peng-Robinson equation for CO_2 mixtures with compositions given in Table 1.1, in comparison with the saturated vapour-pressure curve of pure CO_2.

Figure 2.1. Calculated phase diagrams for CO_2 streams compositions given in Table 1.1., including: a) Selexol (pre-combustion) case; b) Rectisol (pre-combustion) case; c) Post-combustion case 1 (99.93 vol% CO_2); d) Post-combustion case 2 (99.81 vol% CO_2); e) Oxyfuel case 1 (85% CO_2); f) Oxyfuel case 2 (98% CO_2); g) Oxyfuel case 3 (99.94 vol% CO_2). For each case the dash line represents the vapour-liquid saturation curve of pure CO_2, and the solid horizontal line represents the pressure level required to avoid two-phase conditions.

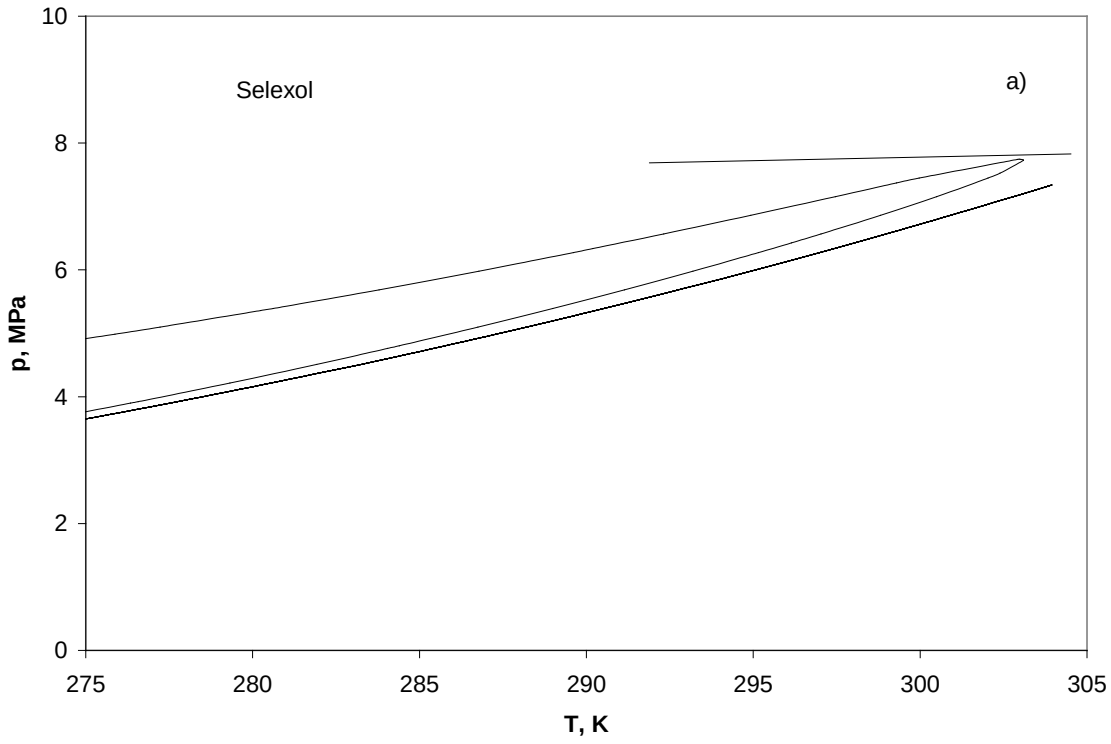

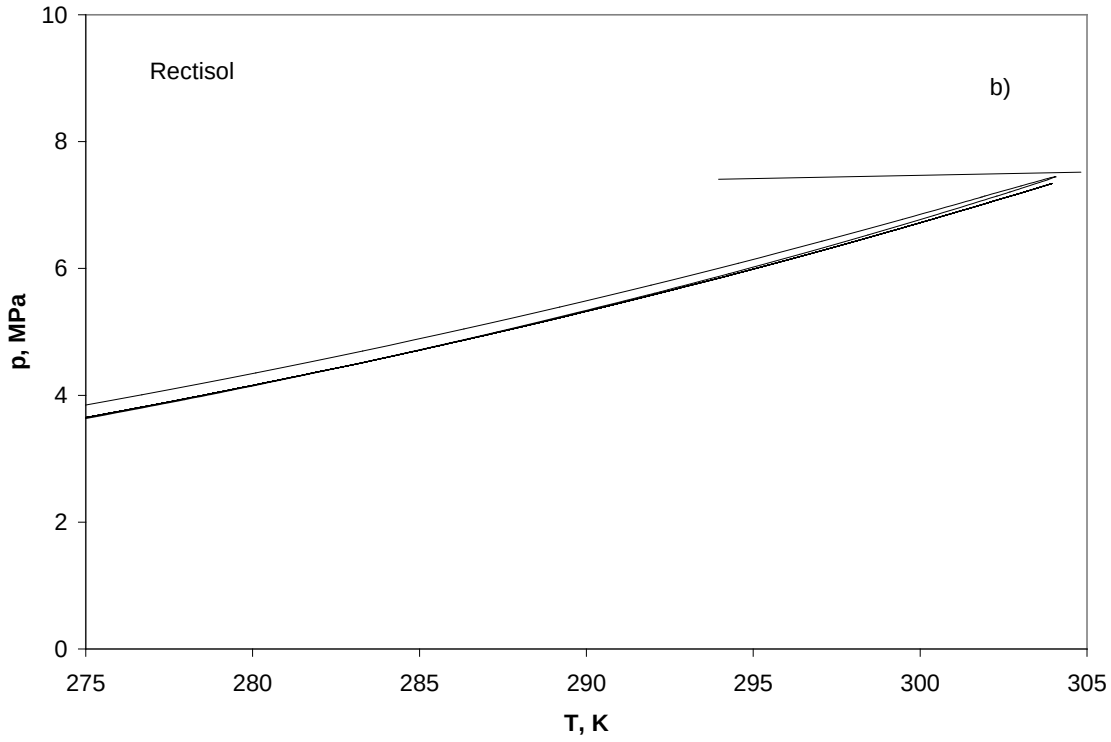
Rectisol
b)
p, MPa
T, K
0
2
4
6
8
10
275
280
285
290
295
300
305

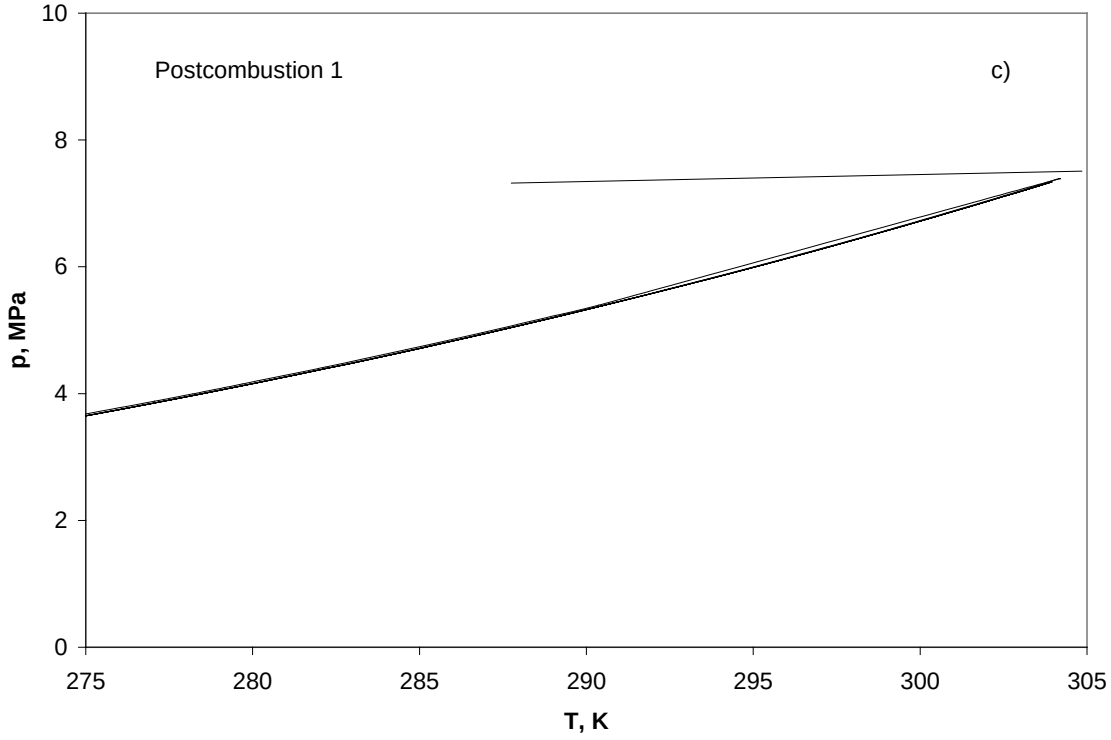
Postcombustion 1
c)
p, MPa
T, K
0
2
4
6
8
10
275
280
285
290
295
300
305

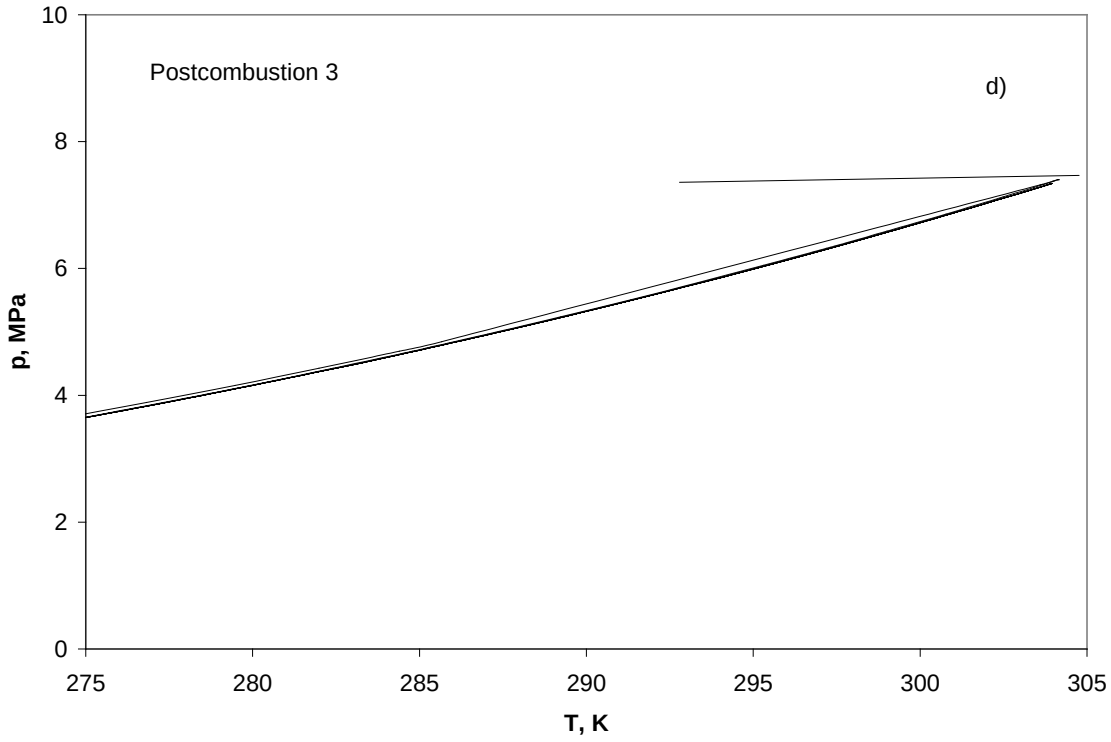
Postcombustion 3
d)
p, MPa
T, K
0
2
4
6
8
10
275
280
285
290
295
300
305

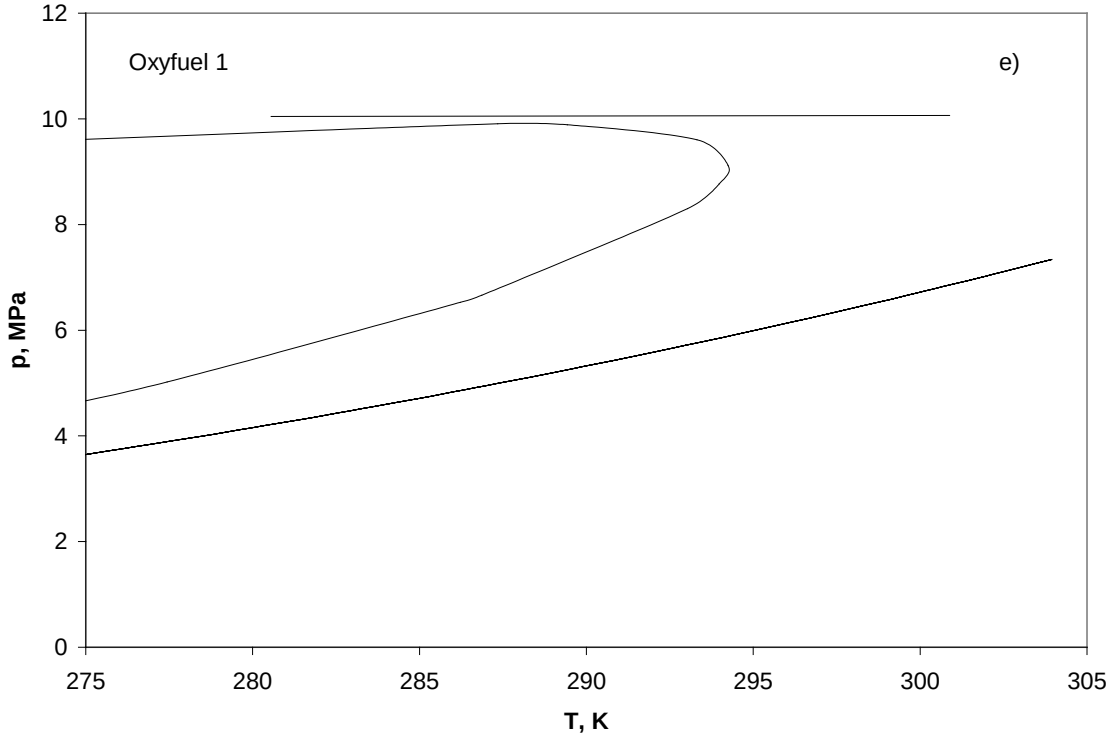
Oxyfuel 1
e)
p, MPa
T, K
0
2
4
6
8
10
12
275
280
285
290
295
300
305

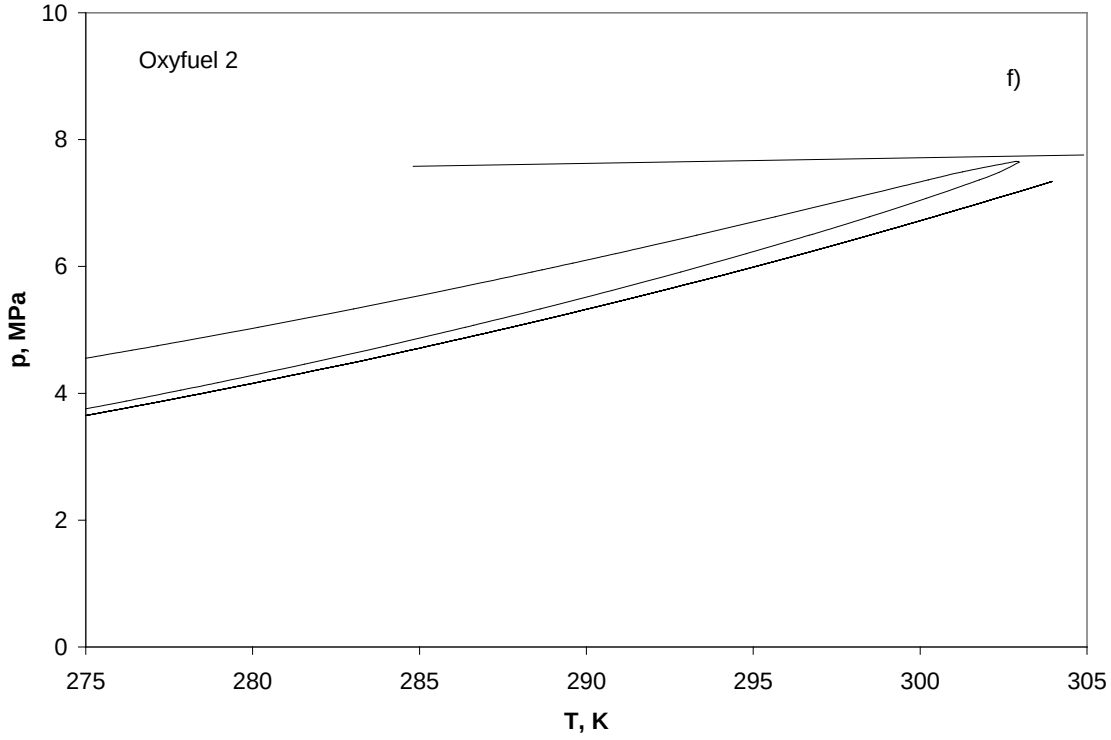
Oxyfuel 2
f)
p, MPa
T, K
0
2
4
6
8
10
275
280
285
290
295
300
305

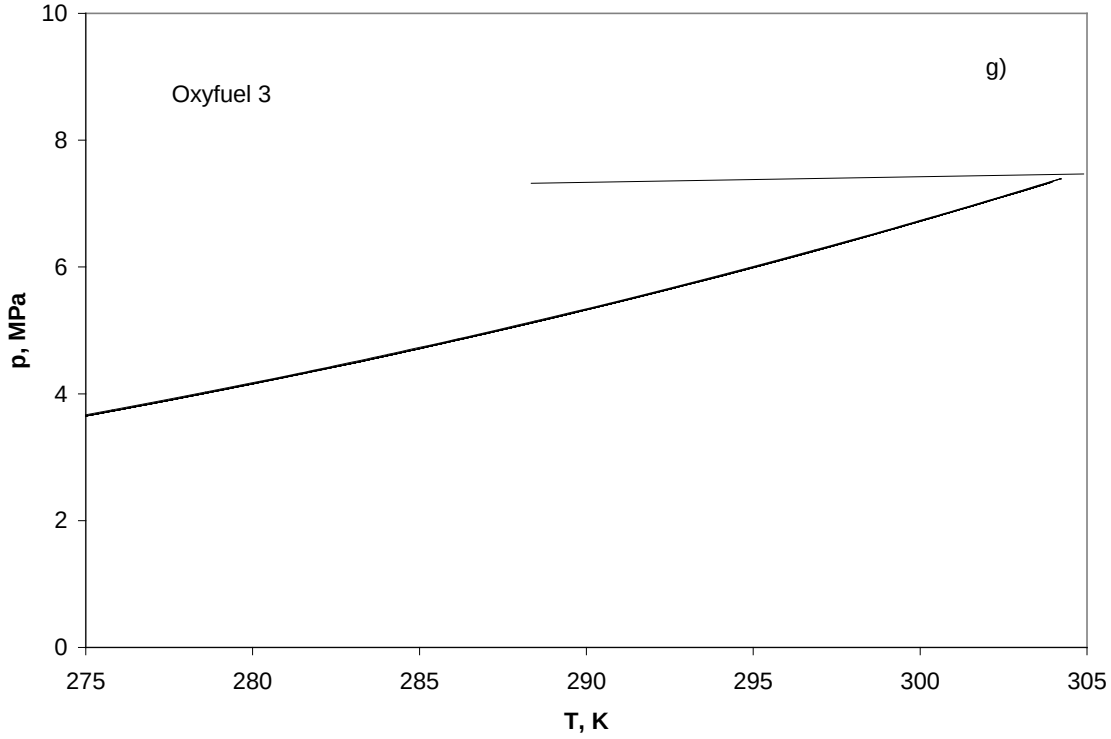
Oxyfuel 3
g)
p, MPa
T, K
0
2
4
6
8
10
275
280
285
290
295
300
305

As can be seen from the diagrams, impurities at high concentration levels affect the phase behaviour significantly. In addition to formation of two-phase regions, the critical temperature and pressure are altered. One extreme case is the high-impurity oxyfuel CO_2 stream containing about 15% N_2, O_2 and Ar, where the critical temperature decreases by about 10°C and the bubble-point pressure increases by over 4 MPa, compared with pure CO_2. Streams with lower impurity levels show smaller changes in the phase behaviour. Particularly, for the two post-combustion CO_2 streams and the low-impurity oxyfuel CO_2 stream (99.94% CO_2), the phase envelopes are very narrow and overlap the vapour-liquid saturation curve of pure CO_2.

Under the studied conditions, non-condensable impurities N_2, O_2 and Ar should have the greatest effect of increasing the vapour-liquid saturation pressures and decreasing the critical temperature, owing to their low critical temperatures. H_2 has a still lower critical temperature, but its effect would be smaller because of its low concentration, as is evidenced in Figure 2.1. The effects of the specific impurity species can be understood from Figure 2.2, where phase diagrams for several CO_2 streams are shown in comparison of the high-impurity oxyfuel CO_2 stream of Table 1.1 (containing 5.8% N_2, 4.7% O_2, 4.47% Ar and other impurities at ppm levels), including

1. CO_2 stream from a typical oxyfuel combustion process, containing 3 vol % O_2, 2 vol % N_2, and 1000 ppm SO_2;
2. CO_2 stream from oxyfuel combustion in a fluidized bed pilot plant combustor in CanmetENERGY, containing 5.2 vol % O_2, 221 ppm CO, 1431 ppm SO_2 and 243 ppm NO (Jia *et al*., 2007);
3. CO_2 stream from a zero-emissions process proposed by CanmetENERGY, containing1.05 vol % CO, 1.7 vol % SO_2, 0.32 vol % H_2 and 690 ppm H_2S (Wang and Anthony, 2008);
4. CO_2 stream from Cansolv® absorption system containing 2.9 vol % SO_2, studied in a previous IEA GHG report (IEA GHG, 2004).

Also shown in this figure are the diagrams for CO_2 mixtures with 5 and 15 vol % Ar, respectively. The 5% Ar mixture is for comparing with cases 1 (3% O_2 and 2 % N_2) and 2 (5.2% O_2), and the 15% Ar mixture is for comparing with the high-impurity oxyfuel CO_2 (containing about 15% N_2+O_2+Ar), with regard to the effects of the three air-derived impurities.

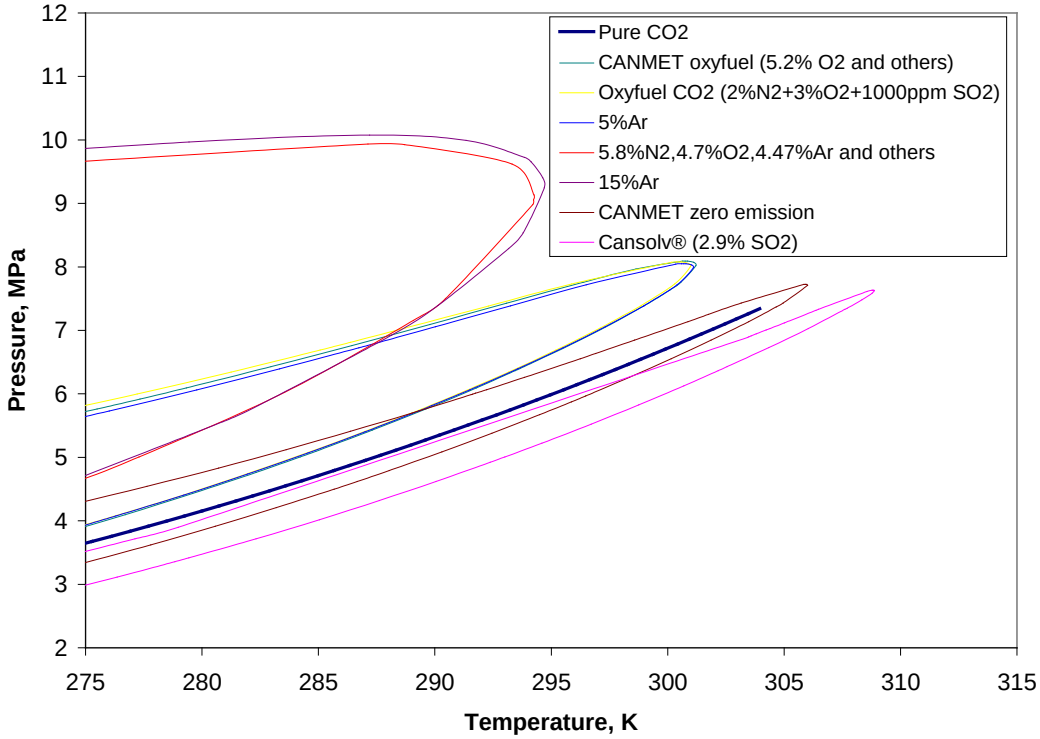

Figure 2.2. Calculated phase diagrams for CO_2 mixtures.

From the phase diagrams it is clear that N_2, O_2 and Ar are responsible for the aforementioned increase in the saturation pressures and decrease in the critical temperature. It is interesting to note that the diagrams of the three cases with about the same content of the air-derived impurities (*i.e.*, 5.2 O_2, 3% O_2 + 2% N_2 and 5% Ar, respectively) practically coincide with each other, suggesting the effects of the three species on the phase behaviour are nearly identical at this concentration level. Even at up to 15% impurity concentration, the effects are quite close, as can be seen from comparison of the diagrams of the high-impurity oxyfuel CO_2 (containing about 15% N_2 + O_2 + Ar) and the 15% Ar CO_2 mixture.

On the other hand, SO_2 results in a decrease in the vapour-liquid saturation pressure and an increase of the critical temperature, as could be expected from the high critical temperature of pure SO_2 (157.6°C). It can also be seen that low-concentration impurities, such as CO and NO_x would not significantly affect the phase behaviour of CO_2.

The changed phase behaviour has significant impacts on pipeline transport of the CO_2 stream. If the impure CO_2 streams were to be transported in liquid phase, lower critical temperature would require lower pipeline temperature. When local temperatures may exceed the critical temperature, better insulation or cooling would be needed. Moreover, although the increased liquefaction pressure is still lower than the injection pressure, and hence the increased power consumption for compression of the stream is not lost in this sense, larger size and higher quality of the pipeline are required, because of lower density

of CO_2 mixtures (and presence of corrosive impurities). Alternatively, if the CO_2 streams were to be transported in supercritical phase, higher pressure would be required to avoid the formation of two phase flow. Furthermore, the size of the pipeline also needs to be larger compared to the case of pure CO_2, due to lower density of the supercritical streams which will be discussed in the next section.

2.2 Storage Capacity

2.2.1 Density of Supercritical CO_2 Stream with Impurities

After injection into underground formations, CO_2 will be in the supercritical state and impurities will affect the volumetric properties of the CO_2 plume. Figure 2.3 shows selected cases of calculated density for supercritical CO_2 with impurities at 330 K, which is in the typical temperature range for CO_2 storage evaluations in western Canada. Two CO_2/Ar mixtures with 5 and 15% Ar, respectively, are included for comparison with the 2% N_2+3% O_2 case and the high-impurities oxyfuel CO_2 case (about 15% N_2 + O_2 + Ar). It can be seen that non-condensable impurities such as O_2, Ar, N_2 and H_2 significantly reduce the density of the supercritical CO_2 stream. The reduced density is largely related to increased volume, except for H_2, where the effect of smaller molecular weight is also significant. All these impurity components in CO_2 would cause a volume increase greater than their molar or volume fractions at standard temperature and pressure (STP) For example, 5 vol %(STP) N_2 + O_2 will result in a volume increase greater than 5 percent in the supercritical CO_2 stream. This can be understood from the fact that non-condensable impurities are less dense than CO_2 and hence take greater volumes. If they have the same molar volume as CO_2 there would be no volume increase, provided the interactions between unlike molecules are negligible.

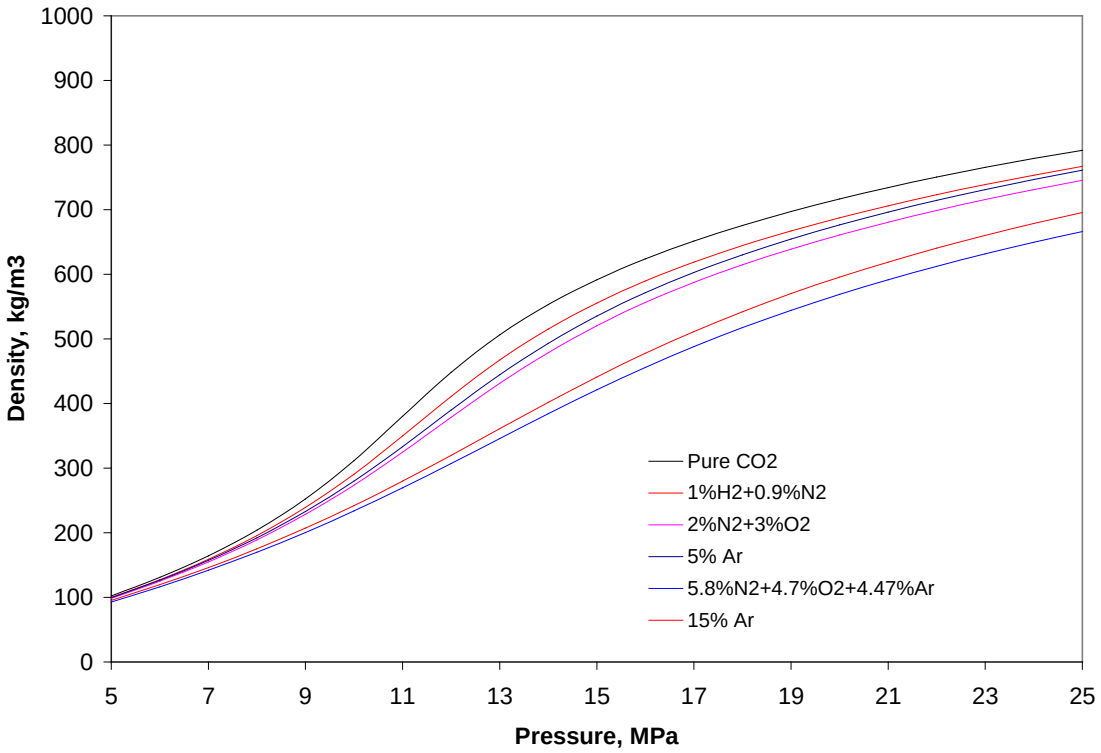

Figure 2.3. Calculated density for CO_2 and CO_2 mixtures as a function of pressure at 330 K.

2.2.2 Quantifying the Effect of Impurities on CO_2 Storage Capacity

The decrease of CO_2 storage capacity due to the contained impurities is thus not only caused by the lower volume fraction of CO_2, but also by the additional volume of less dense impurities. To produce a simple relation regarding the effect of the impurities on the storage capacity for CO_2 for given storage volume, we propose the following expression for the storage capacity (expressed in mass) as a function of the density of the CO_2 stream:

$$\frac{M}{M_0} = \frac{\bar{\rho}}{\rho_0 (1 + \sum_i m_i / m_{CO2})} \qquad (2.5)$$

where M and M_0 denote the mass of CO_2 in the mixture and in the pure stream, respectively, which occupy the same volume, $\bar{\rho}$ and ρ_0 are the density of the mixture and the pure stream, and m_i/m_{CO2} is the ratio of the mass of impurity i to the mass of CO_2 in the mixture. The ratio M/M_0 on the left-hand side of the equation, which can also be viewed as the ratio of the mass of CO_2 per unit volume in the mixture to that in the pure state, represents a normalized storage capacity for CO_2 in its supercritical phase, *i.e.*, the

capacity for structural trapping of CO_2. In the case of pure CO_2 (zero impurity effect) the ratio equals unity. The right-hand side of the equation is a function of temperature, pressure and mixture composition and can be calculated from equations of state. Accordingly, the normalized storage capacity can be determined for given temperature and pressure conditions. Calculated results for the mixtures of Figure 2.3 using the Peng-Robinson equation are shown in Figure 2.4. As can be seen from the figure, in all cases the reduction of capacity is greater than the molar or STP volume fractions of the impurities. More importantly, in all cases there is a maximal reduction of the capacity at a certain pressure, as shown by a minimum in the capacity-pressure curves. With the purity levels considered by IEA GHG (Table 1.1), the maximum reduction is from 9% for the 97.95% CO_2 to 40% for the 85% CO_2 mixtures. The minimal reduction between 9 MPa (corresponding to a shallow storage depth of about 900 m) to 25MPa for the two mixtures is 4% and 25.5%, respectively, which is still about twice the STP volume fractions of the impurities. Whereas the accuracy of the numerical values is limited by the accuracy of the equation of state, the existence of a minimum in the storage capacity appears to be certain, as will be discussed in following sections.

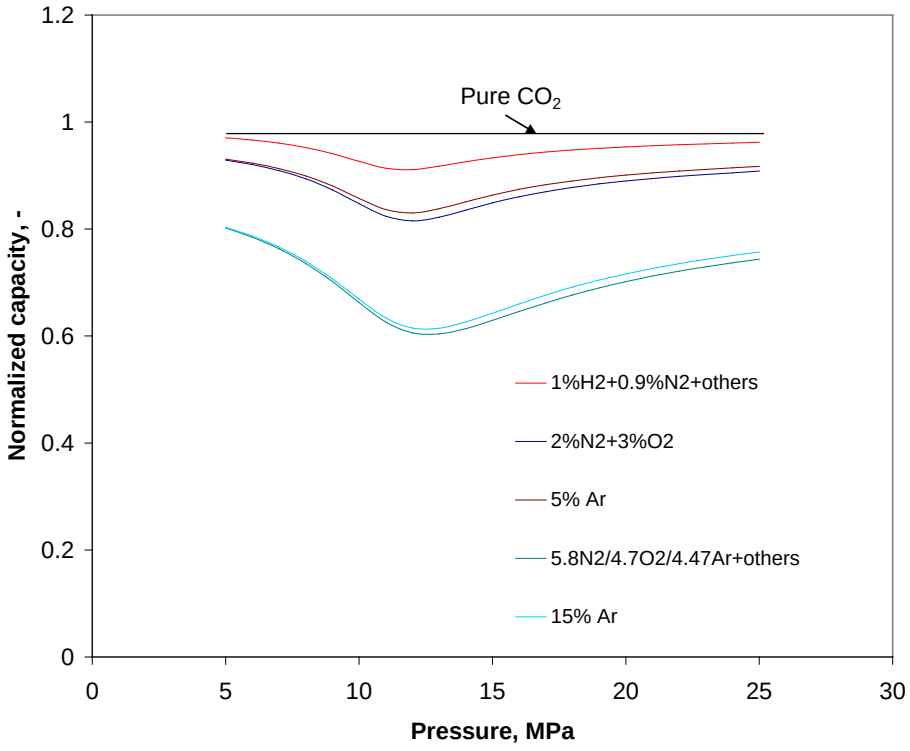

Figure 2.4. Normalized CO_2 storage capacity at 330 K in terms of Equation 2.5, where the densities are calculated with Peng-Robinson Equation.

2.2.3 The Minimum in the Storage Capacity of CO_2 with Non-condensable Impurities

As has been seen, there is a maximum reduction of CO_2 storage capacity, or a minimum capacity, for all cases shown in Figure 2.4. This minimum is revealed through our analysis. Comparison of Figures 2.3 and 2.4 shows that the minimum occurs in the pressure range where the density of CO_2 increases most rapidly, and the pressure corresponding to the minimum increases slightly with increasing impurity concentration. To make sure this generalization is not affected by inadequate representation of the PVT relations by the Peng-Robinson equation, another equation of state (Soave-Redlich-Kwong equation) was used for the same calculations, and similar results were obtained. As this behaviour has important implications for CO_2 storage, we have analyzed it further and concluded that the minimum is a physical reality. The analysis is given as follows.

From Figure 2.4 it can be seen that mathematically the minimum should correspond to

$$\frac{d(M/M_0)}{dp}=0 \tag{2.6}$$

Using Equation 2.5 and noting that $(1+\sum_i m_i/m_{CO2})$ is constant for a given mixture, it follows that

$$\frac{d(M/M_0)}{dp}=\frac{d(\overline{\rho}/\rho_0)}{(1+\sum_i m_i/m_{CO2})dp}=\frac{\frac{d\overline{\rho}}{dp}\rho_0-\frac{d\rho_0}{dp}\overline{\rho}}{(1+\sum_i m_i/m_{CO2})\rho_0^2} \tag{2.7}$$

Thus, Equation 2.6 is satisfied for

$$\frac{d\overline{\rho}}{dp}\rho_0-\frac{d\rho_0}{dp}\overline{\rho}=0 \tag{2.8}$$

A rearrangement of Equation 2.8 yields

$$\frac{d\overline{\rho}}{\overline{\rho}dp}=\frac{d\rho_0}{\rho_0 dp} \quad \text{or} \quad \frac{d\ln\overline{\rho}}{dp}=\frac{d\ln\rho_0}{dp} \tag{2.9}$$

Moreover, when the pressure p is smaller or greater than the pressure corresponding to the minimum, there should be $\frac{d\ln\overline{\rho}}{dp}<\frac{d\ln\rho_0}{dp}$ and $\frac{d\ln\overline{\rho}}{dp}>\frac{d\ln\rho_0}{dp}$, respectively, for the minimum to occur. Since $\frac{d\ln\overline{\rho}}{dp}>\frac{d\ln\rho_0}{dp}$ if $\frac{d\overline{\rho}}{dp}>\frac{d\rho_0}{dp}$ and *vice versa*, we can examine $\frac{d\overline{\rho}}{dp}$ and $\frac{d\rho_0}{dp}$ only. At low pressure we can apply the ideal gas law for simplicity:

$$pV_m=RT \tag{2.10}$$

Rewriting the ideal gas law into

$$\rho = \frac{wp}{RT} \tag{2.11}$$

where ρ is density and w is the molar weight, we have

$$\frac{d\rho}{dp} = \frac{w}{RT} \tag{2.12}$$

at constant temperature. Because the non-condensable impurities result in smaller molar weight, *i.e.*, $w < w_{CO2}$, there must be $\frac{d\overline{\rho}}{dp} < \frac{d\rho_0}{dp}$ according to Equation 2.12 for low pressures. On the other hand, at very high pressures, the density of pure CO_2 in its supercritical state would be close to liquid density and not change appreciably with pressure. By contrast, the density of the mixtures of CO_2 and non-condensable impurities can still increase with pressure because they are farther away from a liquid state in comparison with pure CO_2, that is, $\frac{d\overline{\rho}}{dp} > \frac{d\rho_0}{dp}$. Consequently, from low pressure to very high pressure there must be a transition point, where $\frac{d\overline{\rho}}{dp} = \frac{d\rho_0}{dp}$, which should correspond to the minimum observed in Figure 2.4.

We have looked for reported experimental data to verify the existence of the minimum. Unfortunately, there are no readily applicable data, as no investigations similar to the present one have been undertaken before (at least not to our knowledge). The data we found which could most closely serve our purpose are shown in Table 2.1. The two sets of data were not obtained at the same temperature, but at very close temperatures. After application of Equation 2.5, the data are represented by the curve in Figure 2.5. Although the fraction of CO_2 is much smaller than the cases we evaluated, a minimum is clearly seen at about 13 MPa. Since all CO_2 mixtures with non-condensable impurities would show a minimum according to our analysis, the verification using this single case should suffice.

Table 2.1 Literature data for density of a mixture of 44.696 mol % CO_2 and 55.304 mol % N_2 (Esper *et al.*, 1989) and pure CO_2 (Klimeck *et al.*, 2001) in the supercritical temperature range of CO_2

44.696 % CO_2 and 55. 304 % N_2 at 320 K

Pressure (MPa)	Density (kg/m^3)
21.6035	335.699
14.3676	222.941
9.868	148.051

Pure CO_2 at 323 K

Pressure (MPa)	Density (kg/m^3)
10.0471	389.902
12.031	586.718
14.0034	672.36

6.7848	98.311
4.6323	65.28

16.0213	722.504
18.0289	757.512
21.0388	796.328
24.0253	825.825

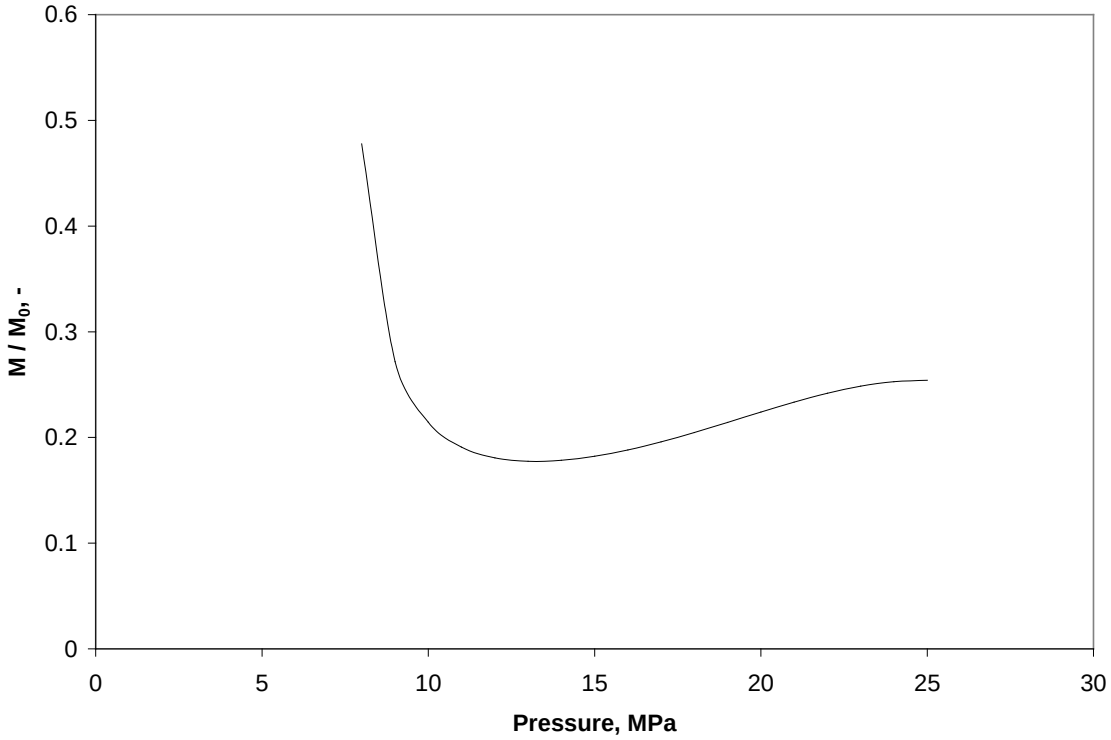

Figure 2.5. Verification of the existence of a minimum in the normalized density for impure CO_2, hence in storage capacity, using literature data given in Table 2.1.

2.2.4 A Maximum of Storage Capacity for CO_2 with SO_2

For impurities which have higher critical temperature than that of CO_2, no storage capacity minimum would occur in the corresponding CO_2 mixture. Rather, a maximum can appear based on an analysis similar to that for the non-condensable impurities. This has been verified with calculated results for the CO_2 mixture with 2.9 vol % SO_2 (the Cansolv® absorption system case presented in the previous IEA GHG report PH4/32). As shown in Figure 2.6, a maximum is seen at about 11 MPa, where the storage capacity is increased by over 5%. It should be noted again that the storage capacity is based on pure CO_2 (see discussion for Equation 2.5). It is, therefore, interesting to see that in this peak region, the CO_2-based capacity is above that of pure CO_2. In other words, SO_2 does not take any but creates space for CO_2. This can be rationalized from the consideration that SO_2 decreases average distance between the molecules of the mixture – an opposite effect of that of the non-condensable gases. This can be taken as one positive effect of the presence of SO_2 on CO_2 storage. However, SO_2 causes more concern with regard to its chemical effects on formation rocks. This will be discussed later.

It is worth mentioning that H_2S would also exhibit a maximum in the storage capacity according to our calculations (see Figure 2.6). However, the maximum is below the capacity of pure CO_2. That is to say, H_2S decreases CO_2 storage capacity. The analysis is more complex, as H_2S has a lower molecular weight but higher critical temperature than CO_2 due to its polar nature, and is not presented here.

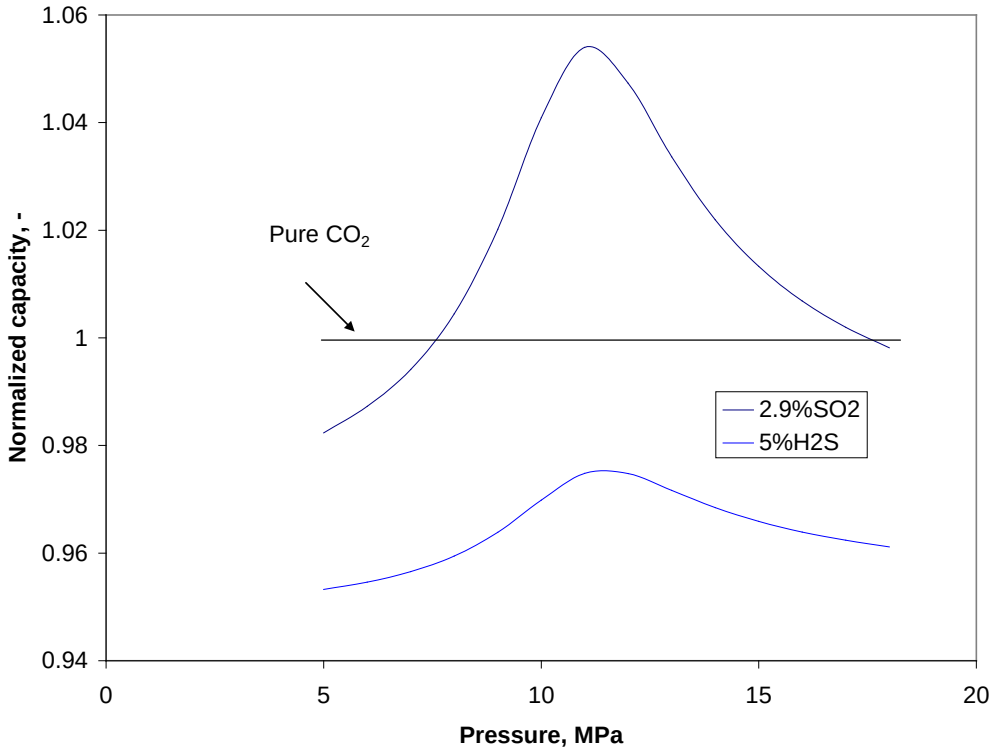

Figure 2.6. Normalized storage capacity for CO_2 with 2.9 vol % SO_2 at 330 K. The result for 5 vol % H_2S is also shown.

2.2.5 Impact of the minimum CO_2 storage capacity

The minimum in the CO_2 storage capacity caused by non-condensable impurities is of practical concern, because these impurities are typical for CO_2 streams from oxyfuel combustion, and the pressure for this minimum falls in the range for CO_2 storage. Calculated pressure dependence of the normalized CO_2 storage capacity at several temperatures for the high-impurity oxyfuel CO_2 stream is shown in Figure 2.7. It can be clearly seen that with temperature increasing, the minimum shifts to higher pressure and the magnitude of the minimum decreases. As is suggested by Figure 2.4, for different impurity levels the pressure corresponding to the minimum storage capacity changes only slightly at constant temperature. Accordingly, similar pressure and temperature dependence behaviour of the minimum shown in Figure 2.7 is expected for CO_2 streams with other impurity levels. In subsurface formations, the pressure and temperature are interrelated as both of them increase with the depth from the surface. At certain depths, the minimums which correspond to the largest decreases of storage capacities may occur

due to pressure and temperature conditions. By assuming a hydrostatic pressure gradient of 10 MPa/km, and geothermal gradients from 20 to 33°C/km for the subsurface and a ground temperature of 15°C (as has been assumed in a recent IEA GHG report, see Gorecki *et al.*, 2009), the impact of the minimum on the CO_2 storage capacity for the high-impurity CO_2 stream is shown in Table 2.2. As can be understood, the storage capacity can decrease to as low as 54.3% at 320 K and 56.4% at 330 K in the case of 33°C/km geothermal gradient. At higher temperature, 350 K, the decrease in the storage capacity is smaller and at still higher temperatures the decrease would be smaller still.

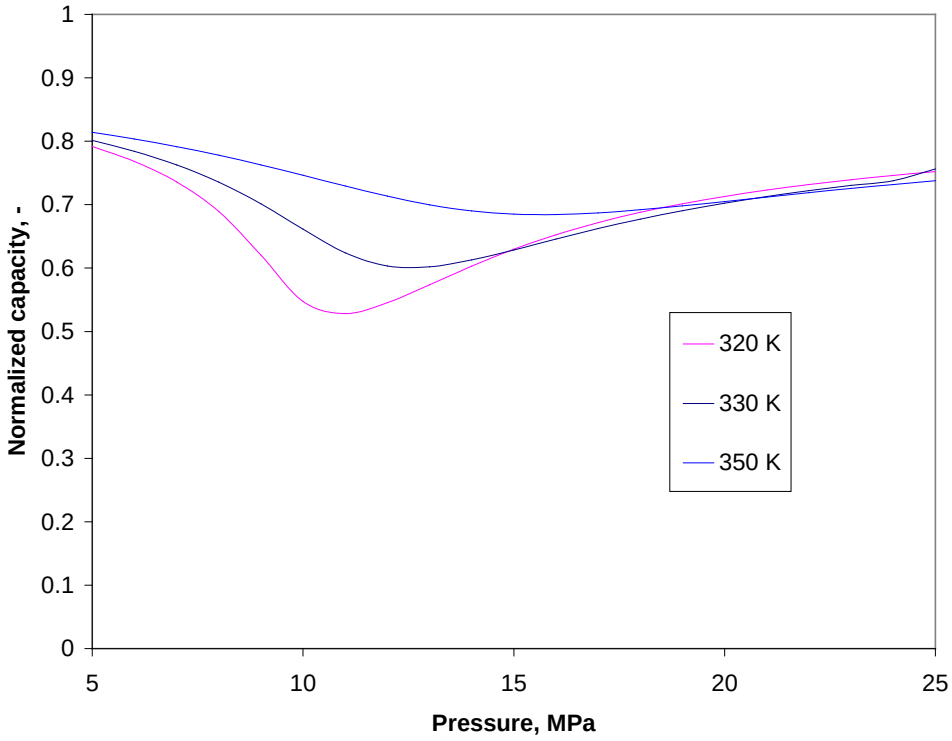

Figure 2.7. Normalized CO_2 storage capacity at different temperatures in terms of Equation 2.5 for the high-impurity CO_2 stream (5.8 vol % N_2, 4.7 vol % O_2, 4.47 vol % Ar and minor amounts of other impurities).

Table 2.2 Normalized CO_2 storage capacity for the high impurity CO_2 stream at several subsurface temperatures*

T gradient	20°C/km		25°C/km		33°C/km	
T (K)	p (MPa)	Capacity (-)	p (MPa)	Capacity (-)	p (MPa)	Capacity (-)
320	16	0.653	13	0.574	10	0.543
330	21	0.723	17	0.672	13	0.564

350	31	0.755	25	0.734	19	0.698

*Hydrostatic pressure gradient of the subsurface is taken as 10 MPa/km.

As structural trapping is deemed the most important trapping mechanism for CO_2 storage at least in the injection phase of a CCS operation, the pressure effect should be taken into account in estimation of the storage capacity for underground formations. Moreover, in storage operations, the minimum would cause reduced storage efficiency. At a given depth, increasing the storage pressure well beyond the level for the minimum would increase storage efficiency. This may be attained for closed formations within the allowable overpressure range. For open formations where higher pressure may not be attainable, one possibility to increase the storage efficiency is to increase the depth of injection and storage. With increasing depth the temperature and pressure will increase so that the capacity decrease can be alleviated, as can be understood from Figure 2.7 and Table 2.2.

2.2.6 Residual Trapping and Interfacial Tension

The discussion of the minimum CO_2 storage capacity in structural trapping should also be applicable to the volume of CO_2 retained in gas bubbles as an immobile phase by the residual trapping mechanism. That is, the decrease of the volume of trapped CO_2 in the bubbles due to the impurities can be greater than the molar fractions or STP volume fractions of the impurities. Moreover, at lower temperatures a minimum may occur at a certain pressure, causing a greater drop in the volume of CO_2. Furthermore, injection at deeper levels may increase the volume of CO_2 in the bubbles because of higher pressure.

The impurities would also affect the efficiency of residual trapping through the interfacial tension (IFT) between the bubbles and water. Higher IFT leads to higher capillary pressure required to move the bubbles and increase residual trapping, and vice versa. Reported data for IFT between water and high-pressure mixtures of CO_2/N_2 (Yan *et al.*, 2001) and CO_2/CH_4 (Ren *et al.*, 2000), respectively, show that the IFT increases with increasing fraction of N_2 or CH_4. Based on these observations, we expect the IFT of the high-impurity oxyfuel CO_2 to be higher than that of pure CO_2. An evaluation of the data is given below.

The reported IFT data for CO_2/N_2 mixtures in the pressure range 10 – 20 MPa and temperature range 313.15 – 373.15 K are selected and plotted in Figure 2.8a, as a function of the mole fraction of N_2. Since the IFT values at different temperatures and pressures fall within a relatively narrow range, it is not easy to see the temperature and pressure dependence from the plot. However, it is evident that the IFT increases with increasing fraction of N_2. In Figure 2.8b, the IFT data for CO_2/CH_4 are plotted. Similarly to the case of CO_2/CH_4, the IFT increases with increasing fraction of CH_4. Given that both N_2 and CH_4 are non-condensable and non-polar gases, and both have higher IFT with water than pure CO_2, it would be reasonable to expect other similar gases, such as O_2 and Ar, to have a similar effect of increasing the IFT of impure CO_2.

The dash lines in Figure 2.8 represent linear interpolations based on IFT of pure CO_2 and N_2 or CH_4, in terms of

$$\sigma = \sigma_{CO2} x_{CO2} + \sigma_i (1 - x_{CO2}) \qquad (2.13)$$

where σ is the IFT; σ_{CO2} and σ_i denote the IFT of CO_2 and the other component, respectively. x_{CO2} is the mole fraction of CO_2. The maximum deviation between the linear predictions and measured data is less than 12% over the evaluated range. It is interesting to note that the IFT of a CO_2 mixture with 30 mol% H_2S has also been found to be close to the molar averages of the two components (Shah *et al.*, 2008), although, unlike N_2 and CH_4, H_2S is polar and its IFT with water is lower than that of CO_2.

Based on the linear interpolations we estimate a moderate increase of the IFT – up to 15% - for the high-impurity oxyfuel CO_2 (ca 15% of N_2, O_2 and Ar). This would have an effect of increasing the bubbles trapped in the pores after water imbibition, and offset the effect of decreasing CO_2 volume in the individual bubbles by the impurities. Measurements should be conducted to determine the actual IFT of impure CO_2 under storage conditions, however.

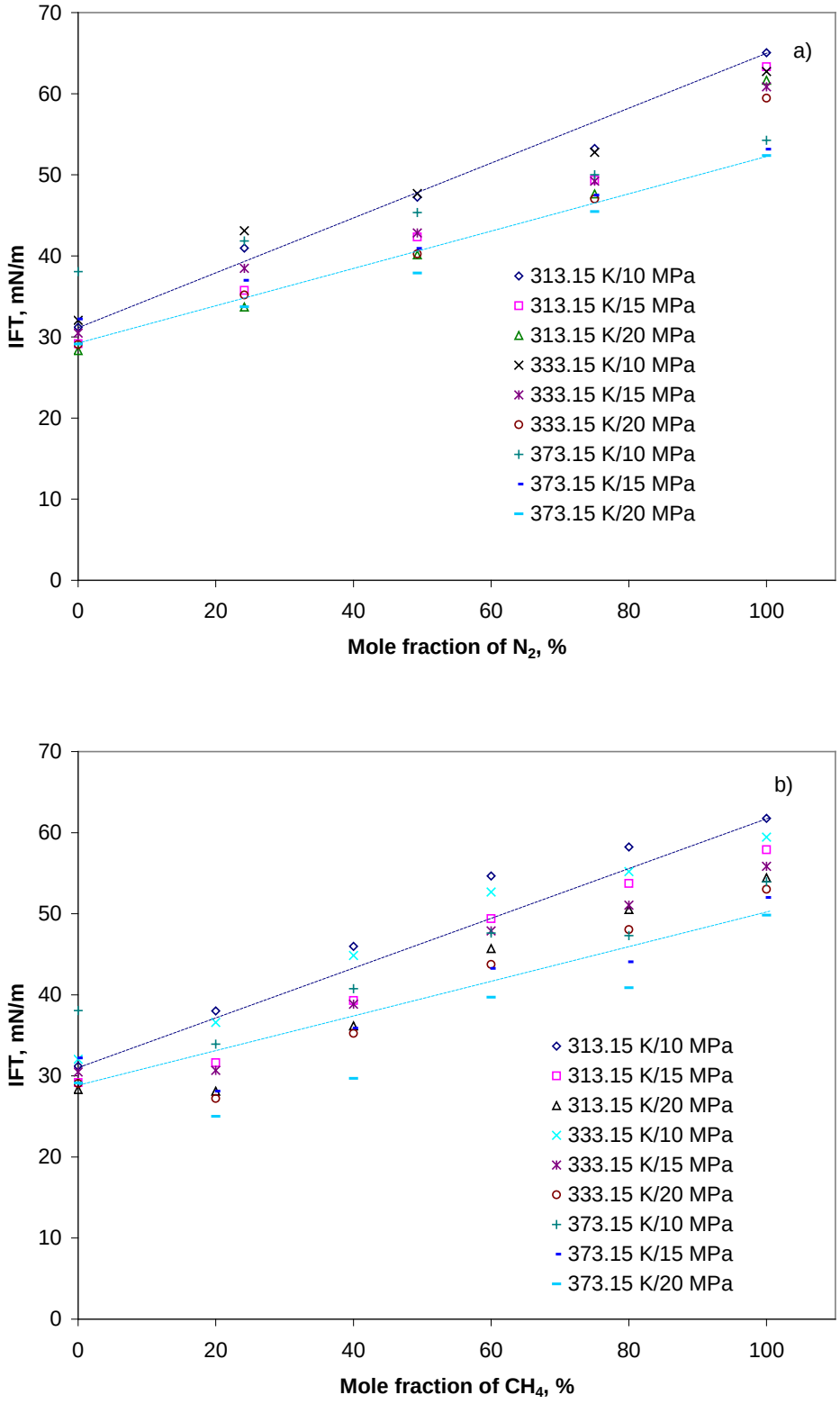

Figure 2.8. Interfacial tension (IFT) of CO_2 mixtures; a) CO_2/N_2, b) CO_2/CH_4. The lines represent interpolations based on Equation 2.13 for upper and lower bound data sets.

2.2.7 Using Ar to Represent Non-condensable Impurities in Oxyfuel CO_2 Streams

CO_2 streams from oxyfuel combustion contain high levels of O_2, N_2 and Ar. As have been discussed, these impurities result in substantial changes to the PVT properties of the CO_2 streams, which impact significantly CO_2 transport and storage. Given the importance of oxyfuel combustion in CO_2 capture, we have further evaluated the PVT properties of CO_2 streams with O_2, N_2 and Ar. The properties of the impure CO_2 streams are dependent on their composition. Computation of these properties for various mixtures requires composition-dependent parameter values that are subject to experimental determination, and can be quite laborious. Measurements of these properties can be more difficult because of the risks of fire, explosion and corrosion of high-pressure oxygen, which demand special materials and extra caution. If the PVT properties of CO_2 mixtures containing O_2, N_2 and Ar can be evaluated using only one impurity component, such as N_2 or Ar, the modeling and laboratory work can be largely simplified. It is for this reason that we included single-impurity (Ar) cases in phase envelope and density calculations, in comparison with the results of multi-impurity (O_2, N_2 and Ar) mixtures at equivalent molar fractions. The concept is based on similar critical properties of the three species, which are shown in Table 2.3. Whereas these properties are common knowledge, the table will serve to show that they lead to similar PVT behaviours of the CO_2 mixtures being discussed. Compared with CO_2, the critical properties of the three gases are quite close. We have considered Ar regarding its representativeness for the other two species, because its critical temperature and pressure are in between the values for the other two, although closer to O_2 than N_2 (Table 2.3).

Table 2.3 Critical properties of CO_2, O_2, N_2 and Ar

Species	Tc (K)	Pc (MPa)
CO_2	304.2	7.38
O_2	155	5.05
Ar	151	4.87
N_2	126	3.39

Comparison of the phase envelopes in Figure 2.2 shows that the calculated result for the 2% N_2 + 3% O_2 and 95% CO_2 mixture is close to that of the 5% Ar and 95% CO_2 mixture. For the high-impurity case with 15% impurities (5.8% N_2, 4.7% O_2, 4.47% Ar and others), the result for the 15% Ar CO_2 mixture essentially coincides with the former over a large part of the dew-point portion. The bubble pressure of the 15% Ar mixture is slightly higher than that of the CO_2 mixture with about 15% N_2 + O_2 + Ar, but the difference is within 2 percent. The difference in critical temperature is less than 1°C.

The results for the supercritical phase are more interesting. Calculated volumes for the CO_2 mixtures with 15% Ar and 15% N_2 + O_2 + Ar, respectively, are practically identical (Figure 2.9), with the maximum discrepancy within 1 percent. An important point is that the density of mixtures can be readily calculated given the volume values. Although the density of the Ar-only mixture is different from the density of the corresponding mixture with multi-impurity components (Figure 2.3), the volumes are practically the same. Once

the volume of the Ar-only mixture is determined, the density of the multi-component mixture can be calculated using the exact mass, which is known for a given composition. As will be discussed, the density of CO_2 mixtures affects not only CO_2 storage capacity, but also permeation and buoyancy of the CO_2 plume. The proposed approach has the potential to substantially simplify related calculations and programming for computer simulations. Moreover, it may largely simplify laboratory experiments for determination of the properties of oxyfuel CO_2 streams, if only Ar is used to simulate the total air-derived gas impurities at various concentration levels. The advantage of avoiding using hazardous high-pressure O_2 is particularly attractive.

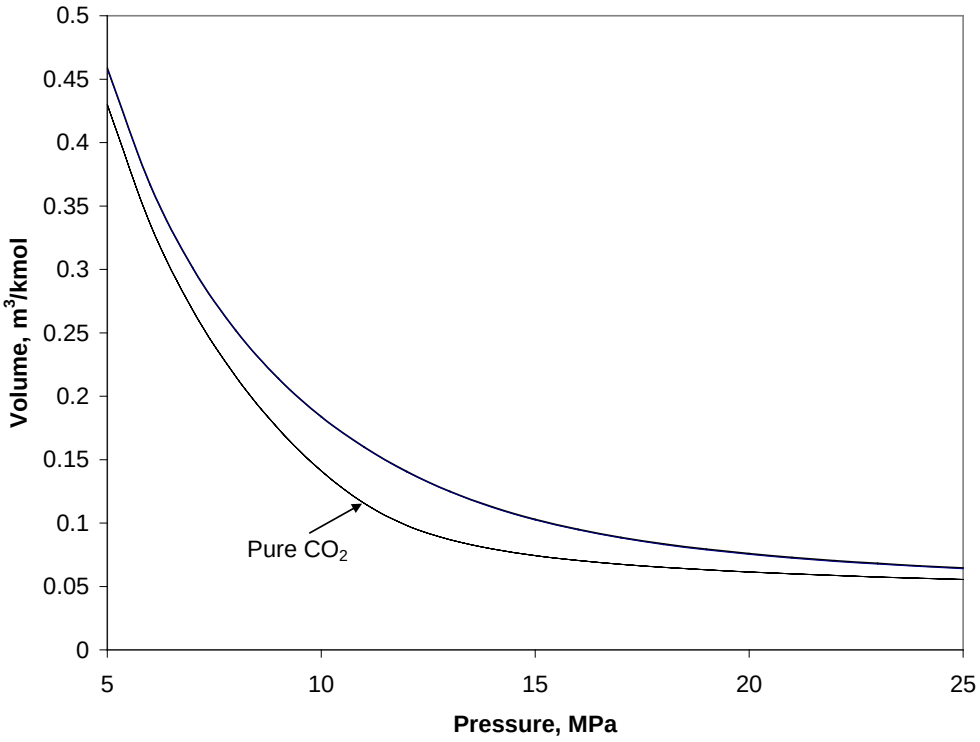

Figure 2.9. Comparison of the volumes of the high-impurity CO_2 mixture (5.8% N_2 + 4.7% O_2 + 4.47% Ar) and the CO_2 mixture with 15% Ar at 330 K. The curves for the two mixtures essentially coincide.

We have not carried out calculations using Ar mixtures at other temperatures, because there is reason to believe that the results would be even better, at least for higher temperatures. This can be demonstrated by use of generalized charts for compressibility factor $Z = pV_m/RT$. For gas mixtures, one can calculate their pseudo-critical temperature, T_c^*, and pseudo-critical pressure, p_c^*, using the Kay's rule (Kay, 1936):

$$T_c^* = \sum_i x_i T_{ci} \qquad (2.14)$$

and

$$p_c^* = \sum_i x_i p_{ci} \qquad (2.15)$$

where T_{ci} and p_{ci} are the critical temperature and pressure of the individual components. Then the compressibility factor of the mixture, *Z*, can be obtained from the generalized charts according to the reduced temperature, $T_r = T / T_c^*$ and reduced pressure, $p_r = p / p_c^*$. The generalized *Z* charts can be found in handbooks such as the Chemical Engineer's Handbook. Once the value of *Z* is determined, the volume can be calculated using the relation $V_m = ZRT/p$. As has been discussed earlier, the critical property values of Ar fall between the two other gases, and all these values are substantially lower than that of CO_2. As a result, the T_r and p_r of the Ar-only mixture and the multi-impurity mixture are very close. A comparison is given in Table 2.4. With values of such small difference, the *Z* values and hence V_m values determined from the generalized compressibility charts will be the same. Since the accuracy of the charts is known to increase with increasing *Z* values, and given the fact that a higher temperature means higher T_r which corresponds to greater *Z*, using Ar-only mixture to replace multi-impurity mixtures for higher temperatures is expected to achieve even higher accuracy than for lower temperatures.

In spite of the merit of not requiring sophisticated computations and information on the interaction factors, the use of compressibility factor charts is unlikely to be popular with the development of more efficient computer programs. Instead, the above discussion shows that the proposed approach of using Ar-only mixtures looks credible, and can be quite useful for quicker evaluation of the impacts of the impurities from oxyfuel combustion on CO_2 storage.

Table 2.4 Comparison of reduced properties for two CO_2 mixtures at 330 K

	5.8% N_2 + 4.7% O_2 + 4.47% Ar	15% Ar
T_r	1.178	1.173
Pressure (MPa)	p_r	p_r
5	1.385	1.401
10	0.6927	0.7004
15	0.4618	0.4669
20	0.3463	0.3502
25	0.2771	0.2801

2.3. Permeation Flux

The presence of impurities would also affect CO_2 injection. Here we discuss their physical effects (no chemical reactions involved) on the injection first. We have discussed the IFT for CO_2 mixtures earlier, which could affect the relative permeability of the CO_2 in two-phase flow. In particular, the presence of N_2, O_2 and Ar in the high-impurity oxyfuel CO_2 may increase the IFT and lead to a lower relative permeability. As two-phase flow also depends on a number of other factors, a quantitative evaluation of the effects of impurities requires additional information. However, for the single-phase flow of injected CO_2, the effects may be analyzed in terms of an expression based on Darcy's Law, for the permeation flux O_2:

$$\dot{M} = \frac{-\rho k}{\mu} \nabla p \qquad (2.16)$$

where $\dot{M}$ is the mass flow per unit area, ρ is the density of injected stream, k is rock permeability, ∇ is the gradient operator, p is the pressure, and μ is the viscosity of the fluid. As the impurities lower the density of the CO_2 stream, the mass flux will decrease for the same pressure drop. However, the impurities also affect the viscosity of the injected fluid. When the viscosity of the impure CO_2 stream is lower than the viscosity of pure CO_2, the flux would increase, hence the decrease in density may be compensated by a corresponding decrease in viscosity. The density and viscosity are functions of temperature and pressure. The permeability and pressure gradient vary case by case. However, for an estimation of the impurity effects under the same permeability and pressure drop conditions, one may use the following relation which is a consequence of Equation 2.16:

$$\frac{\dot{M}_{CO2}}{\dot{M}_0} = \frac{\rho(\mu_0 / \mu)}{\rho_0 (1 + \sum_i m_i / m_{CO2})} \qquad (2.17)$$

where $\dot{M}_{CO2}$ and $\dot{M}_0$ are the mass flow per unit area for CO_2 in the mixture and in its pure state, respectively. ρ_0 and μ_0 are the density and viscosity of pure CO_2, respectively. This expression represents a normalized permeation flux, and should be able to provide a measure of the relative injectivity of the impure CO_2 stream. To evaluate the temperature and pressure dependence of this permeability, knowledge of the viscosity is needed. The calculation of viscosity for high-pressure gas mixtures is less certain, especially in the supercritical region. The viscosity can be quite sensitive to pressure at relatively low temperature. Various methods exist but we could not find reported data to verify calculated results for CO_2 mixtures evaluated. Since the impurity effects are more important for high impurity levels, we only discuss the high-impurity case. The viscosities of pure CO_2 and impure CO_2 shown in Figure 2.10 are calculated using the TRAPP method (Huber and Hanley, 1996; Poling *et al.*, 2001). Whereas the accuracy of the numerical values is not certain, the pattern of the predicted pressure dependence looks plausible. The mixture is seen to have considerably lower viscosity than pure CO_2 at high pressures. At 5 MPa, the lowest pressure for the evaluation, the viscosity of the mixture is

slightly higher. This is not unreasonable given the fact that the viscosities of N_2, O_2 and Ar are all higher than the viscosity of CO_2 at ambient pressure. The pressure dependence of the normalized permeation flux, based on the calculated viscosities, is shown in Figure 2.11. As a trend it can be seen that the injectivity of the impure CO_2 with about 15% N_2/O_2/Ar is lower than that of pure CO_2 by more than 15 percent at lower pressures, but reaches the same level as pure CO_2 after a transition range of pressure. This pressure range is likely related to the minimum of the relative density of CO_2. This will be discussed later on.

As has been discussed, the viscosity of supercritical CO_2 is lowered by the impurities N_2, O_2 and Ar. Consequently, the effect of increased volume on the permeation flux is partly offset. Thus, the overall physical effect of the impurities on the permeation flux would be less important than on the storage capacity. When the impurity level is lower, the effect on CO_2 permeation flux or injectivity would be smaller still.

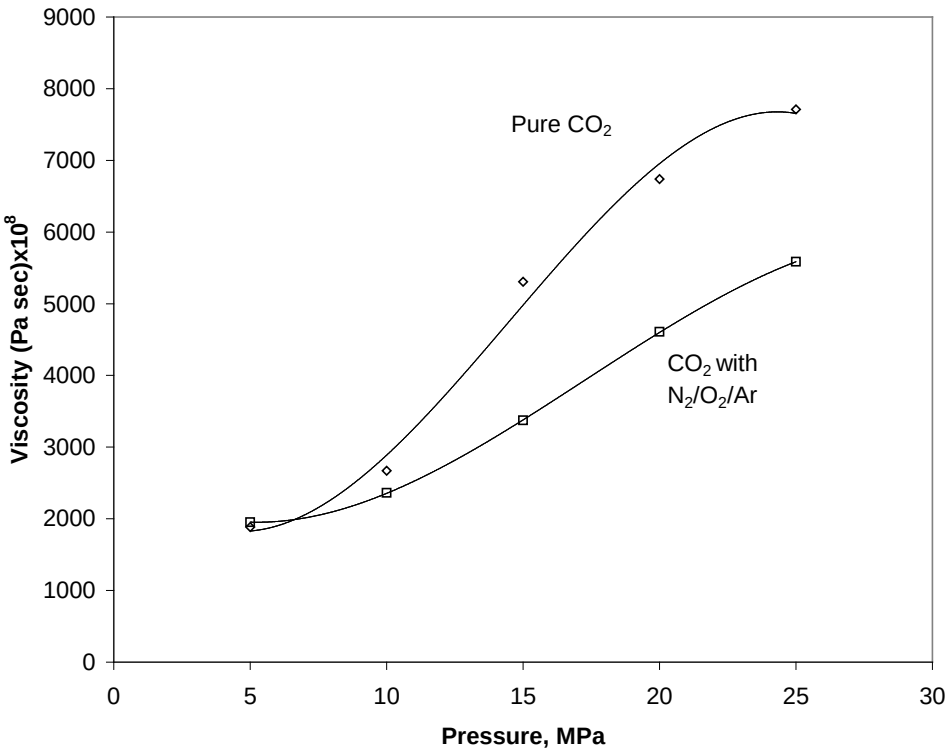

Figure 2.10. Calculated viscosity for 330 K. The symbols represent calculated values and the curves are trend lines.

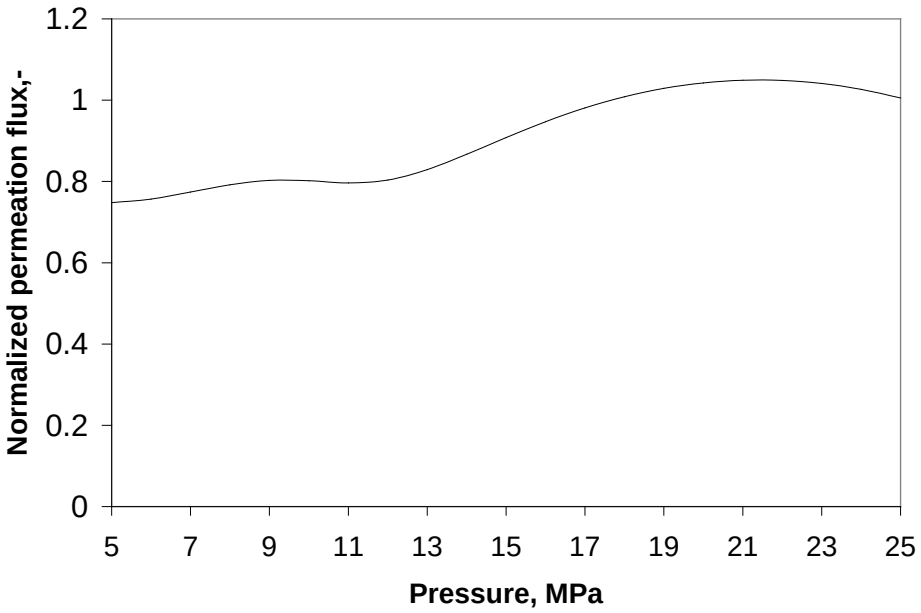

Figure 2.11. Normalized permeation flux for the high-impurity CO_2 stream (5.8% N_2 + 4.7% O_2 + 4.47% Ar) from oxyfuel combustion at 330 K.

2.4 Buoyancy and Rising Velocity

The light-impurity species would result in greater buoyancy for the CO_2 plume, due to the lower plume density they bring about. When a mass of the plume in a unit volume is in contact with the formation water, the buoyancy force can be expressed as

$$F = (\rho_{H2O} - \rho_m)g \qquad (2.18)$$

where ρ_{H2O} and ρ_m are the density of the water and the plume, respectively, and g is the gravitational acceleration. When the changes in relative permeability and capillary pressure are neglected, the effect of impurities on this force with reference to pure CO_2 may be given as

$$\frac{F}{F_0} = \frac{\rho_{H2O} - \rho_m}{\rho_{H2O} - \rho_{CO2}} \qquad (2.19)$$

where F and F_0 are the buoyancy force for the CO_2 mixture and pure CO_2, respectively. The greater the difference between the densities of the mixture and CO_2, the greater the change in the buoyancy would be. The buoyancy also depends on the density of the formation water, assumed constant in these calculations. Figure 2.12 shows the calculated result for the highest impurity case where the density of the formation water (brine) is taken as 1,025 kg/m^3.

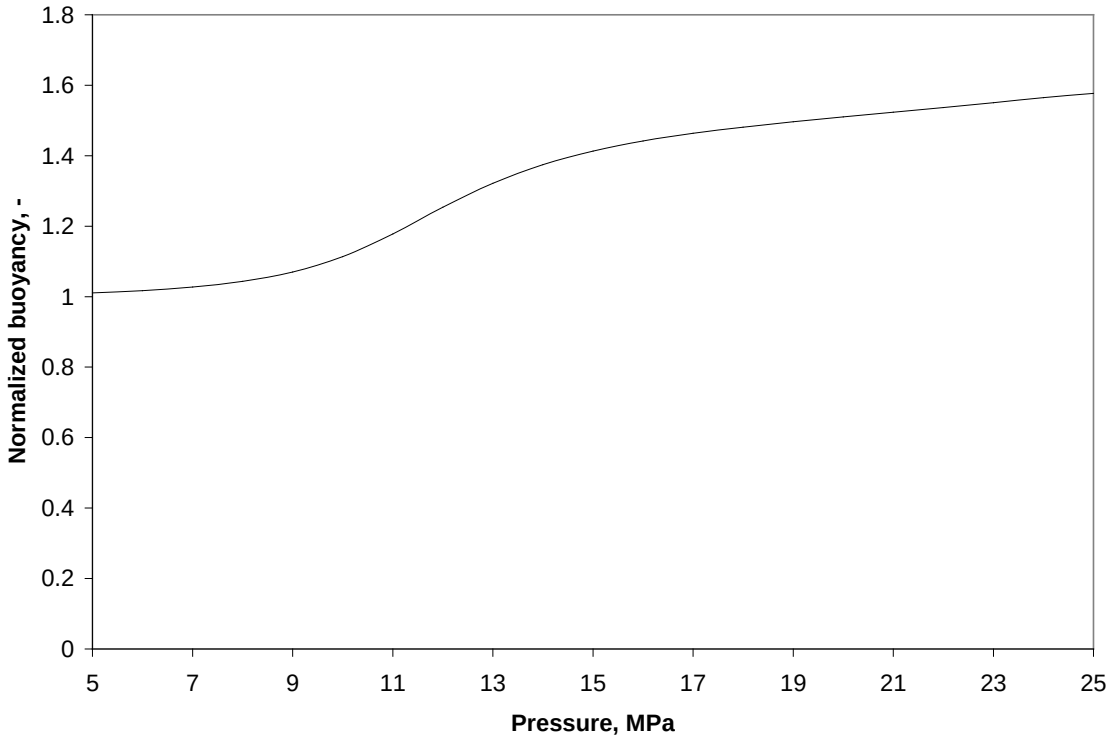

Figure 2.12. Normalized buoyancy for the high-impurity CO_2 stream (5.8% N_2 + 4.7% O_2 + 4.47% Ar) from oxyfuel combustion at 330 K.

As can be seen from this figure, with about 15 vol % non-condensable impurities the buoyancy of the CO_2 plume can increase by over 50% for this high-impurity case. This would significantly increase the rising velocity of the plume. The relation of the velocity and the forces may be given as

$$\frac{dv}{dt} = \frac{F}{\rho} - fv \tag{2.20}$$

where v is the velocity, t is time and f is a coefficient related to frictional resistance to the movement of the plume. As the velocity increases due to increased buoyancy, the resistance also increases. When the two forces are balanced the velocity becomes constant and there is

$$\frac{F}{\rho} = fv \tag{2.21}$$

As f may be taken as being proportional to the viscosity μ, we have

$$\frac{v}{v_0} = \frac{F/(\rho\mu)}{F_0/(\rho_0\mu_0)} \tag{2.22}$$

With the density, viscosity and buoyancy data in Figures 2.2, 2.9 and 2.11, the velocity of the high-impurity plume can reach nearly three times that of the pure CO_2 plume. The high rising velocity would reduce the time for CO_2 contact with water and formation of dissolved species. It would also reduce the formation of a residual phase, because it reduces the spreading of the plume laterally, leaving a smaller area of the aquifer affected by the plume, and hence a smaller area for trapping CO_2 in the pores of rocks. When the plume reaches the caprock it will spread laterally, but the contact with water is only at the interface. Besides, near the caprock the pressure is lower than in the deeper region, and thus the efficiency of CO_2 dissolution and trapping in the pores as a residual phase would be lower. As a result, the potential for CO_2 leakage increases if pathways are available.

Another noteworthy point is that, for both pure CO_2 and the CO_2 mixtures, the buoyancy should decrease with increasing pressure, because of increased density. However, the relative buoyancy with reference to pure CO_2 increases with increasing pressure, as seen in Figure 2.12. This can be understood from Equation 2.19 by rewriting it into

$$\frac{F}{F^0} = \frac{1-\rho_m/\rho_{H2O}}{1-\rho_{CO2}/\rho_{H2O}} \qquad (2.19')$$

As in the investigated range the density of pure CO_2 increases more with pressure than the density of impure CO_2, the ratio of the buoyancy increases with pressure.

Yet another noteworthy point is that from Figure 2.12 a threshold-like transition pressure range is clearly seen, where the buoyancy increases by about 40% from the pure CO_2 level. This transition range is similar to that seen in Figure 2.11 for the normalized injectivity. This behaviour may be related to the pressure which corresponds to the minimum in the relative density of CO_2 discussed earlier. Rearranging Equation 2.19 into

$$\frac{F}{F^0} = \frac{\frac{\rho_{H2O}}{\rho_{CO2}} - \frac{\rho_m}{\rho_{CO2}}}{\frac{\rho_{H2O}}{\rho_{CO2}} - 1} \qquad (2.19'')$$

we recognize the term ρ_m / ρ_{CO2} identified previously, whose pressure dependence shows a minimum, according to the discussions of Equations 2.5 through 2.12. This explains the transition pressure range.

2.5 Dissolution of CO_2 Mixtures in Formation Water

Dissolution of CO_2 into water, which is relevant to solubility trapping of CO_2, increases with pressure but decreases with temperature, salinity and pH. As most high-concentration impurities under consideration have lower solubility in water than CO_2, the presence of these impurities would reduce the partial pressure of CO_2 and, therefore, reduce the dissolution of CO_2 in formation water. Figure 2.13 illustrates the effect of the lowered partial pressure on CO_2 solubility (according to Henry's law) as a function of salinity, where the pure CO_2 solubility is based on literature data (see, *e.g.*, Duan and Sun,

2003). As can be seen, the pressure dependence of pure CO_2 solubility decreases with increasing pressure under the studied conditions. As a consequence, the pressure dependence of impure CO_2 solubility becomes weaker at high pressures. Moreover, the CO_2 will eventually dissolve if the formation is open or the water-to-CO_2 ratio is large, regardless of the presence of impurities. Compared with the other impacts of the impurities discussed earlier, the impact on dissolution appears insignificant.

Acid impurities, such as SO_x and NO_x, would decrease the solubility of CO_2 by decreasing the pH of the formation water. However, dissolved rock minerals can serve as a pH buffer and weaken the effect of acid impurities on CO_2 dissolution. Overall, the effect of impurities is less significant for CO_2 dissolution.

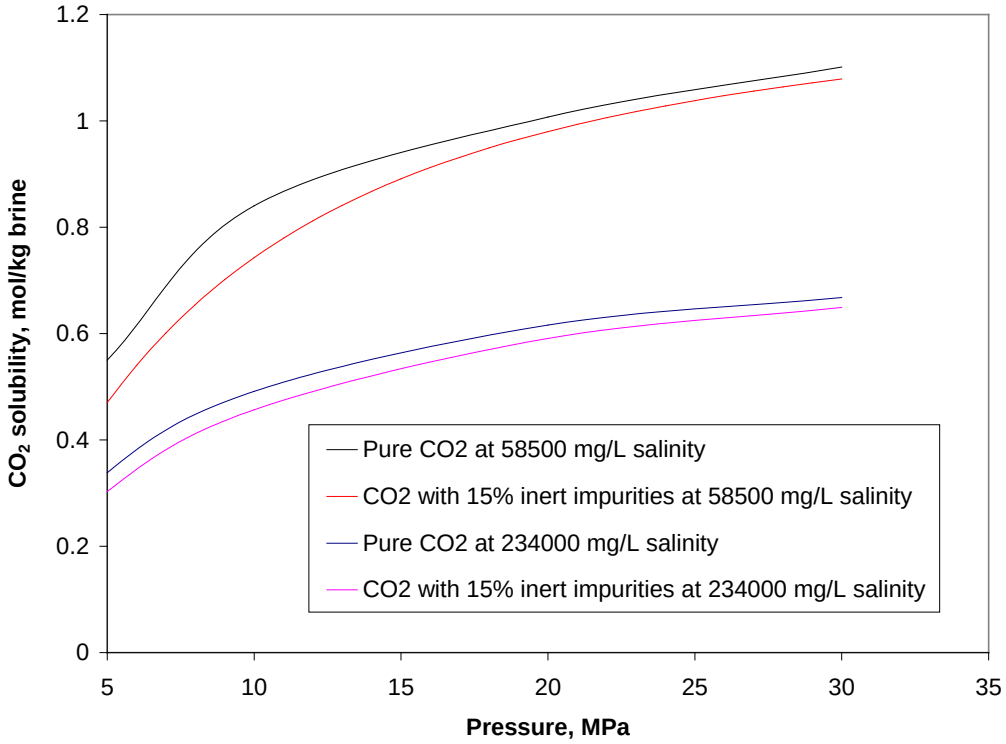

Figure 2.13. The effect of low-solubility impurities on CO_2 solubility in brine at 330 K. The solubility of pure CO_2 is based on literature data and the solubility of impure CO_2 is calculated on account of reduced partial pressures.

3. Chemical Effects

3.1 Impact of Reactive Impurities on Injectivity of CO_2

The most common reactive impurities are H_2S, SO_2, NO_x, whose aqueous solutions are acidic, and CO, which is highly reductive and will be oxidized to CO_2 by oxygen or mineral oxides. There have been several studies on co-injection of H_2S and/or SO_2 with CO_2 (Talman and Perkins, 2009; Knauss *et al.*, 2005; Xu *et al.*, 2007; Bacon *et al.*, 2009;

Jacquemet *et al*., 2009). The general view is that H_2S is not an issue, and it has been co-injected with CO_2 for 20 years in Canada in acid gas disposal. However, SO_2 is believed to alter the geochemistry, causing increased dissolution and precipitation. SO_2 can greatly lower the pH of the formation water and hence enhance the dissolution of rock minerals. When the species become oversaturated precipitation of sulphates would occur, and reduction of pore volume and hence the injectivity of CO_2 is a concern. The effect of the impurities is difficult to quantify. Numerical simulation studies have been performed for one-dimensional cases (Knauss *et al*., 2005; Xu *et al*., 2007; Bacon *et al*., 2009; Jacquemet *et al*., 2009). Trough these studies SO_2 is shown to result in dissolution of minerals in the injection zone and precipitation downstream, causing significant decrease of rock porosity and hence CO_2 injectivity (Xu *et al*., 2007). Such information is valuable for CO_2 injection operations. However, the simulations have either assumed that SO_2 is injected as an aqueous solution or the water in the injection zone is never dry. This would be relevant for injection of CO_2 with water or study of the effects of SO_2 on caprock integrity, but the situation is different from the injection operations where SO_2 migrates with CO_2 in an immiscible plume which results in a desiccation or dry-out zone (see, *e.g.*, Gaus *et al*., 2008; Pruess and Müller, 2009; Pruess, 2009). The important point is that SO_2 is far less reactive when it is dry. Further, continuous dissolution of minerals as in the "wet cases" would not occur in the dry-out zone. The contact of SO_2 with water only occurs on the front of the plume and the two-phase flow zone, and the time would be limited. Therefore, build-up and precipitation of minerals in the downstream which were dissolved in the upstream and carried by water flow would be much less, compared with the "wet cases". In the following we give an analysis for the impact of SO_2 on the injectivity of CO_2.

3.1.1 Formation of Sulphuric Acid from SO_2 and the Roles of O_2 and NO_x

The effect of SO_2 depends on its state. If SO_2 is dissolved and oxidized to form sulphuric acid, it will be highly reactive. The oxidation depends on the availability of O_2. Although the formation of sulphuric acid through disproportionate reaction of SO_2

$$4SO_2 + 4H_2O \rightarrow 3H_2SO_4 + H_2S. \quad (3.1)$$

and oxidation of SO_2 by mineral oxides such as hematite have been proposed, they are not considered to be important in the scenarios of the present study. In CO_2 streams from oxyfuel combustion and post-combustion capture plants the concentration of O_2 will be higher than SO_2, according to the data provided by IEA GHG (Table 1.1). Moreover, in these streams NO_x will also be present. NO_x is known to catalyze SO_2 oxidation and hence formation of sulphuric acid according to the lead chamber process for production of sulphuric acid:

$$2NO_2 + H_2O \rightarrow HNO_2 + HNO_3 \quad (3.2.1)$$

$$SO_2 \text{ (dissolved)} + HNO_3 \rightarrow NOHSO_4 \quad (3.2.2)$$

$$NOHSO_4 + HNO_2 \rightarrow H_2SO_4 + NO_2 + NO \quad (3.2.3)$$

$$SO_2 \text{ (dissolved)} + 2HNO_2 \rightarrow H_2SO_4 + 2NO \quad (3.2.4)$$

$$2NO + O_2 \rightarrow 2NO_2 \quad (3.2.5)$$

NO_2 is soluble in water but NO is barely soluble. For the catalytic process to proceed, the oxidation of NO to NO_2 is essential. The rate of the process depends on various factors such as concentrations of reactants and products, pressure and temperature. To carry out a simulation to evaluate the rate of SO_2 conversion substantial information about the rate constants is required. Moreover, based on our past experience with NO_x and SO_x interactions, we believe these reactions are enhanced on surfaces (liquid and/or solid) (Preto *et al.*, 2004). The surface effect is hard to quantify, but is likely important in rock pores where the ratio of available surface, be it solid or liquid, to the gas phase is high. As the maximum effect of NO_x is to oxidize all SO_2, we assume that all SO_2 can be converted to sulphuric acid and the concentration of SO_4^{2-} ions is equal to that of dissolved SO_2, when NO_x and O_2 are present.

3.1.2 A Simple Model for Evaluation of the Effect of SO_2 on Reduction of Pore Porosity

Here we consider a simple model for a quick estimate of the contribution of SO_2 to the reduction of rock porosity. Because CO_2 in its supercritical state does not mix with water, the water is displaced by injected CO_2. This results in the development of a dry-out zone starting from the injection well (see, *e.g.*, André *et al.*, 2007; Burton *et al.*, 2008; Gaus *et al.*, 2008; Pruess and Müller, 2009; Pruess 2009). In the dry-out zone there may be some trapped water or residual water, but the water would remain immobile and evaporate into the CO_2 phase. Therefore, in the dry-out zone there is no moving water phase. Between the dry-out zone and the front of the CO_2 phase, there is a two-phase flow region where CO_2 and water flow in separate phases. This picture is essentially the same as the one described by Pruess (2009) for injection of pure CO_2, except that the precipitation of salt due to the dry-out is not included. A simplified sketch is shown in Figure 3.1 for a one-dimensional illustration (it will be understood that the concept should also be valid in 3-D cases). SO_2 dissolves into water in the two-phase region and the front of the plume, lowering the pH of the water and causing dissolution of minerals. If the concentration of precipitate-forming positive ions is low, only dissolution will occur and the dissolved ions are carried by water which is pushed by the plume, building up the concentration. Once the concentration of the dissolved species reaches the level for sulphates to precipitate, the precipitation starts. From this point a quasi-steady state is established (the expression ‘quasi’ is used here because the velocity of the front would slow down with time under constant injection rate). The dissolution and precipitation of minerals occur simultaneously and the consumed SO_4^{2-} ions are constantly made up by dissolution of SO_2 from the plume. For a given location ahead of the plume, the dissolution and precipitation start with the arrival of the front of the two-phase zone, and cease once the front of the dry-out zone passes. The dissolvable minerals remaining in the dry-out zone will not contribute to the formation of sulphates, as there is no water and the dry SO_2 passing by is much less reactive compared with the wet situation (we will establish that porosity change due to sulphation by dry SO_2 is insignificant, at least in the injection period). Local dissolution and precipitation may still occur in immobile water left in the dry-out zone, but there is no migration of minerals, and the effect is far more limited

compared with the case where SO_2 constantly passes with water. Thus, the reaction of SO_2 is important only for a limited period of time.

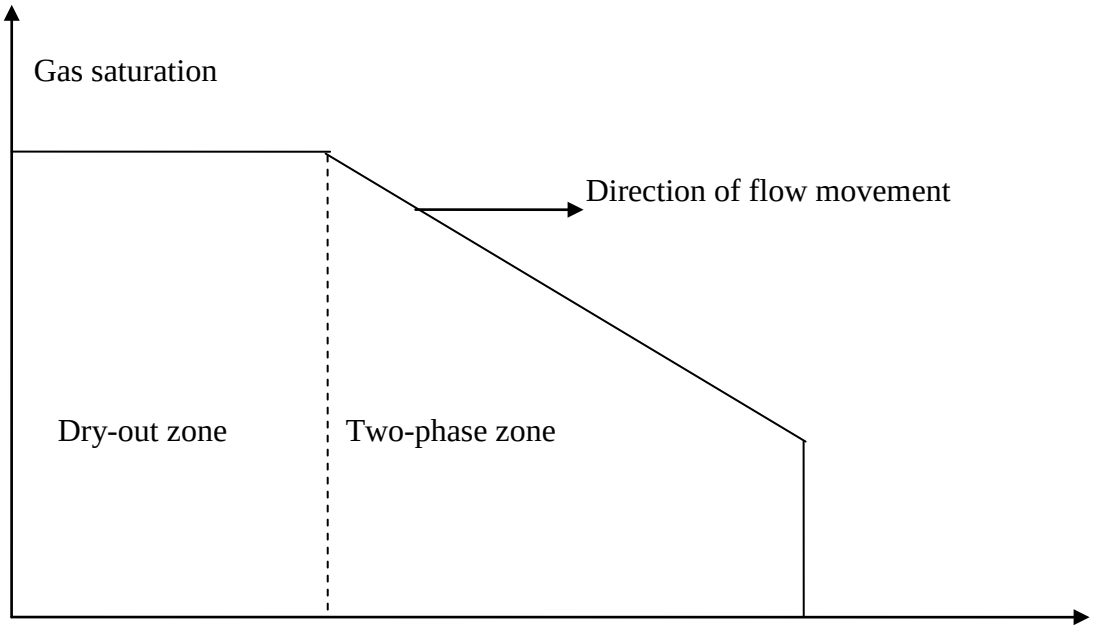

Figure 3.1 Simplified sketch for the movement of injected CO_2.

As can be understood from the above discussion, once the quasi-steady state is established, the rate of dissolution will be equal to the rate of precipitation, and there is no migration of dissolved minerals. These rates depend on mineral species and SO_2 concentration. If the dissolution is very slow, the quasi-steady state will start late. In the extreme case, when the quasi-steady state starts after the injection period ends, there will be no decrease but only increase of porosity, because there is no precipitation. With faster dissolving species, the quasi-steady state starts earlier and more precipitation takes place. The decrease of porosity is of greater concern with fast-dissolving and precipitating species. As calcite and calcium sulphate are representative of such species, we discuss this pair first. The discussion would be relevant to carbonate formations. We will show later that our method also has application in sandstone formations.

Rate constants and equilibrium constants for the dissolution of calcite and precipitation of anhydrite can be found in the literature. Numerical simulations are possible in principle. However, the results would depend on many factors, such as pH, salinity, rock compositions, to mention a few. Such results would be difficult to generalize. As stated, we want a quick estimate of the porosity change for given SO_2 impurity levels, and for this purpose a simple analytical relationship is desirable.

The rate of $CaSO_4$ precipitation depends on the concentration of Ca^{2+} and SO_4^{2-}, but it will not exceed the rate of SO_2 supply. As a limiting case, we consider that all SO_2 passing the reaction zone, *i.e.*, from the front of the two-phase zone to the front of the

dry-out zone, is converted to a precipitate of $CaSO_4$. Because under the quasi-steady state conditions the dissolution and precipitation occur at the same time, the effect on the pore volume is related to the volume change for dissolved $CaCO_3$ to convert to $CaSO_4$. The molar volume of $CaSO_4$ and $CaCO_3$ is 46 and 36.7 cm^3/mol, respectively. The resultant volume increase due to the conversion is 9.1 cm^3/mol.

As illustrated in Figure 3.2, under the quasi-steady state, when the front of the dry-out zone advances a distance *dL*, the front of the two-phase zone also advances *dL*. Since the advance is accompanied with $CaSO_4$ precipitation in the incremental element 2 of the two-phase zone, the consumed SO_4^{2-} is made up by SO_2 from element 1. However, the change can also be viewed as moving element 1 to the position of element 3. After the front of the two-phase zone moves the full length of this zone L, the front of the dry-out zone will also advance the distance L. By denoting dV_p the volume change due to precipitation of $CaSO_4$ in the incremental element, and dV_ϕ the total pore volume of the incremental element, under conditions of the aforementioned quasi-steady state and total conversion of SO_2 to sulphate there should be

$$\frac{dV_P}{dV_\phi} = \frac{(\gamma_{SO2}\dot{M}/\rho)dt}{\phi A dL} \tag{3.3}$$

where $\dot{M}$ is the mass flow of the supercritical phase, γ_{SO2} is the volume fraction of SO_2 in this flow, ρ is the density of the flow, dt is the time increment corresponding to the advance dL, ϕ is the porosity of the rock in the zones, and A is the cross section area.

As $\frac{\dot{M}}{\rho\phi A} = \frac{dL}{dt}$, we have

$$\frac{dV_P}{dV_\phi} = \gamma_{SO2} \tag{3.4}$$

That is, the precipitation is constant and equal to the fraction of SO_2 in the plume, independent of the velocity of the plume and the porosity of the rock. In reality, the conversion of SO_2 to $CaSO_4$ would depend on the moving velocity of the plume: more $CaSO_4$ would form when the plume moves more slowly. However, the maximum conversion limit is γ_{SO2}. With this relation we can estimate the effect of SO_2 on the porosity. By considering that all SO_2 which passes the two-phase zone is consumed by precipitation, the porosity decrease due to SO_2 is $(\frac{9.1\gamma_{SO2}}{w/\rho})$, where *w* is the molar weight (g/mol) of the flow of CO_2 mixture. The estimate of the porosity change increases with pressure and SO_2 fraction. For a high-end estimate we use the CO_2 stream with 2.9 vol % SO_2 (the stream considered in the previous IEA GHG report PH4/32) at 20 MPa and 330K. The resulted pore volume decrease due to SO_2 is 0.44%. It should be emphasized

that this is for the extreme case where SO_2 conversion to $CaSO_4$ is 100 percent. In other words, the maximum effect of SO_2 on the injectivity under the discussed conditions is to decrease the porosity by 0.44%, which is still much less significant compared with the wet cases.

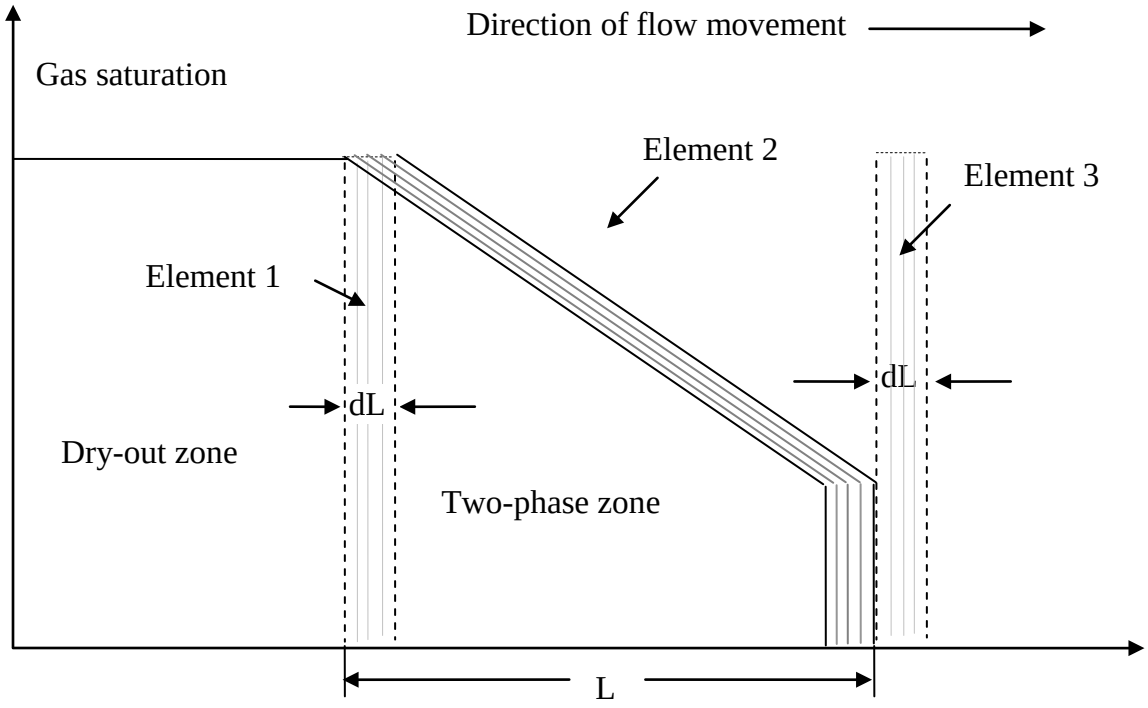

Figure 3.2 Sketch for determination of SO_2 conversion to $CaSO_4$.

For precipitation of other sulphates, such as alunite in sandstone formations (Xu *et al.*, 2007), similar analyses can be made to estimate the impact on the porosity. The key point is that in the two-phase zone, the reaction of SO_2 is limited. Moreover, dissolution accompanies precipitation and the related pore volume decrease is much smaller than in the wet cases, where dissolved species migrate and precipitate in the downstream. With the dry-out effect, precipitation of alunite, which is shown to cause substantial porosity reduction by simulation studies for a "wet case" of sandstone formation (Xu *et al.*, 2007), would not cause much decrease of pore volume. As an example we consider the following thermodynamically-plausible reaction for alunite formation, where the reactants (except dissolved gas species) and products are primary and secondary rock minerals, respectively, of the sandstone formation (Xu *et al.*, 2007):

$$KAlSi_3O_8 + Mg_5Al_2Si_3O_{10}(OH)_8 + 2SO_2 + O_2 + 5CO_2 = KAl_3(OH)_6(SO_4)_2 + 5MgCO_3 + 6SiO_2$$

(K-feldspar) (chlorite) (alunite) (magnesite)

$$\Delta G = -546 \text{ kJ/mol} \qquad (3.5)$$

where ΔG is the change of Gibbs free energy. With the 2.9% SO_2 discussed earlier, the estimated volume decrease associated with the precipitation of alunite is 5.6%. This is a significant decrease, but the value is still less than a quarter of the value calculated from the result of Xu *et al*. (2007). This example again demonstrates that, when the precipitation and dissolution occur simultaneously, the volume effect would be much smaller in comparison with the "wet case".

An important consideration of our model is that SO_2 would not cause dissolution and precipitation of minerals without liquid water. Dry gas injection has been known to cause evaporation of water and precipitation of salts, resulting in reduced injectivity (see, *e.g.*, Pruess and García, 2002; Giorgis *et al.*, 2007; Motealleh and Bryant, 2007; Zuluaga and Lake, 2008), and injection of dry CO_2 could cause the same phenomena (see, *e.g.*, Giorgis *et al.*, 2007; André *et al.*, 2007; Burton *et al*., 2008; Gaus *et al*., 2008; Pruess and Müller, 2009; Pruess 2009). Our model does not include the reduction of injectivity due to the precipitated salts other than sulphates related to SO_2. However, our results suggest that, compared with the predicted effect of the precipitated salts, where the resulted porosity reduction could be over 50% (see, *e.g.*, Burton *et al*., 2008), the effect of SO_2 is insignificant.

Bryant and Lake (2005) have discussed the effect of SO_x and NO_x on CO_2 injectivity, and suggested that the net change in pore volume is likely to be small, and thus the effect on injectivity is likely to be insignificant. With our simple model such suggestions can be verified readily.

A recent study on dissolution of SO_2 impurity from injected CO_2 plume in formation water concludes that even after 1000 years, 65 to 75% of the SO_2 will remain in the CO_2 phase due to mass transfer limitation (Crandell *et al*., 2010). This slow release of SO_2 would largely reduce its impact on brine pH. Although this work does not concern chemical reactions, according to its conclusion SO_2 dissolution into the water will be slower than previously considered. Since low concentration leads to less dissolution and precipitation, the impact of the less than 100 ppmv SO_2 in the present study (see Table 1.1) due to the dissolution/precipitation mechanism would be even less.

3.1.3 Reaction of SO_2 with Rocks in the Dry-Out Zone

Having discussed the reactions of SO_2 with the presence of water, now we consider the reactions of SO_2 in the dry phase. Sulphation of $CaCO_3$ according to

$$CaCO_3 + SO_2 + ½\ O_2 = CaSO_4 + CO_2 \qquad (3.6)$$

has been studied at high temperatures for the application of sulphur removal using limestone from pressurized combustors. At ambient temperature the reaction is thermodynamically favoured but likely too slow to be detected. Based on reported values of rate constants and activation energy determined at high temperatures (Hu *et al.*, 2006), a calculation suggests that sulphation in the gas phase will be slower by some 5 orders of magnitude than in the water phase. It should be noted that in the dry-out zone there can

be some water vapour due to evaporation of immobile water, which would increase the reactivity of SO_2. However, since there is no liquid phase, dissolution and migration of reaction products would not occur. Moreover, if the sulphation does take place, the rate would drop greatly once a layer of $CaSO_4$ forms - because of the larger volume of $CaSO_4$ it will form a dense surface layer and retard mass transfer. For the above reasons it does not appear that sulphation by dry SO_2 will be important for the injectivity, as the injection period may end before the effect can be observed.

3.1.4 The Possibility of Pore Plugging by Elemental Sulphur

Co-injection of H_2S, as mentioned earlier, has been practiced for 20 years in Canada. There were also occasions of injection with water. We have not found any reports of injectivity issues with the co-injection. There have been a number of incidents of acid gas breakthrough at neighbouring producing wells instead. In the absence of O_2, formation of pore-plugging sulphates would be limited. However, if SO_2 and H_2S are co-injected, such as in the case where the same storage site receives CO_2 streams from both pre-combustion removal plants and post-combustion capture plants, a concern has been raised over the possibility of the occurrence of the Claus reaction

$$2H_2S + SO_2 = 3S + 2H_2O \quad (3.7)$$

which would result in deposition of solid sulphur in the rock pores. This reaction can occur at temperatures close to that of CO_2 storage operation: it has been reported that the reaction could take place at temperatures as low as 40-60°C (Ledoux *et al.*, 2000). The reaction needs a catalyst, but it can be catalyzed by alumina on silica. Potential catalytic sites exist in formation rocks such as clay surfaces. Unlike the case of SO_2 in the dry-out zone discussed earlier, the Claus reaction can take place in the gas phase, and produce water. Therefore, the dry-out zone does not exclude the possibility of this reaction occurring, and the reaction may last for the whole period of injection operation. It does not require minerals as reactants and the pore volume decrease due to formation of sulphur could be significant. However, without catalysts the rate of the reaction may become insignificantly low. Thus, in the case the reaction is catalyzed by minerals in the rock pores, after depositing a thin layer of sulphur the rate would drop because of reduced contact with catalysts. How low the rate of the reaction will be without catalysts is unclear. Another matter is that the formation of elemental sulphur will be reduced by H_2, which co-exists with H_2S in CO_2 streams from pre-combustion capture. With the reaction

$$H_2 + S = H_2S \quad (3.8)$$

the deposition of elemental sulphur should be alleviated. In this scenario the impurity H_2 has a positive effect. Finally, O_2, which co-exists with SO_2, could play a positive role by:

$$3O_2 + 2H_2S = 2SO_2 + 2H_2O \quad (3.9)$$

$$O_2 + S = SO_2 \quad (3.10)$$

thus preventing or reducing sulphur deposition. On the other hand, potentially H_2 and O_2 may react to form water if catalyzed and be unavailable for the above reactions.

Unfortunately, there are many uncertainties in this reacting system. Given the potential of the Claus reaction to severely reduce the injectivity of CO_2 over many years, we recommend investigating the envisaged reaction system experimentally under CO_2 injection conditions, and we ourselves have plans to do this.

3.2 Reactions with Caprocks and Mineral Sequestration of CO_2

Unlike the injectivity issue, which concerns only a relatively short period of time, the impacts of impurities on the integrity of caprocks need to be considered over the long term. Moreover, reactions in the presence of water need to be assessed, as the acid-forming impurities would dissolve in water eventually together with CO_2, given a sufficiently long time. For carbonate rocks the effects of reactive impurities such as SO_2 and NO_x have already been discussed. In the presence of water they would form H_2SO_4 and HNO_3 and promote dissolution of rocks. H_2SO_4 may also cause precipitation but HNO_3 will not. Unless these impurities are all retained by formation water before they reach the caprock in the CO_2 plume, they would negatively impact on caprock integrity.

Thermochemical evaluations are deemed useful for the study of the long-term effects, because the reactions with minerals can be very slow. We have made assessments for the reactions using thermochemical calculations. Regarding caprock integrity, we have used quartz, K-feldspar and limestone as model species, with the latter two representing reactive constituents for sandstone and carbonate caprocks, respectively, which are susceptible to acid attack. Quartz is used to represent pure sandstone. According to our results dissolution of quartz is not affected by SO_2 and NO_x thermochemically. In the case of K-feldspar, whose dissolution has been well studied in modeling of the impact of CO_2 injection on caprocks (see, *e.g.*, Johnson *et al.*, 2002; Gaus *et al.*, 2005), the dissolution increases slightly in the presence of SO_x and NO_x. The most pronounced effect of SO_x and NO_x is seen in limestone, where the dissolution increases by 50% with the presence of 1.5 vol % total concentration of SO_x and NO_x. However, the effect decreases with decreasing concentration. When the total concentration of SO_x and NO_x in the CO_2 stream is reduced to below 200 ppm, as in the case considered by IEA GHG, the increase in the dissolution becomes negligible. The calculation results will be shown later in the section of evaluations for selected scenarios.

The effect of O_2 would be mainly related to oxidation of SO_2 to form H_2SO_4 and oxidation of NO to form NO_2 and hence HNO_3. By itself O_2 can react with certain minerals. As an example, dissolved O_2 can combine with minerals in rocks which contain reduced forms of iron, manganese, etc., causing decomposition of the rocks. If the only iron mineral is hematite, for instance in the case studied by Xu *et al.* (2007), O_2 would have no impact. If dissolved ferrous ions are present in the water, however, O_2 could react with them to form ferric oxide-hydrate or ferric hydroxide, which has the potential to block permeable formations even in small quantities (Zettlitzer *et al.*, 2010). Oxidation of sulphides in rocks can produce sulphates. For example, oxygen can react with pyrite (FeS_2) to form $FeSO_4$. The sulphate, $FeSO_4$, is soluble in water (*ca.* 260 g/L at 50°C). This would result in very acidic local pockets, facilitating dissolution of the rock. If the oxidized location is not in contact with bulk water, hydrates which are soluble would form. The resultant mechanical stress in the rock may lead to cracks. However, the above

reaction requires relatively large amounts of O_2. In the case of low O_2 levels, or where most O_2 has been consumed by oxidation of metallic minerals and/or retained in the residual CO_2 phase (unlike the acidic impurities, O_2 has low solubility and would stay in the CO_2 phase) before the plume reaches the top rock, the impact on caprock integrity would be limited. Alternatively, if the caprock has low sulphide content, the impact of O_2 would also be expected to be small.

Concerns over the chemical effects of two other impurities CO and H_2 have also been raised (Jacquemet *et al.*, 2009). As has been discussed, CO is highly reductive and can be easily oxidized to CO_2. Particularly, in water CO can be oxidized by the reaction

$$CO + H_2O = CO_2 + H_2 \quad (3.11)$$

As a result, the concentration of CO should be low. H_2 is also reductive but not toxic nor corrosive. CO and H_2 may react with certain minerals, *e.g.*, $CaSO_4$ and reduce it to CaS, but dissolution and precipitation will not be involved. With regard to chemical effects, CO and H_2 are not expected to be as important as SO_2, NO_x and H_2S.

As for other impurities shown in Table 1.1, COS exists in trace amounts in CO_2 streams from pre-combustion capture. It can decompose to CO and H_2S and its toxicity is lower than those two species. NH_3 can exist in ppm levels in CO_2 from post-combustion capture. In water it can form NH_4OH which is weakly basic and can increases the pH; however, given the likely low concentration level such effects are expected to be limited.

3.3 Corrosion of Well Materials

Reactive impurities themselves will increase the corrosion potential. Dissolved oxygen is known to be a major source of corrosion by water. H_2S, SO_2, NO_2 are all corrosive. In addition, chlorine is very corrosive for pipeline and concrete structures. In oxyfuel combustion, coal chlorine will be released to the gas phase as HCl. However, most of the chlorine can be removed together with condensed water. Under high-pressure conditions of transport and injection, the partial pressure of the low-concentration impurities could increase to significant levels, leading to increased corrosion potential. The impurity effects on steels have been addressed in a recent IEA GHG report (IEA GHG 2010).

Acid solutions are very corrosive for cements. The most corrosive acids in this regard are believed to be those that produce easily soluble calcium salts, such as nitric, hydrochloric or acetic acid (Pavlík, 2000). The acids react with hydrated cement compounds and unhydrated cement residues, leaching out the prevailing calcium ions into the solutions. A soft and porous layer of decalcified corrosion products remains on the surface, which has practically no binding and protective properties (Pavlík and Unčík, 1997).

NO_x in CO_2 streams would be very harmful to cements because of its relatively high concentration (from oxyfuel combustion) and the resultant HNO_3, whose calcium salts are soluble. Moreover, sulphuric acid or sulphate attack on cements is well known (see, *e.g.*, Gaus *et al.*, 2008). Sulphates, HSO_4^- and SO_4^{-2}, react with cements to produce additional gypsum, $CaSO_4.2H_2O$, and ettringite, $(CaO)_3(Al_2O_3)(CaSO_4)_3 \cdot 32H_2O$, which

could cause volume expansion and loss of cohesion of the cement matrix, leading to cracking, pitting and spalling. As SO_2 in the CO_2 streams has a high potential to form sulphates when NO_x and O_2 are present, the damaging effect of SO_2 on cements is anticipated. Once the protection by cements is lost, the steel casings of the wells would be under attack by acids and O_2. Through the damaged cements and/or damaged casings, leakage of injected CO_2 with toxic impurities could occur.

In acid gas injection operations in western Canada, H_2S and CO_2 are co-injected into deep hydrocarbon reservoirs and saline aquifers, with the H_2S content ranging from 2 to 83%. Bachu and Gunter (2004) pointed out that as H_2S is more corrosive than CO_2, the success of acid-gas injection operations indicates that the engineering technology for CO_2 geological storage is in a mature stage. However, the acid gas does not contain SO_2, NO_x and O_2. With these impurities CO_2 would be more corrosive than with H_2S alone. Small amounts of SO_2, NO_x and O_2 have been injected with CO_2 into oil reservoirs since at least the 1960s, according to a review by Taber (1985), but the concentration ranges are not known. Taber (1985) noted that operators of the injections normally insisted that the SO_2 and NO_x concentrations be reduced to minimize corrosion before the gas went through the high-pressure stages in the compressors. Corrosion of wells was not mentioned, and presumably was not a concern as long as the compressors do not fail. However, we have not found reports subsequent to Taber's on injection of SO_2, NO_x and O_2. Very recently a review on sulphur from oxyfuel combustion (Stanger and Wall, 2011) briefly discussed the effect of SO_2 on CO_2 storage, where only Taber's work was cited, suggesting no other significant reports have been available.

As the impurities are much less reactive in the absence of water, during the injection period, corrosion may not be a severe issue owing to the desiccation of the well zone. However, after the injection period when water is once again present, the acidic impurities would increase the corrosion. In the case that the steel casings are taken out prior to well abandonment (IEA GHG, 2010), only corrosion of the cements needs be assessed. The corrosive effects of the impurities in the high-impurity oxyfuel CO_2 stream are assessed in the section of evaluation for selected scenarios.

4. Fate of Hazardous Impurities

Table 4.1 shows the fate of several hazardous impurities according to thermochemical calculations using the software and database package FactSage™ for selected conditions. CO, SO_2, H_2S and NO_x would form dissolved and/or precipitated species, although it can take a very long time for these species to form. Elemental mercury is volatile at combustion temperatures and present in CO_2 streams from oxyfuel combustion. However, at lower temperature it can be adsorbed and oxidized, by coal chlorine, for example, on solid surfaces. The oxidized mercury species are soluble. Based on the calculated results of Table 4.1, the end products are all dissolved species. Therefore, as long as the brine does not contaminate fresh-water aquifers, the Hg would be retained in the aqueous phase.

In the event of CO_2 leakage, the dissolved hazardous impurities could be released and enter the atmosphere together with CO_2. However, since CO_2 at high concentrations is

hazardous by itself if breathed in for prolonged periods, causing adverse health effects varying from headache to death (see, *e.g.*, United States OHSA Regulated Hazardous Substances Vol. 1), the effects of the impurities may become a secondary issue. This will be assessed in another study.

Table 4.1 Fate of reactive impurities according to thermochemical calculations*.

Species	End Product
CO	$CaCO_3$, CO_2(aqueous), HCO_3^-, CO_3^{2-}
SO_2	$CaSO_4$, SO_4^{2-}, HSO_4^-
H_2S	H_2S(aqueous), HS^-, SO_4^{2-}, HSO_4^-
NO_x	NO_3^-,NO_2^-, HNO_2
Hg	$HgCl^+$, $HgCl_2$, $HgCl_3^-$, $HgCl_4^{2-}$

* Calculated using FactSage™ for the conditions of 330 K, 10-20 MPa, 1 molal CO_2 and 50000 mg/L salinity.

Another important point is that the recommended impurity limits for CO_2 transport (Table 1.2) have taken into account short-term exposure limits for H_2S, CO, SO_x and NO_x in CO_2. The limits give the maximum amount of a substance that one can be exposed to without adverse health effects for 15 minutes. As can be seen from Tables 1.1 and 1.2, in the CO_2 streams considered by IEA GHG, the concentrations of H_2S, CO, SO_x are lower than the recommended levels and the concentration of NO_x is the same as the recommended level. Therefore, at least for short-term exposures, the hazard of the impurities leaked from storage sites is less than that due to sudden leakages from pipelines.

5. EOR and Depleted Gas Fields

In the above discussions we have focused on CO_2 storage in saline formations, which have the largest storage potential. For EOR and depleted gas fields, CO_2 streams from oxyfuel combustion with high levels of O_2 may be a concern. Pipitone and Bolland (2009) discussed O_2 concentration requirement for EOR, and showed that O_2 in three existing EOR projects is at ppm levels. Higher O_2 concentration can cause:

1. Overheating at the injection point;
2. Oxidation in the reservoir with higher oil viscosity and increased extraction cost;
3. Increased biological growth with unknown effects on oil production.

They also recommended that due to the lack of fundamental research development and industrial experience, acceptable tolerance to O_2 should be evaluated case by case.

High level of O_2 would promote the growth of aerobic bacteria, which cause biodegradation of crude oil and adversely affect oil recovery and refining (see, *e.g.*, Palmer, 1993; Jones *et al.*, 2008). The bacteria, along with other types of bacteria which

do not require O_2, would also cause corrosion and plugging of equipment and injection wells (see, *e.g.*, Collins, 1977).

Wilkinson *et al.*(2010) discussed the risk of formation of elemental sulphur when O_2 contacts H_2S. This is the same issue related to the Claus reaction discussed earlier.

As has been mentioned earlier, small amounts of SO_2, NO_x and O_2 have been injected with CO_2 into oil reservoirs for more than 30 years (see, *e.g.*, Taber, 1985). Although the concentrations were not reported, according to an IEA GHG expert's information, in at least one instance, O_2 at about 2% concentration level has not affected the EOR operation.

With the low-impurity oxyfuel stream (Case 3 in Figure 1.1) where O_2 concentration is 100 ppm, no negative impacts are foreseen for either EOR or depleted gas field operations. Bryant and Lake (2005) have discussed the effect of SO_x and NO_x on EOR, with respect to the factors which affect the effectiveness of the operations such as minimum miscibility pressure, mobility ratio and gravity number. The conclusion is that the impurities at typical flue gas levels are unlikely to affect the recovery adversely. Regarding depleted gas fields, Nogueira and Mamora (2008) studied experimentally the effects of flue gas impurities, including N_2, O_2, H_2O, SO_2, NO_2, and CO, with the conclusion that injection with less than 1 vol % impurities would have little effect on the volume of CO_2 to be stored, but allow savings of separation cost.

6. Evaluations of Selected Scenarios

As the impact of impurities increase with their concentrations in the CO_2 streams, and oxyfuel streams have the highest levels of both non-condensable impurities (*ca*. 15 vol % N_2, O_2 and Ar) and most acidic impurities (NO_x and SO_x) (Table 1.1), we use the high-impurity CO_2 stream from oxyfuel combustion to assess significant impurity effects for selected cases in the following.

6.1 Storage Capacity and Injectivity under Representative Reservoir Conditions

The most significant impact is reduction of storage capacity. IEA GHG sponsored a study of storage coefficients for CO_2 storage in deep saline formations and depleted hydrocarbon reservoirs (Gorecki *et al*., 2009), aiming at more accurate estimation of storage capacity of available resources. We have applied our findings to estimation of storage capacity for several representative cases evaluated in that IEA GHG study. In Table 6.1, storage conditions and storage coefficients for the representative cases are shown, where the storage coefficient is defined as

$$E = \frac{G_{CO2}}{V_{CO2}\rho_{CO2}} \tag{6.1}$$

where G_{CO2} is the estimate of storage capacity in terms of CO_2 mass, V_{CO2} is the total pore space available for CO_2 storage and ρ_{CO2} is the density of CO_2. As can be understood, the estimate of storage capacity is based on pure CO_2. With non-condensable impurities in the CO_2 stream the storage capacity will be smaller. Here we introduce an impurity factor F for estimation of the storage capacity for impure CO_2:

$$G_{CO2} = V_{CO2}\rho_{CO2}EF \tag{6.2}$$

where F is the ratio of the CO_2 storage capacity in the presence of impurities to that in the absence of impurities. This ratio is numerically equal to the normalized storage capacity defined by Equation 2.5. The value of F is evaluated for each case in Table 6.1 and shown in the last column. As can be seen, in the shallow formation with a depth of 895 m the CO_2 storage capacity drops to about 40% of that for pure CO_2. In other words, more than double the number of storage resources will be required for storing the same quantity of CO_2 in the high-impurity stream.

Table 6.1 Effect of impurities on CO_2 storage capacity

Cases	Depth (m)	P (MPa)	T (°C)	T grad (°C/m)	E[a] (-)	Storage Capacity (kg CO_2/m^3 pore)		F[b] (-)
						Pure	Impure	
Shallow-Low Temp	895	9.2	33	0.020	0.07	647.68	253.96	0.392
Shallow-Mid Temp	895	9.2	38	0.025	0.10	540.97	231.20	0.427
Shallow-High Temp	895	9.2	45	0.033	0.09	364.48	208.72	0.573
Median-Low Temp	2338	24	62	0.020	0.12	750.04	550.35	0.734
Median-Mid Temp	2338	24	75	0.025	0.13	675.00	493.67	0.731
Median-High Temp	2338	24	92	0.033	0.13	584.92	432.23	0.739
Deep-Low Temp	3802	38.8	92	0.020	0.15	777.66	611.13	0.786
Deep-Mid Temp	3802	38.8	113	0.025	0.16	700.29	551.25	0.787
Deep-High Temp	3802	38.8	141	0.033	0.17	611.35	485.19	0.794

[a] Storage coefficient.
[b] Capacity factor given as the ratio of the CO_2 storage capacity in the presence of impurities to that in the absence of impurities.

However, as the depth of the formations increases, the effect of impurities on CO_2 storage capacity decreases. As shown in Table 6.1, at a depth of 3802 m, the capacity approaches 80% of that for pure CO_2.

The effects of the impurities on CO_2 injectivity, based on Equation 2.17, are shown in Table 6.2. As has been discussed earlier, the injectivity is dependent on density and viscosity. As the impure CO_2 stream has lower viscosity, the effect of lower density is

partly compensated and the injectivity reduces by a smaller degree compared with the storage capacity. Both the density and viscosity increase with pressure and decrease with temperature, and the resultant injectivity is relatively insensitive to the depth of injection. For the scenarios of Table 6.2: the relative injectivity at the median temperature changes little with increasing depth. It can also be seen that the relative injectivity is less sensitive to temperature at greater depths. This would be generally true, as the density difference of pure and impure CO_2 decreases with increasing pressure, and the viscosity difference decreases with increasing temperature, which corresponds to increasing depth.

Table 6.2 Effect of impurities on CO_2 injectivity

Cases	Depth (m)	P (MPa)	T (°C)	T grad (°C/m)	Viscosity[a] (-)	Injectivity[b] (-)
Shallow-Low Temp	895	9.2	33	0.020	0.38	1.0
Shallow-Mid Temp	895	9.2	38	0.025	0.45	0.94
Shallow-High Temp	895	9.2	45	0.033	0.77	0.74
Median-Low Temp	2338	24	62	0.020	0.72	1.0
Median-Mid Temp	2338	24	75	0.025	0.75	0.98
Median-High Temp	2338	24	92	0.033	0.79	0.93
Deep-Low Temp	3802	38.8	92	0.020	0.81	0.97
Deep-Mid Temp	3802	38.8	113	0.025	0.83	0.95
Deep-High Temp	3802	38.8	141	0.033	0.87	0.91

[a] Relative viscosity given as the ratio of the viscosity in the presence of impurities to that in the absence of impurities.

[b] Relative injectivity given as the ratio of the injectivity in the presence of impurities to that in the absence of impurities.

6.2 Storage Integrity

With regard to the chemical effects of impurities, dissolution of caprock, a major concern related to storage integrity has been evaluated by use of representative rock minerals. As has been mentioned earlier, dissolution of quartz is not affected thermodynamically by acid impurities. The results of thermochemical calculations (using the software and database package FactSage^{TM}) for dissolution of K-feldspar and calcite and formation of secondary minerals are shown in Tables 6.3 and 6.4. As can be seen, the effect of SO_x and NO_x on K feldspar dissolution is small. With 5000 ppm SO_x + 1 mol% NO_x, the dissolution increases only by about 3.5%. When the total concentration of SO_x and NO_x is reduced to 150 ppm, the effect on dissolution is negligible. Moreover, potential secondary minerals dawsonite and muscovite would result in cementation of the surface layer of the rock and thus compensate for the effect of dissolution. In the case of calcite, the impurity effect is appreciable. With a total SO_x and NO_x concentration of 1.5 mol%

the dissolution of calcite increases by 50%. However, the effect decreases quickly with decreasing concentration of the acid impurities. When the total concentration of SO_x and NO_x is reduced to 150 ppm, the difference with the pure CO_2 case is less than 0.4%. On the other hand, the precipitation of anhydrite is not significant and cementation of the rock would be limited.

Table 6.3 Dissolution of K-feldspar and formation of secondary minerals*

	K-feldspar dissolution (mol/L)	Dawsonite formation (mol/L)	Muscovite formation (mol/L)
CO_2 alone	1.8706	0.7774	0.3644
Impure CO_2			
50 ppm SO_x+100 ppm NO_x	1.8709	0.7773	0.3645
500 ppm SO_x+1000 ppm NO_x	1.8742	0.7772	0.3657
5000 ppm SO_x+1 mol% NO_x	1.9403	0.7763	0.3779

*Conditions: 50°C; 20 MPa; 50000 mg/L salinity; 100 g CO_2; 1 L H_2O; 4000 cm^3 $KAlSi_3O_8$; SO_x and NO_x are assumed to be fully oxidized to H_2SO_4 and HNO_3. All possible compounds in the FactSage™ database are considered as potential products.

Table 6.4 Dissolution of calcite and precipitation of anhydrite*

	Calcite dissolution (mol/L)	Anhydrite precipitation (mol/L)
CO_2 alone	0.03734	-
Impure CO_2		
50 ppm SO_x+100 ppm NO_x	0.03748	-
500 ppm SO_x+1000 ppm NO_x	0.03894	0.0001670
5000 ppm SO_x+1 mol% NO_x	0.05644	0.01052

*Conditions: 50°C; 20 MPa; 50000 mg/L salinity; 100 g CO_2; 1 L H_2O; 4000 cm^3 $CaCO_3$; SO_x and NO_x are assumed to be fully oxidized to H_2SO_4 and HNO_3. All possible compounds in the FactSage™ database are considered as potential products.

The impact of the acid impurities on injection wells is evaluated with regard to dissolution of $Ca(OH)_2$ and CSH (calcium silicate hydrate), the major cement components. As has been discussed, the greatest concern is over the post-injection stage, where acids formed in water attack well cements. The results of thermodynamic calculations for dissolution of $Ca(OH)_2$ and $Ca_3Si_2O_7{\cdot}3H_2O$ and formation of gypsum are shown in Table 6.5. With increasing concentration of SO_x and NO_x, calcium ion concentration in the solution increases and pH decreases consistently. The necessity of reducing the acid impurities is evident.

Table 6.5 Dissolution of $Ca(OH)_2$ and $Ca_3Si_2O_7{\cdot}3H_2O$ and formation of gypsum*

Solid species	Gas composition	$CaSO_4{\cdot}2H_2O$ formation (mol/L)	Ca^{++} in water (mol/L)	pH of water

$Ca(OH)_2$	CO_2 alone	-	0.00869	11.515
	50 ppm SO_x+100 ppm NO_x	-	0.00884	11.512
	500 ppm SO_x+1000 ppm NO_x	-	0.01026	11.479
	5000 ppm SO_x+1 mol% NO_x	0.00094	0.01911	11.344
$Ca_3Si_2O_7 \cdot 3H_2O$	CO_2 alone	-	0.4307	10.805
	50 ppm SO_x+100 ppm NO_x	-	0.4309	10.805
	500 ppm SO_x+1000 ppm NO_x	0.00074	0.4322	10.804
	5000 ppm SO_x+1 mol% NO_x	0.01096	0.4423	10.800

*Conditions: 50°C; 20 MPa; 50000 mg/L salinity; 100 g CO_2; 1 L H_2O; 4000 cm^3 $Ca(OH)_2$ or $Ca_3Si_2O_7 \cdot 3H_2O$ (approximate); SO_x and NO_x are assumed to be fully oxidized to H_2SO_4 and HNO_3. All possible compounds in the FactSage™ database are considered as potential products.

With 150 ppm total concentration of SO_x and NO_x, the Ca^{++} concentration in water increases by over 1.5% compared with the CO_2 - alone case with $Ca(OH)_2$, suggesting increased dissolution. By contrast, the Ca^{++} concentration with $Ca_3Si_2O_7 \cdot 3H_2O$ does not increase appreciably. The formation of gypsum is not predicted under this low acid-impurity level. The increase of calcium dissolution in $Ca(OH)_2$ is more significant than that seen in dissolution of calcite and K-feldspar. With the loss of the protection by cements, the steel casings will also be attacked. Appropriate measures for countering the adverse impact, such as improving cement sheath and casing quality (if the casings are not taken out) prior to sealing the wells, may be required.

7. Impact of Impurities on the Cost of CO_2 Storage

The most significant impact of impurities on the cost in the scope of the present study would arise from lower density of impure CO_2, which results in lower mass flow rate of CO_2 streams with given size of pipeline and lower injectivity. We have evaluated the impact of the impurities using a cost curve for CO_2 storage in North America developed by Dahowski *et al*. (2004). The cost curve is based on available data for over 300 onshore candidate geological reservoirs, including deep saline aquifers and depleted oil and gas fields, in the United States and Canada with estimated storage capacities. The storage cost, which includes the cost of injection and any offsetting revenue related to resultant enhanced oil or gas recovery, is given as a function of cumulative CO_2 to be stored. For deep saline aquifers it is assumed that the injection only requires injection wells. The cost curve shows that deep saline aquifers account for a majority of the storage capacity and the related storage cost is 12-15 USD per tonne CO_2, with an average of $12.5/tonne CO_2. In our estimation of the impact of the impurities on the cost, we consider that the lower injectivity of impure CO_2 requires an increase of the number of injection wells, assuming the wells are standardized for pure CO_2. From Table 6.2 we take an average value of injectivity 0.94 for impure CO_2 stream. To inject the same amount of CO_2 using the standardized wells, the number of the wells needs to increase to 1/0.94 = 1.06 times that for pure CO_2, and hence the cost of injection increases by 6%. The resultant cost curve for impure CO_2 is shown in Figure 7.1, along with the original cost curve for pure CO_2. In this figure the predominant flat portion corresponds to the storage cost in deep saline

aquifers. As this storage capacity is used up, the cost will increase drastically because more costly storage sites will be required. Here the impact of the storage capacity on the cost is seen, since impurities would cause a decrease of the storage capacity and the lower cost saline aquifers would be used up earlier. The storage capacity for impure CO_2 is taken as the average value in Table 6.1 (0.75 of the capacity for pure CO_2). It should be noted that the storage capacity of the original cost curve is based on the capacity of solubility trapping. As solubility trapping would only become important in the long term, on the order of hundreds to thousands of years (Dahowski *et al.*2004), we have transformed the curve in terms of structural trapping, which would be prevailing over the foreseeable period of CO_2 injection operations. Obviously, for lower-impurity CO_2 the average cost would lie between the two curves of Figure 7.1.

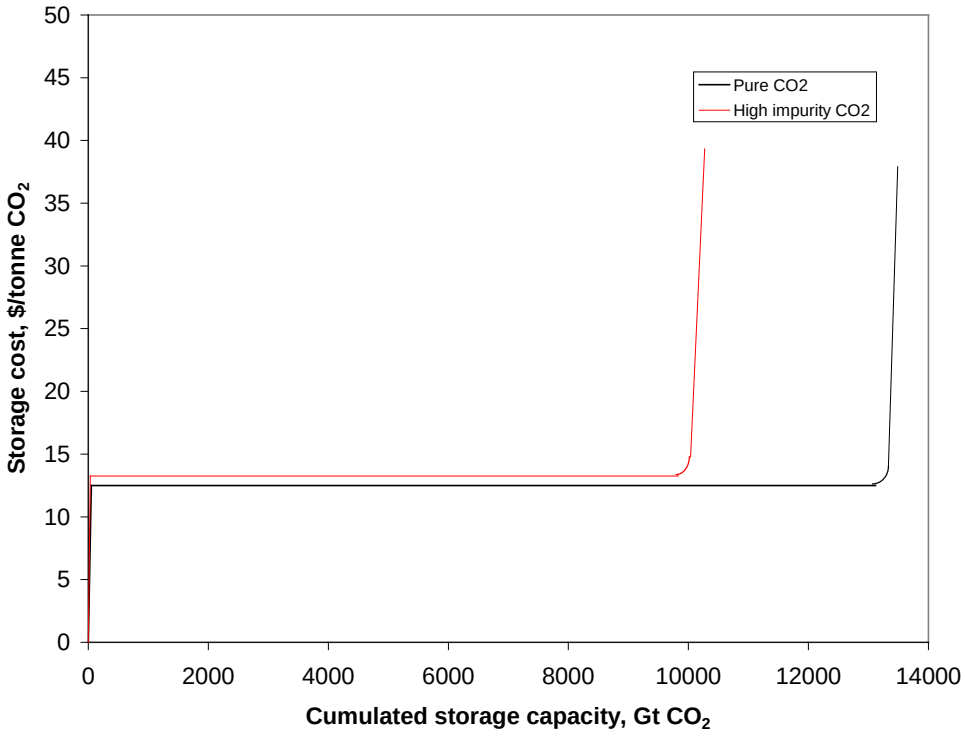

Figure 7.1 Impact of impurities on storage cost curve for North America.

It should be emphasized that Figure 7.1 is only for illustration purposes, as the analysis is very much simplified (based on the simplification by Dahowski *et al.*, 2004, where the storage cost is only related to injection wells), and the parameter values used in the calculations are subject to updating and improvement. Nevertheless, Figure 7.1 is qualitatively informative, particularly for understanding how the impurities alter the cost curves evaluated for pure CO_2. Clearly, with impurities the cost curves will be above those for pure CO_2, and the cumulated capacity corresponding to the start of the high cost range will decrease. Moreover, the concept should be applicable to produce more accurate cost curves with the development of more accurate costing methods.

8. Uncertainties and Recommended Studies

We have already discussed uncertainties with respect to the occurrence of the Claus reaction, which may plug the pores of formation rocks and reduce the injectivity. Other uncertainties of importance are discussed in the following.

8.1 The Accuracy of Equations of State

For pure CO_2 there are reported experimental P-V-T data and equations of states which are more accurate than cubic equations of state in the supercritical range. However, there are no data for CO_2 mixtures under the studied conditions. Equations of state require experimental data to calibrate parameter values, and the predicted results are expected to be reliable only in the calibrated range. In this study we have mainly used the Peng-Robinson equation for both pure CO_2 and the mixtures because of its relative simplicity. The results are not expected to be highly accurate. However, they are expected to be reasonable and show the correct trends. It is possible to use experimental data or more accurate equations of state for pure CO_2, but for mixtures no results of other equations of state can be proved to be better than that from the Peng-Robinson equation, as there are no data for validation. For accurate quantification of the effects of impurities, experimental data under the conditions of CO_2 storage operations are required both for calibration of the parameters of equations of state and validation of the predictions by the equations.

8.2 Viscosity

Viscosity affects injectivity and migration of the CO_2 stream. Several methods exist which enable calculation of the viscosity of gas mixtures under high pressure (Poling *et al.*, 2001). However, we have not found experimental data for gas mixtures under the conditions of the present study to validate the results.

Whereas the effect of impurities on the viscosity is not expected to impact CO_2 storage operations as much as in other regards, such as density and buoyancy, for computer simulations the viscosity value is required as a function of composition, pressure and temperature. Accordingly, experimental data in the storage operation range are needed to verify calculated results, modify calculation methods, or establish empirical formulas.

8.3 Effects on the Reactivity of Supercritical CO_2 Phase

In this study we have not considered the effects of impurities on the reactivity of supercritical CO_2 phase, particularly water-saturated supercritical CO_2 phase. Jacquemet *et al.* (2008) reported that a dry H_2S-CO_2 supercritical phase (66 mol % H_2S) at 50 MPa and 120-200°C showed significant reactivity with crushed cement. With regard to water-saturated supercritical CO_2, Choi *et al.* (2010) reported that addition of 4 mol % O_2 and 1 mol % SO_2 drastically increased the corrosion rate of a 13 Cr steel at 8 MPa and 50°C. Aqueous phase reactions have been the focus of the studies on the chemical reactions in CO_2 storage, and the observations of reactions in the supercritical CO_2 phases are new.

Given the low concentration levels in our studied CO_2 streams, we do not expect the effects of the impurities on the supercritical phase reactivity to be significant. However, investigation of such effects is certainly desirable.

8.4 Potentially Useful Properties of Impurities for Monitoring

As has been mentioned earlier, Bachu and coworkers (2009 a, b) investigated partitioning of impurities. The partitioning may influence the flow characteristics such as the relative permeability, through the change of interfacial tension between water and the CO_2 phase (Bachu and Bennion, 2009 a). We have discussed possible increase of the interfacial tension and decrease of the relative permeability due to the presence of N_2, O_2 and Ar. Although O_2 and Ar have not been investigated with regard to the partitioning phenomenon, we expect them to be enriched together with N_2 in the front of the CO_2 flow as a result of partitioning, due to their similar properties to N_2, and decrease the relative permeability. Here we consider another application of the partitioning effect: Ar impurity may serve as a trace species for monitoring CO_2 leakage. Noble gases including Ar have long been used in volcanic gas monitoring (see, *e.g.*, Magro and Pennisi, 1991). Ar has also been used as a tracer to monitor underground movement of injected CO_2 (see, *e.g.*, Bennaceur *et al.*, 2004). Ar concentration in air is 0.934%, but in the CO_2 stream from oxyfuel combustion, it can comprise over 4%. Considering the high pressure of the injected stream, Ar level may have a noticeable increase near the ground. The point is that Ar may reach the ground surface faster than CO_2, due to chromatographic partitioning by soil (after the gas passes through the caprock) as well as by porous formation rocks. It would be of great interest if Ar can serve as an indicator of potential leakage. For instance, with monitoring Ar level at the ground surface, higher than normal Ar level at a local area could suggest that the CO_2 is not far away from the surface. Emergency measures should then be taken for potential leakage, and this would leave more time than dealing with an eruption. Ar detectors can be maintained at locations with highest risks of leakage (abandoned injection wells, for instance), in addition to CO_2 monitors. In this way, the Ar impurity could make a positive contribution.

Compared with N_2, in the high-impurity case (5.8% N_2, 4.7%O_2 and 4.47% Ar) argon would give a more noticeable change of the ground air composition. Ar is concentrated to 4.8 times its level in air, but N_2 is not concentrated. The partial pressure of Ar in CO_2 is nearly 1 MPa if the total pressure is 20 MPa. The longer the storage, the higher the Ar concentration in CO_2, as Ar dissolves less. Moreover, Ar has lower adsorption on certain inorganic sorbents than N_2 and much lower than CO_2, which would make the partition more effective. We also consider that Ar may serve as a tracer in fresh water aquifers which have higher risk of contamination by CO_2 stored underneath, as Ar may emerge earlier than CO_2.

H_2 is the candidate for streams from pre-combustion capture when its concentration is appreciable. It has low solubility in water and low levels in air. In the high-H_2 stream (1 vol % H_2) studied in this work, it is concentrated 20,000 times its level in air. It also has high permeability (high diffusivity and low adsorption level) so that it would more readily get to the ground surface than CO_2. However, its reactions with other impurities (O_2, for example) and rock minerals are uncertain. If it is mostly consumed by reactions,

especially in the long term (this is thermodynamically favoured), its concentration in the gas phase may not be appreciable.

9. Conclusions

The effects of various impurities on CO_2 may be generalized into two categories: physical and chemical. Physical effects are concerning phase behaviour, storage capacity, permeation flux, buoyancy, etc. Chemical effects are concerning rock-porosity related injectivity, caprock integrity, corrosion of well materials, hazardousness in the event of leakage, etc. Based on the results of the investigations the effects of non-condensable gas impurities, mainly N_2, O_2 and Ar, are considered physical, except for the enhancement of chemical effects by O_2 through oxidation of SO_2 to sulphuric acid and others.

In the studied scenarios of impure CO_2 streams where O_2, N_2 and Ar have the highest levels, the greatest impact of the impurities is physical, *i.e.*, reducing the storage efficiency and the injectivity.

The most significant effect under the studied conditions is the reduction of storage capacity. It has been shown that the non-condensable impurities can cause the reduction of the structural trapping capacity by a degree greater than their molar fractions in supercritical CO_2 streams. Particularly, there is a maximum reduction of the storage capacity in a certain pressure range, where the capacity can drop to below 50% of the pure CO_2 cases. Non-condensable impurities N_2, O_2 and Ar are also expected to cause an increase of the interfacial tension between the CO_2 phase and water. This would lead to decreased relative permeability of the CO_2 flow but increased residual trapping. The injectivity of impure CO_2 streams reduces as a result of lower density. However, due to the compensation by increased viscosity the reduction of injectivity is smaller than that of storage capacity. The higher buoyancy of impure CO_2 streams would reduce the efficiency of CO_2 dissolution in formation water and CO_2 trapping in rock pores, and thus reduce the security of CO_2 storage in the near to medium terms. The adverse effects on storage efficiency and security may be alleviated by increasing the depth of injection and storage.

SO_2 can increase CO_2 storage capacity and there will be a maximum increase at a certain pressure. However, in the studied scenarios the concentration of SO_2 is low and no appreciable increase of capacity can be expected.

Under the studied conditions, Ar has been shown to have the potential to represent total N_2, O_2 and Ar for CO_2 streams from oxyfuel combustion with regard to the physical effects. The applicability for more general cases should be validated by experimental data. Once the validity is confirmed, the benefits of using Ar-only mixture for both computer simulations and experimental evaluations will be substantial.

With regard to chemical effects on the rocks, the most significant species are SO_x, NO_x and H_2S. NO_x can catalyze the oxidation of SO_2 to sulphuric acid according to the lead chamber process. Although the effect of catalysis is hard to quantify, when NO_x and O_2

are present, SO_2 could be taken as completely converted to sulphuric acid and would cause mineral dissolution and precipitation. However, the impact of SO_2 on reduction of rock porosity and injectivity appears much smaller than previously thought, because its contact with water is limited with the development of the dry-out zone. NO_x would also promote dissolution of minerals, but would not cause precipitations and reduction of rock porosity. H_2S on its own has not been found to reduce the injectivity in acid gas injection operations and computer simulations. However, if H_2S and SO_2 are co-injected, deposition of elemental sulphur, as a result of the Claus reaction, in the pores over the whole injection period can be a serious concern. Experimental evaluation of this issue is recommended.

For evaluation of the chemical effects on caprock integrity, the presence of water has been taken into account to assess the worst-case scenario. Thermochemical calculations show that SO_x and NO_x increase dissolution of carbonate rocks and aluminosilicate rocks. However, for CO_2 streams considered by IEA GHG in this study where SO_x and NO_x concentrations are within 100 ppm, the impact on the dissolution of the rocks would not be significant.

Corrosion of injection well materials may not be serious when the CO_2 stream is dry, due to desiccation of the well zone in the injection period. However, after termination of injection and return of water, corrosion by the acidic impurities will be an issue of concern. Results of thermochemical calculation suggest that the effect of acid impurities on dissolution of cement constituents is more significant than on dissolution of rocks. When protection by the cement sheaths is lost, the steel casings will also be attacked. Appropriate measures for countering the adverse effects, such as improving cement and casing quality (if the casings are to not taken out) prior to sealing the wells may be required.

Hazardous impurities CO, SO_2, H_2S, NO_x and Hg will form dissolved and/or precipitated species eventually. In the event of CO_2 leakage, the dissolved hazardous impurities may be released. However, in the CO_2 streams of the studied scenarios, the concentrations of the hazardous impurities are generally lower than the limits recommended for pipeline transport of CO_2, where short-term exposure limits have been taken into account. Accordingly, at least for short-term exposures, the hazard of the impurities would be less than that due to sudden leakages of CO_2 pipelines.

Concerning CO_2 storage costs, we have shown that, based on an existing approach for cost estimation which only considers costs of injection wells, the impact of impurities looks modest. On the other hand, decreased CO_2 storage capacity by the impurities can result in earlier reduction of the storage capacity, and increase the storage costs afterwards. We have also illustrated how impurities would impact cost curves evaluated on the basis of pure CO_2. With the development of more accurate costing methods, the impact of impurities could be evaluated more accurately.

Acknowledgment

Drs. Stephan Bachu and Ernie Perkins of Alberta Innovates as well as Charles Gorecki and Jordan Bremer of the Energy and Environmental Research Centre reviewed the draft report. Their invaluable comments are greatly appreciated.

Notations

A: cross section area (m^2).
a: parameter in equation of state (Pa $m^6 mol^{-2}$)
b: parameter in equation of state ($m^3 mol^{-1}$).
F : buoyancy force density (N m^{-3}).
F_0 : buoyancy force density of pure CO_2(N m^{-3}).
f : a coefficient related to frictional resistance (s^{-1}).
g: gravitational acceleration (9.8 m s^{-2}).
k : permeability of rock (m^2).
k_{ij}: binary interaction constant for components i and j (-).
m_i : mass of impurity species i (kg).
m_{CO2} : mass of CO_2 in mixture (kg).
L : distance (m).
M: mass of CO_2 in mixtures stored in given volume (kg).
M_0: mass of CO_2 in pure stream stored in given volume (kg).
$\dot{M}$: mass flux (kg s^{-1}).
p : pressure (Pa or MPa).
p_c : critical pressure (Pa or MPa).
p_c^* : pseudo-critical pressure (Pa or MPa).
R: universal gas constant (8.314 J mol^{-1} K^{-1}).
T : temperature (K).
T_c, critical temperature (K).
T_c^* pseudo-critical temperature (K).
t : time (s).
V_m: molar volume (m^3).
V_p : volume of sulphate precipitate (m^3).
V_ϕ : pore volume (m^3).
v: velocity (m s^{-1}).
w: molar weight (g mol^{-1}).
Z: ($= pV_m/RT$); compressibility factor (-).

Greek symbols

α : parameter in equation of state (-).
γ_{SO2} : volume fraction of SO_2 in CO_2 stream (-).
μ : viscosity (Pa s).
μ_0 : viscosity of pure CO_2 (Pa s).
ρ : density (kg m^{-3}).
$\overline{\rho}$: density of impure CO_2 stream (kg m^{-3}).
ρ_0 : density of pure CO_2 (kg m^{-3}).
σ : interfacial tension (N m^{-1})

ϕ: porosity of rock (-).
ω: acentric factor (-).

References

André, L., Audigane, P., Azaroual, M., Menjoz, A.(2007). Numerical modeling of fluid-rock chemical interactions at the supercritical CO_2-liquid interface during CO_2 injection into a carbonate reservoir, the Dogger aquifer (Paris Basin, France). Energy Conversion and Management 48 (6), pp. 1782-1797.

Bachu, S., Gunter, W.D. (2004). Overview of acid-gas injection operations in western Canada. In: Proceedings of the 7th International Conference on Greenhouse Gas Control Technologies. Volume 1: Peer-Reviewed Papers and Plenary Presentations, Vancouver, BC, September 5-9, 2004.

Bachu, S. (2008). CO_2 storage in geological media: Role, means, status and barriers to deployment. Progress in Energy and Combustion Science 34 (2), pp. 254-273.

Bachu, S., Bennion, D.B. (2009 a). Chromatographic partitioning of impurities contained in a CO_2 stream injected into a deep saline aquifer: Part 1. Effects of gas composition and in-situ conditions. International Journal of Greenhouse Gas Control 3 (4), pp. 464-473.

Bachu, S., Pooladi-Darvish, M., Hong, H. (2009 b). Chromatographic partitioning of impurities (H_2S) contained in a CO_2 stream injected into a deep saline aquifer: Part 2. Effects of flow conditions. International Journal of Greenhouse Gas Control 3 (4), pp. 458-463.

Bacon, D.H., Sass, B.M., Bhargava, M., Sminchak, J., Gupta, N. (2009). Reactive transport modeling of CO_2 and SO_2 injection into deep saline formations and their effect on the hydraulic properties of host rocks. Energy Procedia 1 (1), pp. 3283-3290.

Bennaceur, K., Monea, M., Sakurai, S., Gupta, N., Ramakrishnan, T.S., Whittaker, S., Randen, T. (2004). CO_2 Capture and Storage—A Solution Within. Oilfield Review 16 (3), pp. 44-61.

Bryant, S., Lake, L. (2005). Effect of impurities on subsurface CO_2 storage processes, Carbon Dioxide Capture for Storage in Deep Geologic Formations - Results from the CO_2 Capture Project, v. 2: Geologic Storage of Carbon Dioxide with Monitoring and Verification, S.M. Benson (ed.), Elsevier, London. pp. 983-998.

Burton, M., Kumar, N., Bryant, S.(2008). Time-dependent injectivity during CO_2 storage in aquifers. In: SPE 113937, SPE/DOE IOR Symposium, Tulsa, OK, 19–23 April 2008.

Choi, Y., Nesic, S., Young, D. (2010). Effect of impurities on the corrosion behavior of CO_2 transmission pipeline steel in supercritical CO_2-water environments. Environmental Science and Technology 44 (23), pp. 9233-9238.

Clifford, A.A. (2007). Calculation of Thermodynamic Properties of CO_2 using Peng Robinson equation of state. Available at Critical Processes Ltd. site: http://www.criticalprocesses.com/index.htm.

Collins, A.G. (1977). Enhanced oil injection waters. In: Oil Field Subsurface Injection of Water, ASTM STP 641 (Wright, C.C., Cross, D., Ostroff, A.G., Stanford A. G. eds), America Society for Testing and Materials, pp. 2-23.

Crandell, L.E., Ellis, B.R., Peters, C.A. (2010). Dissolution potential of SO_2 co-injected with CO_2 in geologic sequestration. Environmental Science and Technology 44 (1), pp. 349-355.

Dahowski, R.T., Dooley, J.J., Davidson, C.L., Bachu, S. Gupta, N. (2004). A CO_2 cost supply curve for North America. Report for IEA GHG (Contract IEA/CON/02/82).

de Visser, E., Hendriks, C., Barrio, M., Mølnvik, M.J., de Koeijer, G., Liljemark, S., Le Gallo, Y. (2008). Dynamis CO_2 quality recommendations. International Journal of Greenhouse Gas Control 2 (4), pp. 478-484.

de Visser, E., Hendriks, C., de Koeijer, G., Liljemark, S., Barrio, M., Austegard, A., Brown, A. (2009). CO_2 quality recommendations. Dynamis-Hypogen project: Deliverable D 3.1.3. http://www.dynamis-hypogen.com/publications/public_reports.htm.

Duan, Z., Sun, R.(2003). An improved model calculating CO_2 solubility in pure water and aqueous NaCl solutions from 273 to 533 K and from 0 to 2000 bar. Chemical Geology 193 (3-4), pp. 257-271.

Ellis, B.R., Crandell, L.E., Peters, C.A. (2010). Limitations for brine acidification due to SO_2 co-injection in geologic carbon sequestration. International Journal of Greenhouse Gas Control 4 (3), pp. 575-582.

Esper, G.J., Bailey, D.M., Holste, J.D., Hall, K.R. (1989). Volumetric behaviour of near-equimolar mixtures for CO_2+CH_4 and CO_2+N_2. Fluid Phase Equilibria, 49, pp. 35-47.

Gaus, I., Azaroual, M., Czernichowski-Lauriol, I. (2005). Reactive transport modelling of the impact of CO_2 injection on the clayey cap rock at Sleipner (North Sea). Chemical Geology 217 (3-4), pp. 319-337.

Gaus, I., Audigane, P., André, L., Lions, J., Jacquemet, N., Durst, P., Czernichowski-Lauriol, I., Azaroual, M. (2008). Geochemical and solute transport modelling for CO_2 storage, what to expect from it? International Journal of Greenhouse Gas Control 2 (4), pp. 605-625.

Giorgis, T., Carpita M., Battistelli, A. (2007). 2D modeling of salt precipitation during the injection of dry CO_2 in a depleted gas reservoir, Energy Conversion and Management 48(6), pp. 1816–1826.

Gorecki, C.D., Sorensen, J.A., Bremer, J.M., Ayash, S.C., Knudsen, D.J., Holubnyak, Y.I., Smith, S.A., Steadman, E.N., Harju, J.A. (2009) Development of storage coefficients for carbon dioxide storage in deep saline formations and depleted hydrocarbon reservoirs. Report for IEA GHG.

Hu, G., Dam-Johansen, K., Wedel, S., Peter Hansen, J. (2006). Review of the direct sulfation reaction of limestone. Progress in Energy and Combustion Science 32 (4), pp. 386-407.

Huber, M.L., Hanley, H.J.M. (1996). The Corresponding-States Principle: Dense fluids, In: Transport Properties of Fluids: Their Correlation, Prediction and Estimation. Millat, J., Dymond, J.H., Nieto de Castro, C.A. (eds), Cambridge University Press. p. 283.

IEA GHG (2004). Impact of impurities on CO_2 capture, transport and storage. Report No. PH4/32.

IEA GHG (2010). Corrosion and materials selection in CCS systems. Report 2010/03.

Jacquemet, N., Pironon, J., Saint-Marc, J.(2008). Mineralogical changes of a well cement in various H_2S-CO_2(-brine) fluids at high pressure and temperature. Environmental Science and Technology 42 (1), pp. 282-288.

Jacquemet, N., Le Gallo, Y., Estublier, A., Lachet, V., von Dalwigk, I., Yan, J., Azaroual, M., Audigane, P. (2009). CO_2 streams containing associated components-A review of the thermodynamic and geochemical properties and assessment of some reactive transport codes. Energy Procedia 1 (1), pp. 3739-3746.

Jia, L., Tan, Y., Wang, C., Anthony, E.J. (2007). Experimental study of oxy-fuel combustion and sulfur capture in mini-CFBC. Energy and Fuels 21 (6), pp. 3160-3164.

Johnson, J.W., Naito, J.J. Steefel, C.I. (2002). Fundamental elements of geologic CO_2 sequestration in saline aquifers. American Chemical Society Fuel Chemistry Division Preprints 47(1), pp.41-42.

Jones, D.M., Head, I.M., Gray, N.D., Adams, J.J., Rowan, A.K., Aitken, C.M., Bennett, B., Huang, H., Brown, A., Bowler, B.F.J., Oldenburg, T., Erdmann, M. Larter, S.R. (2008). Crude-oil biodegradation via methanogenesis in subsurface petroleum reservoirs. Nature 451 (7175), pp. 176-180.

Kather, A. (2009). Presented at 2nd Working Group Meeting on CO_2 Quality and Other Relevant Issues (September 2009, Cottbus, Germany).

Kay, W.B. (1936). Gases and vapors at high temperature and pressure - density of hydrocarbon. Industrial and Engineering Chemistry 28:pp.1014-1019.

Klimeck, J., Kleinrahm, R., Wagner, W. (2001). Measurements of the (p, ρ, T) relation of methane and carbon dioxide in the temperature range 240 K to 520 K at pressures up to 30 MPa using a new accurate single-sinker densimeter. Journal of Chemical Thermodynamics 33 (3), pp. 251-267.

Knauss, K.G., Johnson, J.W., Steefel, C.I. (2005). Evaluation of the impact of CO_2, co-contaminant gas, aqueous fluid and reservoir rock interactions on the geologic sequestration of CO_2. Chemical Geology 217 (3-4 SPEC. ISS.), pp. 339-350.

Ledoux, M.J., Pham-Huu, C., Keller, N., Nougayrède, J.-B., Savin-Poncet, S., Bousquet, J.(2000). Selective oxidation of H_2S in Claus tail-gas over SiC supported NiS2 catalyst. Catalysis Today 61 (1), pp. 157-163.

Li, H., Yan, J. (2009 a). Impacts of equations of state (EOS) and impurities on the volume calculation of CO_2 mixtures in the applications of CO_2 capture and storage (CCS) processes. Applied Energy 86 (12), pp. 2760-2770.

Li, H., Yan, J. (2009 b). Evaluating cubic equations of state for calculation of vapor-liquid equilibrium of CO_2 and CO_2-mixtures for CO_2 capture and storage processes. Applied Energy 86 (6), pp. 826-836.

Magro, G, Pennisi, M. (1991). Light noble gases and nitrogen in the crater fluids at vulcano (Italy): special survey from June to September 1988. Acta Vulcanologica 1, pp. 215-218.

Motealleh, S., Bryant, S.L.(2007). Predictive model for permeability reduction by small wetting phase saturations. Water Resources Research 43 (12), art. no. W12S07.

Nogueira, M., Mamora, D.D. (2008). Effect of flue-gas impurities on the process of injection and storage of CO_2 in depleted gas reservoirs. Journal of Energy Resources Technology, Transactions of the ASME 130 (1), pp. 0133011-0133015.

Oosterkamp, A., Ramsen, J. (2008). State-of-the-art overview of CO_2 pipeline transport with relevance to offshore pipelines. Polytech Report No: POL-O-2007-138-A.

Palandri, J.L., Kharaka, Y.K. (2005). Ferric iron-bearing sediments as a mineral trap for CO_2 sequestration: Iron reduction using sulfur-bearing waste gas. Chemical Geology 217 (3-4), pp. 351-364.

Palmer, S. E. (1993). In: Organic Geochemistry (Macko, S. A., Engel, M. H. eds), pp. 511–534, Plenum Press, New York).

Pavlík, V., Unlink, S. (1997).The rate of corrosion of hardened cement pastes and mortars with additive of silica fume in acids. Cement and Concrete Research 27 (11), pp. 1731-1745.

Pavlík, V. (2000). Effect of carbonates on the corrosion rate of cement mortars in nitric acid. Cement and Concrete Research 30 (3), pp. 481-489.

Peng, D., Robinson, D.B. (1976). A New Two-Constant Equation of State. Industrial and Engineering Chemistry: Fundamentals 15, pp.59–64.

Pipitone, G., Bolland, O. (2009). Power generation with CO_2 capture: Technology for CO_2 purification. International Journal of Greenhouse Gas Control 3 (5), pp. 528-534.

Poling, B.E., Prausnitz, J.M., O'Connell, J. P. (2001). Properties of Gases and Liquids (5th Edition). McGraw-Hill.

Preto, F., Wang, J., Jia, L., Anthony, E.J.(2004). A study on mechanisms of nitrous oxide formation in post-combustion flue gases. Atmospheric Environment 38(8), pp. 1123-1131.

Pruess, K., García, J.(2002). Multiphase flow dynamics during CO_2 injection into saline aquifers. Environmental Geology 42(2-3), pp. 282 - 295.

Pruess, K., Müller, N. (2009). Formation dry-out from CO_2 injection into saline aquifers: 1. effects of solids precipitation and their mitigation. Water Resources Research 45 (3), art. no. W03402.

Pruess, K. (2009). Formation dry-out from CO_2 injection into saline aquifers: 2. analytical model for salt precipitation. Water Resources Research 45 (3), art. no. W03403.

Ren, Q., Chen, G., Yan, W., Guo, T. (2000). Interfacial tension of (CO_2 + CH_4) + water from 298 K to 373 K and pressures up to 30 MPa. Journal of Chemical and Engineering Data 45 (4), pp. 610-612.

Sass, B.M., Farzan, H., Prabhakar, R., Gerst, J., Sminchak, J., Bhargava, M., Nestleroth, B., Figueroa, J. (2009). Considerations for treating impurities in oxy-combustion flue gas prior to sequestration. Energy Procedia 1 (1), pp. 535-542.

Seevam, P.N., Race, J.M., Downie, M.J. (2007). Carbon dioxide pipelines for sequestration in the UK: An engineering gap analysis. Global Pipeline Monthly 3 (6).

Shah, V., Broseta, D., Mouronval, G., Montel, F.(2008). Water/acid gas interfacial tensions and their impact on acid gas geological storage. International Journal of Greenhouse Gas Control 2 (4), pp. 594-604.

Soave, G. (1972).Equilibrium constants from a modified Redlich-Kwong equation of state. Chemical Engineering Science, 27 (6), pp. 1197-1203.

Stanger, R., Wall, T. (2011). Sulphur impacts during pulverised coal combustion in oxy-fuel technology for carbon capture and storage. Progress in Energy and Combustion Science 37(1) pp. 69-88.

Taber, J.J. (1985). Fate of small concentrations of SO_2, NOx and O_2 when injected with CO_2 into oil reservoirs, Argonne National Laboratories.

Talman, S.J., Perkins, E.H. (2009). Concentration gradients associated with acid gas injection. International Acid Gas Injection Symposium 2009, Calgary, AB, Canada.

Wang J., Anthony, E.J. (2008). Clean combustion of solid fuels. Applied Energy 85 (2-3), pp. 73-79.

White, D.J., Johnson, J.W. (2009). Integrated geophysical and geochemical research programs of the IEA GHG Weyburn-Midale CO_2 monitoring and storage project. Energy Procedia 1 (1), pp. 2349-2356.

Wilkinson, J.R., Leahy-Dios A., Teletzke, G. F., Dickson, J.L. (2010). Use of CO_2 containing impurities for miscible enhanced oil recovery, presentation at CPS/SPE International Oil & Gas Conference and Exhibition Beijing, China, 8-10 June 2010.

Xu, T., Apps, J.A., Pruess, K., Yamamoto, H. (2007). Numerical modeling of injection and mineral trapping of CO_2 with H_2S and SO_2 in a sandstone formation. Chemical Geology 242 (3-4), pp. 319-346.

Yan, W., Zhao, G. , Chen, G., Guo, T. (2001). Interfacial tension of (methane + nitrogen) + water and (carbon dioxide + nitrogen) + water systems. Journal of Chemical and Engineering Data 46 (6), pp. 1544-1548.

Zettlitzer, M., Moeller, F., Morozova, D., Lokay, P., Würdemann, H. (2010). Re-establishment of the proper injectivity of the CO_2-injection well Ktzi 201 in Ketzin, Germany. International Journal of Greenhouse Gas Control, in press.

Zuluaga, E., Lake, L.W.(2008). Modeling of experiments on water vaporization for gas injection using travellng waves. SPE Journal 13 (2), pp. 248-256.

Appendix A – Properties of Components in CO_2 Streams

The following table contains physical properties of the components in CO_2 streams that are discussed in this work. The data are compiled from a number of sources, including CRC Handbook of Chemistry and Physics, Gas Encyclopaedia (available at http://encyclopedia.airliquide.com/Encyclopedia.asp), and others which are indicated in the table).

Component	**W_M**	**T_c (K)**	**P_c (MPa)**	**ρ (kg/m^3)**	**ω (-)**	**μ (μPa·s)**	**S (mol/L)**
CO_2	44.01	304.21	7.38	1.842	0.22362	14.73	0.039
O_2	32	154.58	5.04	1.331	0.02218	20.34	0.0014
N_2	28.02	126.20	3.4	1.165	0.03772	17.49	0.00068
Ar	39.95	150.86	4.9	1.661	0.00000	22.35	0.0015
SO_2	64.06	430.75	7.88	2.279	0.24538	12.70	2.1
SO_3	80.06	490.85	8.21	1.970 [1)]	0.42396	n/a	reaction
NO	30	180.15	6.48	1.249	0.58294	18.97	0.00033 [3)]
NO_2	46.01	431.15	10.13	3.400 [2)]	0.85109	13.2	reaction
H_2S	34.08	373.53	8.96	1.434	0.09417	12.42	0.11
CO	28.01	132.92	3.5	1.165	0.04816	17.45	0.001
H_2	2.016	33.19	1.31	0.0893	-0.21599	8.88	0.0008
CH_4	16.043	190.56	4.6	0.668	0.01155	11.03	0.0014
H_2O	18.02	647.13	22.6	0.749	0.34486	n/a	n/a

where:

W_M - molecule weight
T_c - critical temperature
P_c - critical pressure
ρ - density at NTP (normal temperature and pressure, defined as 20°C and 1 atm)
ω - acentric factor (the values are from SIMSCI databank incorporated in process simulator PRO/II (http://iom.invensys.com/EN/Pages/SimSci-Esscor.aspx))
μ - viscosity at NTP
S - solubility in water at NTP (data are from "Solubility of Gases in Water", available at http://www.engineeringtoolbox.com/gases-solubility-water-d_1148.html)

[1)] vapor density at 25°C
[2)] vapor density at 22°C
[3)] at 0°C and 1 atm

Appendix B – Binary Interaction Constants for Equations of State

The following table lists the values of binary interaction constants used in this study for calculations with the Peng-Robinson equation and Soave-Redlich-Kwong equation. The values are from SIMSCI databank incorporated in the process simulator PRO/II (http://iom.invensys.com/EN/Pages/SimSci-Esscor.aspx) unless indicated otherwise.

Component pair	k_{ij}	
	Peng-Robinson	**Soave-Redlich-Kwong**
CO_2/O_2*	0.1140	0.1160
CO_2/N_2	-0.017	-0.0300
CO_2/Ar*	0.1630	0.1800
CO_2/SO_2*	0.0460	0.0480
CO_2/H_2S	0.1000	0.1000
CO_2/CO	-0.0300	0.0500
CO_2/H_2	-0.1622	-0.3426
CO_2/CH_4	0.0919	0.0933
CO_2/H_2O	0.2100	0.2300
O_2/N_2	-0.0119	-0.0078
O_2/Ar	0.0104	0.0178
O_2/CH_4	0.0500	0.0600
N_2/SO_2	0.0800	0.0578
N_2/H_2S	0.1800	0.1700
N_2/CO	0.0120	0.0400
N_2/H_2	-0.0300	0.0233
N_2/CH_4	0.0350	0.0300
N_2/H_2O	0.5080	0.5300
Ar/CH_4	0.0230	0.0252
SO_2/CH_4	0.1356	0.1279
H_2S/CO	0.0544	0.0367
H_2S/H_2	0.1000	0.0830
H_2S/CH_4	0.0850	0.0900
H_2S/H_2O	0.1640	0.1350
CO/H_2	0.0900	0.0400
CO/CH_4	0.0300	0.0322
CO/H_2O	0.2000	0.2000
H_2/H_2O	0.5630	0.4000
H_2/CH_4	0.0160	-0.0200
CH_4/H_2O	0.5000	0.5200

* from Li and Yan (2009 b)